Geoscience Laser Altimeter System (GLAS)

Algorithm Theoretical Basis Document
Version 4.2

GLAS ATMOSPHERIC DATA PRODUCTS

Prepared by:

Steve Palm[1], William Hart, Dennis Hlavka
Science Systems and Applications, Inc.
Lanham, MD

Ellsworth J. Welton
Ashwin Mahesh
Goddard Earth Science and Technology Center
University of Maryland, Baltimore County

James Spinhirne
NASA Goddard Space Flight Center
Greenbelt, MD

October 2002

Corresponding Address: Code 912, Goddard Space Flight Center, Greenbelt, MD 20771
Email: spp@virl.gsfc.nasa.gov

Table of Contents

.

ii

Summary of Changes to this Version

Most of the major changes made to this version (4.2, October 2002) of the ATBD are in the GLA02, GLA09, GLA10 and GLA11 modules. In particular, section 3.6.2 details the multiple scattering algorithm and in section 3.1.1.3 we have added considerably more detail to the calibration process. Also, section 3.3.1.2 has been expanded. It now gives more detail on the cloud/aerosol layer discrimination algorithm.

1 Introduction

Scheduled for launch in late 2002, the Geoscience Laser Altimeter System (GLAS) is an atmospheric lidar in addition to a surface altimeter. GLAS will provide high resolution measurements of global topography with special emphasis on the determination of the temporal changes of ice sheet mass over Antarctica and Greenland. These measurements, obtained continuously for a period of 10 to 15 years, will enable scientists to determine whether the ice sheets are growing or shrinking which has implications for climate change. The atmospheric objectives of GLAS are the global laser profiling of atmospheric aerosols and clouds. Knowledge of the height, coverage and thickness of cloud layers is essential in modeling the radiative fluxes at the surface and within the atmosphere. Clouds frequently occur in multi-layer systems on many spatial scales. Satellite based radiometers and imagers do an excellent job of viewing the cloud tops, but are limited in their ability to distinguish multi-level cloud formations and determine the true vertical distribution of clouds. Passive remote sensors also tend to underestimate the fraction of optically thin clouds, while overestimating the percent of broken, optically thick clouds. Recent sensitivity studies using calculations based on ISCCP (International Satellite Cloud Climatology Project) data indicate that the largest uncertainty in long wave radiative flux at the surface is caused by the lack of knowledge of the amount of cloud overlap or multi-layering (Wielicki et al. 1996).

Anthropogenic aerosol is also known to have important implications for the earth's radiative balance. Both direct (scattering and absorption of sunlight) and indirect (changing of cloud radiative properties) forcing by mainly sulfate aerosols has recently been shown to cause net regional cooling (IPCC, 1994). With current passive sensors, our ability to map the amount and extent of global aerosol is limited. Passive sensing provides essentially no information on vertical distribution and there are formidable analysis problems, especially over land. GLAS will significantly enhance our ability to measure atmospheric aerosol, both natural and anthropogenic. This has implications for improving climate models by providing better knowledge of the anthropogenic direct aerosol forcing, which at this point can only be estimated from sulfate source models.

The primary atmospheric science goal of the GLAS cloud and aerosol measurement is to determine the radiative forcing and vertically resolved atmospheric heating rate due to cloud and aerosol by directly observing the vertical structure and magnitude of cloud and aerosol parameters that are important for the radiative balance of the earth-atmosphere system, but which are ambiguous or impossible to obtain from existing or planned passive remote sensors. A further goal is to directly measure the height of atmospheric transition layers (inversions) which are important for dynamics and mixing, the planetary boundary layer and lifting condensation level. Towards these goals, the various level 2 data products which will be generated on the GLAS ground processing system are:

1. GLA07 - Profiles of calibrated cloud and aerosol attenuated backscatter cross section
2. GLA08 - Planetary Boundary Layer (PBL) height
3. GLA08 - Elevated tropospheric aerosol layer height
4. GLA09 - Cloud top (and bottom when possible) heights
5. GLA10 – Attenuation-corrected backscatter cross section for clouds and aerosol layers
6. GLA10 - Cloud and aerosol extinction cross sections

7. GLA11 - Thin cloud and aerosol layer optical depth

The intent of this document is limited to a description of the theoretical basis and the approach that is to be pursued in developing processing algorithms for the GLAS level 1 and 2 atmospheric data products. The actual development of the algorithms will involve modeling and testing over the next two years. We anticipate subsequent revision(s) of the GLAS atmospheric products ATBD as we collectively continue to code these algorithms and exercise them on various simulated GLAS data sets. The level 1 and 2 products described are those that will be produced by real time processing of data. The basis for the initial approach is described. More sophisticated approaches and improvements from post processing are to be developed. To date almost all resources that have been available for the development of algorithms for atmospheric products have gone into the development of comprehensive, bit level, simulation of GLAS data as a tool for instrument design studies (Spinhirne and Palm, 1997) and calculations of multiple scattering effects on surface ranging (Duda et al. , 1999a and b). The level 1 and 2 data products only involve data input from the GLAS instrument and other ancillary information that is available in real time, such as atmospheric temperature profiles. Level 3 products and improvement of level 2 products from post processing will involve measurements and retrievals from other satellites and models. The further research for these will be described in section IX.

To begin, we will first review some of the prior lidar work which is pertinent to the GLAS data products discussed here, before presenting the details of the individual algorithms in section 3. Section 4 discusses the practical applications and implementation issues of each algorithm including examples of output. Section 5 briefly addresses multiple scattering induced ranging error and section 6 lists a number of possible browse products which can be used to monitor the algorithm output. Section 7 discusses the algorithm development plan with section 8 providing details on the pre and post launch validation plan. Finally, section 9 touches on ideas for future research.

2 Overview and Background

2.1 History

The purpose of this document is to develop and present a detailed description of the algorithm theoretical basis for each of the GLAS data products. Most of the expertise for this endeavor is the result of many years work with aircraft and ground-based lidar systems. Each of the authors have had many years experience designing and coding algorithms for the retrieval of atmospheric parameters from lidar data. The Cloud and Aerosol Lidar System (CALS), which flies on the NASA ER-2 high altitude aircraft, has been employed in many field experiments around the world and algorithms have been developed to analyze these data for a number of atmospheric parameters. CALS data have been analyzed for cloud top height, thin cloud optical depth, cirrus cloud emittance (Spinhirne and Hart, 1990) and boundary layer depth (Palm and Spinhirne, 1987, 1998). Work by others also demonstrate the utility of lidar for deriving cloud optical properties, especially when combined with passive, multispectral radiometric observations (Platt et al, 1980; Spinhirne and Hart, 1990). We believe the methods developed to analyze CALS data can be adapted for use with GLAS data and will produce the best atmospheric data products possible.

2.2 Description of GLAS Atmospheric Channel Data

The atmospheric channel of GLAS will provide a record of the vertical structure of backscatter intensity from the ground to a height of about 41 km with 76.8 meter vertical resolution. Two channels will be employed, the Nd:Yag fundamental wavelength of 1064 nm and the frequency doubled 532 nm wavelength in the visible portion of the spectrum (green channel). The green channel will be the primary atmospheric signal, using a photon counting detector and will be for the detection of thin cirrus, elevated aerosol and haze layers and the planetary boundary layer. When the densest clouds are encountered, the 532 channel will saturate but will still provide an accurate measure of the height of the cloud tops. In this instance, the IR channel can then be used directly or as a way of estimating what the data from the green channel would have been had it not saturated.

The basic equation which describes the atmospheric return signal p(z) is the standard lidar equation

$$(2.1) \quad p(z) = \frac{CE\beta(z)T^2(z)}{r^2} + p_b + p_d$$

where $\beta(z)$ is the total atmospheric backscatter cross section at an altitude z, T(z) is the transmission from the top of the atmosphere to altitude z, r is the range from the spacecraft to the altitude z, E is the transmitted laser pulse energy and C is a dimensional constant referred to as the calibration constant. There are two range independent background terms, p_b from scattered solar radiation and p_d for any detector dark signal. In the case where p would be the signal in watts returned to the receiver detector, the calibration constant is given as

$$(2.2) \quad C=cAT_s/2$$

where c is the light speed constant , A the area of the receiver and T_s the optical transmission of the receiver system.

For the GLAS 532 nm atmospheric channel the signal will be acquired as the photo-electron count rate from the detector n(z). In this case the calibration constant will be given as

$$(2.3) \quad C=AT_s\lambda q/2h$$

where λ is the wavelength, q is the photon detection probability or quantum efficiency, and h is the Plank constant. The background radiance signal in terms of photo-electron count rate will be

$$(2.4) \quad n_b=AT_sI_b\Omega\Delta/hc$$

where I_b is the background radiance and Ω is the receiver solid angle and Δ is the optical bandwidth. The additional background signal will be any detector dark photo-electron count rate n_d.

The 1064 um detector for GLAS is the same silicon APD detector that will be used for the surface return signal although a separate lower speed A/D signal acquisition will be used. The signal in this case is a voltage from the detector amplifier V(z). The calibration constant will be

(2.5) $C = AT_s crg_v/2$

where r is the detector responsivity in amps/watt, and g_v is the voltage gain of the detector preamplifier. The detector background signal will be $i_d g_v$ where i_d is the detector dark current.
The accuracy of the received GLAS atmospheric signals will be limited by the fundamental probability, or signal shot noise of the signal. For the case of the 532 nm photon counting signal, the noise factor is given by Poisson statistic. The signal to noise ratio will then be given by

(2.6) $$S/N = \frac{n(z)}{\sqrt{n(z) + n_b + n_d}}$$

Where n(z) is the number of photons detected by the lidar at range z. In the case where the signal is voltage derived from a detected current the basic signal to noise will be:

$$S/N = \frac{i_s}{\sqrt{2\Delta f(i_s + i_b + i_d)e}}$$

(2.7)

where i_s is the detector current produced by the backscattered signal, i_b is the detector current produced by background ambient light i_d is the detector dark current, Δf is the system electronic bandwidth, and e is electron charge. The signal noise defines the degree to which the lidar data may be usefully applied.

2.3 Instrument Description

The GLAS atmospheric measurements will be obtained from the 600 km polar orbiting platform both day and night using two separate channels. The 532 nm, photon counting channel will be the most sensitive and will provide the highest quality data obtaining both aerosol and cloud returns. This channel will employ an etalon filter which will be actively tuned to the laser frequency, providing a very tight bandpass filter of about 30 picometers. This, together with a very narrow (150 µr) receiver field of view (FOV), will enable high quality daytime measurements even over bright background scenes. There are 8 separate photon counting detectors for this channel which will significantly increase the available dynamic range while providing some degree of redundancy in the case of detector failure. The 1064 nm channel will use an Avalanche Photo Diode (APD) detector with a much wider (0.1 nm) bandpass filter and FOV (475 µr). The sensitivity of the 1064 channel will be limited by the inherent detector noise. It will, however, provide sufficient signal to noise to profile optically thick clouds and will be used to supplement the 532 channel when and if it becomes saturated. The 1064 data will not be used to retrieve atmospheric parameters since the signal to noise ratio of the 532 channel will be much better. The only exception to this would be in the case of problems or complete failure of the 532 channel, at which point the 1064 channel data would be used for cloud height retrieval only. Table I lists the major GLAS system parameters which ultimately affect system performance and data quality.

GLAS will carry three identical and redundant 40 Hz, solid state Nd:YAG lasers onboard, each with an expected lifetime of about 2.5 billion shots, or approximately 2 years of continuous operation. If

a laser malfunctions, or simply comes to the end of its normal lifetime, switching to one of the other lasers is straightforward. The laser will transmit short (5 nanosecond) pulses of laser light (in the nadir direction) that will produce a footprint 70 meters wide upon striking the surface, and each footprint will be about 175 meters apart. The backscattered light from atmospheric clouds, aerosols and molecules will be digitized at 1.953 MHz, yielding a vertical resolution of 76.8 meters. The horizontal resolution will be a function of height. For the lowest 10 km, each backscattered laser pulse will be stored. Between 10 and 20 km, 8 shots will be summed, producing a horizontal resolution of 5Hz or 1.4 kilometers. For the upper half of the profile (20-40 km), which is entirely within the stratosphere, 40 shots will be summed, providing a horizontal resolution of about 7.5 kilometers. This approach was adopted for a number of reasons. First, the atmospheric processes of interest have more variability and smaller scales in the lower troposphere (particularly the boundary layer) than in the mid and upper troposphere. Second, the amount of molecular and aerosol scattering in the upper troposphere and stratosphere is so small that summing multiple shots is required to obtain a non zero result. Lastly, this approach will help to reduce the amount of data that has to be stored on board the spacecraft and transmitted to the ground.

Table I. GLAS System Parameters

Parameter	532 Channel	1064 Channel
Orbit Altitude	600 km	600 km
Laser Energy	36 mJ	73 mJ
Laser Divergence	110 μ rad	110 μ rad
Laser Repetition Rate	40 Hz	40 Hz
Effective Telescope Diameter	95 cm	95 cm
Receiver Field of View	150 μ rad	500 μ rad
Detector Quantum Efficiency	60 %	35 %
Detector Dark Current	3.0×10^{-16} A	50.0×10^{-12} A
RMS Detector Noise	0.0	2.0×10^{-11}
Electrical Bandwidth	1.953×10^6	1.953×10^6
Optical Filter Bandwidth	0.030 nm	0.800 nm
Total Optical Transmission	30 %	55 %

3 GLAS Atmospheric Algorithms

This section will address in detail the structure and content of the six algorithms which comprise the level 1A, 1B and level 2 GLAS atmospheric data products. A theoretical description will be given for each algorithm followed by error quantification and a description of the confidence (quality) flags which attempt to assign a confidence level to the quality of the algorithm output. Section 4 will discuss the issues related to the practical application and implementation of the algorithms.

3.1 Normalized Lidar Signal (GLA02)

3.1.1 *Theoretical Description*

3.1.1.1 Normalized Lidar Signal

The normalized lidar signal is a level 1A data product which applies the fundamental corrections and normalizations to the raw data as well as providing an estimate of the height of the first cloud top and/or the bin location of the ground return. Additionally, it will flag each 532 nm channel bin which has reached saturation so that it may be corrected in later processing. The algorithm applies range and laser energy normalizations, computes and subtracts out the ambient background signal, and performs dead time correction to the photon counting (532 nm) channel. The dead time correction is performed by using a look-up table which contains a dead time corrected value for each possible output from the photon counting channel (sum of 8 individual photon counting detectors). The raw (not dead time corrected) signal from the photon counting channel will range from zero to about 100 photons per bin (0.512 microsecond). Thus, the lookup table need have only 100 or so entries. The exact content of the lookup table will be determined by careful laboratory calibration procedures prior to launch. In the case of the 1064 channel, the digital counts that are output from the analog to digital converter must first be converted back to a voltage using a lookup table which has been calibrated and tested in the laboratory. The background subtraction, energy and range corrections are then applied to the data.

The basic output of GLA02 is the generation of what we call normalized lidar signal ($P'(z)$). From (2.1) we first subtract the background, then multiply by the square of the range (in km) from the lidar receiver to the return bin (R^2) and divide by the laser energy (E, in millijoules). Here, we have combined the detector dark current (P_d) and the ambient background light (P_b) into one background term (B). We must also perform dead time correction on the raw photon counts (for the 532 channel) and convert from digital counts to volts in the case of the 1064 channel. Now, a further consideration for the 532 channel is the etalon transmission. For the 532 channel, a narrow-band etalon filter is used for rejection of background light. The etalon bandpass is about 25 picometers wide. The laser frequency may shift considerably on a shot to shot basis, which could result in a loss of return signal, since the laser frequency is not centered on the fliter bandpass. On board the spacecraft, a part of the laser energy will be split off and sent through the etalon. The amount of energy passing through the etalon will be measured and sent down in the telemetry. In the telemetry spreadsheet this is known as "Dual Pin A." The ratio of this to the outgoing laser energy at 532 times a calibration coefficient gives us a relative measure of the etalon transmission. The calibration coefficient (γ) will be determined by laboratory measurement. Thus, if we let $\alpha = \gamma$ DPA /

E_{532} where DPA is the "Dual Pin A" output, the equation to produce the normalized signal for the 532 channel is:

$$(3.1.1) \qquad P'_{532}(z) = C_{532}\beta_{532}(z)T^2_{532} = (DC[S_{532}(z)] - DC[B_{532}])R^2/(\alpha E_{532})$$

where DC denotes the dead time correction lookup table discussed above. Note that in the denominator, the transmit energy cancels as: $\alpha E_{532} = \gamma DPA$

For the 1064 channel, we must first convert the digital counts to voltage for both the background (V_b) and the atmospheric return signal (V_s) before computing the normalized signal.

$$3.1.2 \qquad V_b = (B_{1064}F_v - V_0)/(GA)$$

$$3.1.3 \qquad V_s(z) = (S_{1064}(z)F_v - V_0)/(GA)$$

where B_{1064} is the 1064 nm background (computed from equation 3.14 below), F_v is a constant (0.01560) relating digital counts to volts (volts per count), V_0 is the voltage offset (currently set to 0.90), G is the amplifier gain (currently set to 18.0) and A is the 1064 programmable attenuation setting (which will be a factor such as 1, 1/1.77, 1/3.16, 1/5.6, 1/10). Next we compute the normalized return signal

$$(3.1.4) \qquad P'_{1064}(z) = C_{1064}\beta_{1064}(z)T^2_{1064} = D_r(V_s(z) - V_b)R^2/E_{1064}$$

The range from the spacecraft to the return bin (R) should be in kilometers and the laser energy (E) should be in millijoules. The voltage must then be multiplied by the detector responsivity factor (D_r = 4.4x10^{7}) which has units watts per volt. The units for the 1064 channel are watts*km^2/mJ. The units for the 532 channel will be photons/bin*km^2/mJ.

Note also that the 8 shot and 40 shot summed data from the middle and upper layers must be normalized by the number of shots summed in that layer before equations 3.1.1 and 3.1.3 can be applied. Thus, all data from the 5 Hz middle layer must be divided by 8 and all data from the upper layer (532 only) must be divided by 40 before application of equations 3.1.1 and 3.1.3.

3.1.1.2 Background Computation

The background signal (B) for the two channels is computed for each laser shot (40 Hz) from time integrated measurements of the background intensity at two separate times relative to laser fire. The first is prior to the laser beam reaching the atmosphere (about 80 km altitude), and the second is well after the beam strikes the Earth (approximately 40 km below ground). The two background measurements for each channel will be stored as two byte values and must be normalized before use in equations 3.1.1 and 3.1.2. Letting T_b equal the background integration time in microseconds, and I_{532} and I_{1064} the integrated background signal for T_b microseconds, the background values (counts per bin) to be used in equations 3.1.1 and 3.1.2 are:

(3.1.3) $\qquad B_{532} = I_{532}/(1.953T_b(\lambda))$

(3.1.4) $\qquad B_{1064} = I_{1064}/(1.953T_b(\lambda))$

The background integration time is not the same for the two channels. $T_b(532)$ will be 265 microseconds, while $T_b(1064)$ will be half that or 128 microseconds. The background will be computed in this manner for the two integration periods. Although it is not definite, most likely the second of the two background measurements (the one taken at –40 km) will be used in equations 3.1.1 and 3.1.2. However, it is possible that the average of the two measurements would be used. The profiles defined by 3.1.1 and 3.1.2 will have the same format as the raw input data. This means that from –1 to 10 km altitude, both the 532 and 1064 channels will be 40 Hz, between 10 and 20 km the profiles will be at 5 Hz, and between 20 and 41 km we have only 532 data at 1 Hz. Note that the background computation as described above will be performed at 40, 5 and 1 Hz (the 5 and 1 Hz backgrounds are computed by averaging the 40 Hz background measurements) for the 532 channel and at 40 and 5 Hz for the 1064 channel. Care must be taken to use the appropriate background in equations 3.1.1 and 3.1.2 as dictated by the given layer (40 Hz background for the lowest layer, 5 Hz background for the middle layer and 1 Hz background for the upper layer). This also applies to the laser energy as well, as it is reported at 40 Hz. The 5 and 1 Hz laser energies must be calculated and the appropriate one applied according to which layer is being processed. Both the background and laser energies at 40, 5 and 1 Hz are stored as part of the GLA02 output.

In addition to the background being calculated from the high and low integration periods, it is also calculated from the last 8 bins of the lidar profile for both 532 and 1064. A fourth element is added to the background array stored on the product:
BG(1) – upper background
BG(2) – lower background
BG(3) – Background used in computing NRB
BG(4) – Background computed from the last 8 bins of the profile

3.1.1.3 Calibration Pre-Processing, Predicted Cloud Height and Ground Return Bin

A major change has been made to version 4 of the ATBD. In GLA02 we now are going to calculate average normalized lidar signal at two calibration heights for segments of data roughly 10 minutes in length continuously throughout the entire orbit. The first calibration height is constant at 30 km (or at least read in from the constants file) and will be used for the 532 channel only. The second calibration height will be calculated from the data comprising that segment and will occur at the height of the minimum average signal between 8 and 15 km. It is understood that the calibration pre-processing described below will most likely not be a part of the GLA02 process, but may be implemented as a stand alone module that will run after GLA02 completes. For the purpose of discussion, we will call the calibration pre-processing module the 'Segment Averaging Module' or SAM for short. After SAM is run, another module is run which uses the output of SAM to compute the actual calibration constants. The general processing scenario for SAM is as follows:

1. Construct a 1 Hz continuous profile of P' from –1 to 41 km for the 532 channel and from –1 to 20 km for the 1064 channel.
2. Add the background to 'summing' variables for each channel

3. Sum the P'$_{532}$ data from H$_1$ to H$_2$ km and add it to a 'summing' variable. The values of H$_1$ and H$_2$ will be roughly 29 and 31, respectively, but will be changeable and read in from the constants file. Increment an 'upper counter'.
4. Check for clouds from 22 km to 8 km above ground. If clouds were not found for this second, then do the following (number 5 below):
5. Add the 1 Hz data (each bin) between 8 and 15 km to a 'summing' array for each channel. Increment a ' lower counter'.
6. If you have been doing this for t minutes, where t is read in from the constants file (default value: t=10), and at least 50 percent of the expected number of seconds have been summed (based on the 'upper counter'), then do the following:
    a. compute the average 532 signal from H$_1$ to H$_2$ km for the entire 't' minute segment. Call this P2(532) from the sum generated in step 3 above.
    b. If the 'lower counter' exceeds 50 percent of the expected number of seconds, then perform c,d, and e below. Otherwise, set P1(532) and P1(1064) to invalid and skip c,d and e. This effectively means that clouds have made calculations impossible at the lower height.
    c. Compute the average 532 and 1064 profiles between 15 and 8 km from the summing array produced in steps 4 and 5 above.
    d. Find the height of the minimum in the 532 average profile between 8 and 15 km call this hmin – this is the lower calibration height
    e. Compute the average of the data between hmin+D and hmin-D km for both the 532 and 1064 channels, where D is in km and is read from the constants file (default = 1km). Call these P1(532) and P1(1064).
    f. Compute the average background for the segment for each channel call these B532 and B1064
    g. Output to a file: P1(532), P1(1064), P2(532), B532, B1064, hmin, D, H$_1$, H$_2$ and: the latitude, longitude and time at 'm' points along the segment, where m is a variable read from the constants file, not to exceed 30. A default value for m is 20. These points would be t/m minutes apart.

7. If after 't' minutes, less than 50 percent of the expected number of seconds have been summed (based on the 'upper counter'), then output missing values (invalid) for P1(532), P1(1064), P2(532), B532, B1064, and the other output described in 6g above.
8   Zero out summing variables, summing array and counters
9   Process next 't' minute segment in the same manner

(3.1.5) $$PC = H_{sat} - [H_{min} - H_{off\,min}] - 41km + PC_{bias}$$

A complication arises in that the data read in by GLA02 are not vertically aligned from second to second. Onboard the spacecraft, the start of data (the height above the ellipsoid of the top most bin) is calculated from equation 3.1.5. The spacecraft position (updated every second) is used to retrieve the Digital Elevation Model (DEM) value corresponding to the spacecraft location. The DEM is a 1x1 degree land surface elevation in km above the ellipsoid. H$_{min}$ - H$_{offmin}$ represents the minimum elevation for a particular grid box, and H$_{sat}$ is the height of the spacecraft above the ellipsoid from onboard GPS measurements. The subtraction of 41 km in equation 3.1.5 insures that the top of the profile for any given second will be 41 km above the minimum ground elevation for the current DEM grid box. This also means that the bottom bin of the profile will be 1 km below the

minimum elevation for the current DEM grid box (since the total lidar profile is 42 km in length). PC_{bias} can be used to shift the whole lidar profile up (when negative) or down (when positive), but will normally be zero. Because this process is happening each second, the bin that corresponds to a given height above mean sea level may change from second to second. Thus, to accomplish steps 4 and 5 above, the DEM value that was used onboard the spacecraft must be known to SAM so that it can compute the height of a given lidar bin number. Either that or simply the range from the spacecraft to the start of data. For the case where the onboard DEM value is used, $H = (548-n)*0.0768 + [H_{min} - H_{offmin}] - 1.0 - PC_{bias}$, gives the rough height in km above the ellipsoid for any bin n, where n=1 is the topmost lidar bin of the complete profile. 548 represents the total number of bins in a complete profile (as constructed in step 1 above). Thus, as an example, the bin number corresponding to H = 36 km would be: $n = 548 - ((36 + 1.0 + PC_{bias} + H_{offmin} - H_{min}) / 0.0768)$. Note that these heights are calculated with respect to the ellipsoid, which can depart as much as 200 meters from mean sea level.

The intent of this process (SAM) is produce the average signal (P'_{532}) at the two calibration heights and P'_{1064} at the lower calibration height every 't' minutes. Depending on the magnitude of 't', this will correspond to about 6 - 10 points per orbit. The file created by SAM will be read in by a 'CALibration Module' (CALM) that will produce the calibration constant for each of the segment averages output by SAM. It is suggested that CALM be a stand alone module that is run prior to GLA07. It is also possible to combine SAM and CALM together as one module. This is an implementation decision. The processing flow of the CALM module is described below:

1) Read in the output from the segment averaging utility (run after GLA02 completes). This output contains segment averages (maybe 20-30 per granule) at the two calibration heights. For each segment average, there is maybe 10-20 latitude/longitude pairs (these are the m points along the orbit segment, described in 6g above). **NOTE: If the SAM and CALM modules are combined into one module, obviously this step is skipped.**

2) For each segment that has a valid (not invalid) P1(532), P1(1064) or P2(532) do steps 3-6 below. If all 3 of these are invalid, then there is no need to perform steps 3-6, below. In this case, we set the 3 calibration values to invalid and skip to step 9 below)

3) At each lat/lon point, compute the average attenuated molecular backscatter at the two calibration heights using ATBD equations 3.2.5 and 3.2.11 (here average means a vertical average – nominally 2 km). This requires access to the MET data at that lat/lon.

4) At each lat/lon point, compute the ozone transmission from the top of the atmosphere to the calibration height (ATBD, equation 3.2.8).

5) Compute the average attenuated molecular backscatter for the segment at the two calibration heights and the average ozone transmission for the segment (average of the values calculated in steps 3 and 4).

6) Compute the calibration constant as the ratio of the segment signal average to the average attenuated molecular backscatter times the average ozone transmission (ATBD, equation 3.2.6).

7) Repeat steps 2-6 for each of the 20-30 segment averages. This will yield 20-30 of the following: C1(532) – the lower 532 calibration constant, C1(1064) – the 1064 calibration constant and C2(532) – the upper 532 calibration constant.

8) Compute mean and standard deviation of the C values in the current granule. Throw out (set to invalid) those C values that are x (default x=1) standard deviations from the mean, where x is a

variable read in from the constants file. This is done separately for each of C1(532), C1(1064) and C2(532). Call these standard deviations σ1(532). σ1(1064) and σ2(532).

9) For each segment, write out to a file the following: 1) The start and end time for the segment, 2) the 3 calibration values (532 upper and lower, and 1064 lower), 3) the standard deviations of the C values (σ1(532), σ1(1064) and σ2(532)), 4) the three segment signal averages (532 upper and lower, 1064 lower), 5) the segment average attenuated molecular backscatter at the two calibration heights, 6) the segment average ozone transmission from the top of the atmosphere to the calibration height, 7) the center height and thickness of the upper calibration zone, 8) the center height and thickness of the lower calibration zone, 9) the segment average 532 background (B532). Note that if calibration points are thrown out during step 8 above, they are still output to the file, but have the value of 'invalid'.

GLA07 will then read the output from CALM (the calibration constants spaced roughly 't' minutes apart) and will compute a calibration constant for each second. This process is discussed in section 3.2.1.1.

The cloud search will rely on a simple threshold method, where if two consecutive bins exceed the threshold, then a cloud is considered found. The cloud will be output on the GLA02 product as 'the predicted height of first cloud top'. The cloud search is not intended to be exhaustive or the most sensitive. It is only meant to provide a means of detecting the first fairly dense cloud encountered. It will probably not be capable of detecting thin cirrus. This will be done in later processing (GLA09). The cloud height thus defined will be in kilometers above the local ground surface.

The ground search begins at the end of the 1 Hz profile and works upward for a maximum of 25 bins. The signal is searched until one bin exceeds a preset threshold value. This threshold is much larger than the threshold for cloud detection and was determined through simulation to be about 25 photons per bin. Once the ground is detected, the maximum of that bin and the following 3 is stored as the 'ground return peak signal'.

3.1.1.4 Saturation Flag Profiles

The photon counting channel will at times become saturated by strong signals from very dense clouds. When this occurs, the data are no longer valid. Therefore, it is important to be able to recognize and flag this condition so that we can apply a correction in later data processing. The 532 channel saturation flag will take the form of a profile (SF(z)) and will have a one-to-one correspondence with the 532 channel return signal bins. Each bin of the 532 channel will be checked against a maximum value (L_s) above which the signal will be considered saturated. This value will be determined in the laboratory and will likely be about 80 counts per bin (or 156 photons per microsecond, prior to dead time correction). This is shown as:

$$SF(z) = 0 \quad \text{FOR} \quad S_{532}(z) < L_s N_{sum}$$
$$SF(z) = 1 \quad \text{FOR} \quad S_{532}(z) \geq L_s N_{sum}$$

where N_{sum} is the number of shots summed for a given layer (1, 8 or 40). Note that this test is done on the raw data, not the normalized signal as produced by equation 3.1.1. Thus, it should be done

first. Parameters which will be read in by the algorithm and passed through as part of the output include but are not limited to:

1. Location of waveform peak (from altimeter channel)
2. 1064 programmable gain amplifier setting (1 Hz)
3. Etalon filter settings (532 channel only)
4. Integrated 532 nm signal (P'_{532}) from 41 to 20 km

3.1.2 *Error Quantification*

In this section we will try to first identify the main sources of error in the computation of normalized lidar signal and then attempt to quantify their magnitudes. Referring to equations 3.1.1 and 3.1.2, the main sources of error stem from incorrect knowledge of the laser energy (E) and inaccurate dead time correction factors for the 532 channel, and digital to analog conversion factors for the 1064 channel. The laser energy will be estimated by splitting off a small portion of the beam and sending it to an energy measuring device. The total energy of the beam transmitted to the atmosphere is then computed from this measurement. Generally, this approach to measuring the laser energy is accurate only to about 5 percent. The other major error in computing the normalized signal is the inaccuracy of the dead time correction table. This is much harder to characterize and has the added problem of changing with time. As the photon counting detectors age, and are exposed to continuous radiation in the space environment, their response characteristics, as well as the amount of detector dark current, will change. This in turn affects the dead time correction table. It is hoped that the detector change with time can be quantified by using 'calibration targets' – places where the return signal should not change with time. Examples of this are the upper troposphere or lower stratosphere where, barring strong volcanic eruptions, known backscatter cross section with time should prevail. Additionally, certain areas of the Earth's surface (providing that the atmospheric conditions are nearly the same) should give the same ground signal independent of time. This would be true over the ocean surface or desert areas where the surface albedo does not change appreciably. It may be possible to use such 'targets' to keep track of detector changes.

Other factors affecting data quality are laser performance, boresite accuracy and, in the case of the 532 channel, how well the etalon filter is tuned to the laser frequency. We anticipate that occasionally, the laser footprint (spot on the ground) will drift from the telescope field of view. This will cause loss of signal until a boresiting procedure can be run to re-align the system (via an onboard software procedure). Likewise, signal loss will occur if the etalon filter is not tuned to the laser frequency. There should be some measure of the etalon tuning stored in the GLAS data stream, but the specifics of this are uncertain at this time. In the next section we will develop a set of confidence flags which are intended to provide a measure of data quality.

3.1.3 Confidence Flags

Confidence flags are meant to give an indication of data quality and our confidence that the data are at a level where all science objectives can be met. As mentioned above, there will be circumstances where the caliber of the data is reduced due to a variety of causes. A useful measure of the data quality can be obtained in a number of ways. The simplest and most straightforward is to integrate the entire signal from 20 km to the end of the profile and compute the

average signal and standard deviation. The average and standard deviation should fall within known limits if the data are good. Another approach is to develop a histogram of the lidar return. If the signal were pure background noise, the photon counting signal (532 channel only) would tend to follow a Poisson distribution. Thus, the degree to which the histogram deviates from a Poisson distribution would tell us something about how much signal is contained in the return. For instance, if the system were totally out of boresite, then the lidar would receive only background, which should closely follow a Poisson distribution. If the system were in boresite, the histogram should deviate from the Poisson distribution, depending on how much cloud or aerosol signal were contained therein. One problem with this approach is that if the atmosphere is totally clean (devoid of cloud or aerosol), then the only signal contained in the return would be from the molecular return and the ground signal. The histogram in this case may not deviate much from the Poisson distribution.

Other ideas for quality flags are discussed in section 4.1.4.

3.2 Attenuated Backscatter Cross Section (GLA07)

3.2.1 Theoretical Description

3.2.1.1 Overview of Processing

The attenuated backscatter cross section falls easily from the normalized lidar signal developed in section 3.1. Essentially, the only computation required to obtain the attenuated backscatter is the calculation of the lidar calibration constant (C). The calibration constant can be approximately obtained from first principles (equations 2.2 and 2.3), but in practice it is much easier and in the long run more accurate, to obtain C from the data itself, provided sufficient signal is available. This approach is beneficial because it overcomes the problems associated with instrument drift and is self-regulating. Our simulations indicate that the 532 photon counting channel will have adequate signal for the computation of C from the data itself, but it is unlikely that we may do so with the 1064 channel. We have therefore decided to use the laboratory calculation of C for the 1064 channel, but will calculate C from the lidar data itself for the 532 channel. Even so, the calibration processing routines (SAM and CALM, discussed in section 3.1.1.3) are structured to compute the 1064 calibration constant from the data, but it will most likely not be used in the computation of calibrated attenuated backscatter unless we can verify its integrity in post processing.

Recall that what we called 'calibration pre-processing' (see the descriptions of SAM and CALM in section 3.1.1.3) computes the calibration constant at points 't' minutes apart along the orbit. This is a change implemented in version 4.1 of the ATBD. The first thing which GLA07 must do (prior to any other processing) is to read the file output by CALM and compute the calibration constant which will be used for each second of the current granule. This process is envisioned as being a subroutine that is called once by GLA07 at the very beginning of its processing for a given granule. For ease of discussion, we will call this the calibration fitting module (CFM). The function of the CFM routine is simply to read in the output of CALM (C values) for the current granule and the C values within 1 hour prior to the start of the current granule and apply some type of fitting procedure to the points to obtain a C value for each second of the current granule. These values are then used by GLA07 to compute the attenuated, calibrated backscatter as per equations 3.2.12 and 3.2.13. The following steps summarize the procedure:

1.) Read in the output from the CALibration Module (CALM).
2.) Based on the value of a flag (0/1, meaning no/yes), eliminate all C values (532 nm upper and lower and 1064) with corresponding 532 nm background values greater than a threshold value (default = 2 photons/bin). Both the flag and the threshold value are read in from the constants file.
3.) Compute the ratio of the 532 nm calibration constant computed at the lower calibration height (about 10 km) to the 532 nm C value computed at the upper height for all points in the granule. If this ratio is less than 1.0 – x, or if this ratio is greater than 1.0 + x, then eliminate (throw out) the corresponding 1064 C value. Where x is read in from the constants file and has a default value of 0.10. Note that when the 532 nm C value at the lower calibration height is missing (invalid), then the value used for it in computing the ratio will be zero.
4.) Read in the C values that are within 1 hour prior to the start of the current granule. We now have x upper 532 nm Calibration points, y lower 532 calibration points and z 1064 calibration points.

Based on the value of a flag variable (0,1,2,3), which is read in from the constants file, the code then does the following:

Flag=0: Granule mean
5.) Compute a mean of the x upper 532 calibration values and the z 1064 calibration values and use the mean for the whole granule.
Flag=1: Granule mean
6.) Compute a mean of the y lower 532 calibration values and the z 1064 calibration values and use the mean for the whole granule.
Flag=2: Running smoother
7.) Using the x upper 532 calibration points, and the z 1064 calibration points compute an m point running average. Linearly interpolate between smoothed points to obtain the calibration constant for each second. The number of points to use in the running smoother (m) is read in from the constants file. A default value for m is 3.
Flag=3: Running smoother
8.) Using the y lower 532 calibration points, and the z 1064 calibration points compute an m point running average. Linearly interpolate between smoothed points to obtain the calibration constant for each second. The number of points to use in the running smoother (m) is read in from the constants file. A default value for m is 3.

Note that there will be a default calibration value for the 1064 channel that will be read in from the constants file. If this number is negative, then the software will use the calculated value of the 1064 calibration constant. If this default calibration value read in from the constants file is positive, then use it for the computation of 1064 calibrated backscatter, ie. do not use the calculated value. No such default mechanism is planned for the 532 channel.

Next, GLA07 will compute the calibrated attenuated backscatter (β') for both channels at 5 Hz and 40 Hz, and correct the 532 channel β' for times when it became saturated. Another important function that GLA07 will perform is the vertical alignment of the data so that each bin is referenced to height above mean sea level. The data acquired by GLAS (as well as the data output from

GLA02) range in height from 41 to –1 km for the 532 channel and 20 to –1 km for the 1064 channel. This height is with respect to the height above the local topography at the sub-satellite point. This is based on a DEM onboard the spacecraft which can have different values for each second of lidar data as discussed in section 3.1.1.3. The equations which are evaluated onboard the spacecraft each second to calculate the 532 nm channel (PC) and the 1064 channel (CD) range gates at which to start taking data are:

$$PC = H_{sat} - [H_{min} - H_{off\,min}] + PC_{bias}$$

$$CD = H_{sat} - [H_{min} - H_{off\,min}] + CD_{bias}$$

where H_{sat} is the height of the spacecraft (from the onboard GPS which is referenced to the ellipsoid), H_{min} is the DEM minimum, H_{offmin} is the offset associated with H_{min} and Pc_{bias} and Cd_{bias} are the offsets to apply to the 532 and 1064 channels, respectively. H_{offmin} is set to a default of 1.125 km. The PC and CD biases will usually be –41 km, but can be used to move the profile either up (when made less than –41 km) or down (when made greater than –41 km). These will only be changed (from –41 km) for off-nadir pointing. The PC and CD values effectively represent the distance from the spacecraft to the top of the data. In the figure below, this range is denoted as R_0. These equations are evaluated in real time aboard the spacecraft and the results are sent down in the telemetry data. Note that the only difference between the two equations is the bias term, which can be different for each channel. Also note that even though the cloud digitizer board begins taking data at the same height (41 km above the local DEM value) as the photon counting channel (assuming PC_{bias} = CD_{bias}), the flight software will only send down in the telemetry those 1064 nm data beginning 268 bins from this point (20.58 km).

16
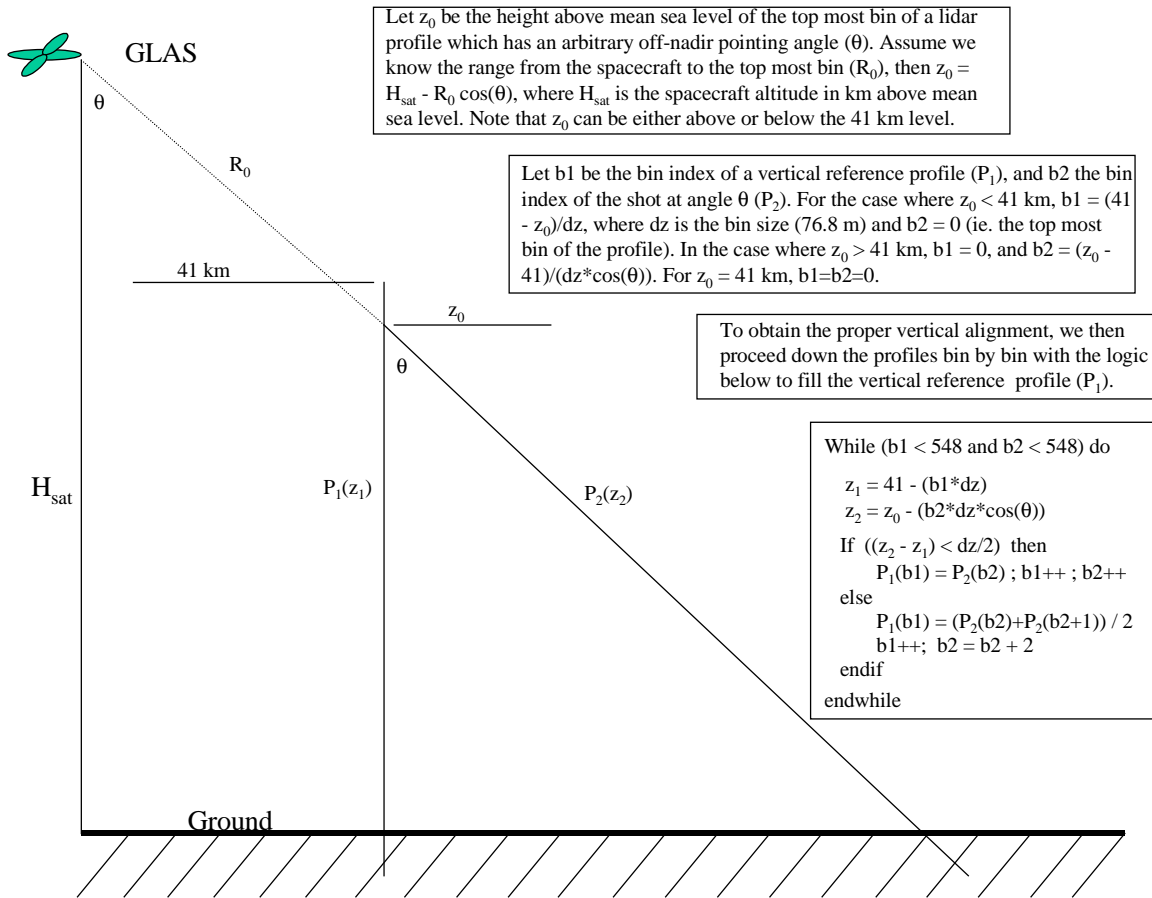
Figure 3.2.1 The logic and algorithm that will be used to correct for vertical errors introduced by off-nadir pointing, which may at times approach 25 degrees, and the correction to account for the vertical shifting of profiles from second to second as described in the text.

Referring to figure 3.2.1, this means that the range from the spacecraft to the top most bin of the lidar profile (R_0) can potentially change from second to second, especially over areas of varying terrain. Thus, the same lidar bin number can correspond to different heights above mean sea level from second to second. The data will have to be shifted in the vertical to account for this. GLA07 must know the altitude of the spacecraft and the range from the spacecraft to the top bin of the lidar profile. Another factor that must be considered for the GLA07 processing is the pointing angle of the laser beam. Normally, GLAS will be pointing very close to nadir, with pointing angles less than 3 degrees. In this case, the effect of the pointing angle on the vertical position of the lidar return bins can be neglected. There will, however, be times when the pointing angle exceeds 3 degrees and may (very infrequently) be as high as 25 degrees. The effect of pointing off nadir is to cause the vertical distance covered by a lidar range bin to decrease by the cosine of the pointing angle. If this effect is neglected for larger off-nadir pointing angles, it will cause a misalignment of the bins in the vertical. We will therefor take the pointing angle into account when we vertically align the data and place it in a coordinate frame referenced to mean sea level.

A solution to the vertical alignment and angle correction problem is shown in the figure above. It is a simple algorithm and can be applied to all the data, regardless of the pointing angle. Referring to figure 3.2.1, most of the time z_0 will be above 41 km, as this corresponds to the situation for land elevations greater than zero. Over mountainous regions and high plateaus, z_0 can be considerably higher than 41 km. Over mount Everest, for example, z_0 will be about 50 km. In these cases, the portion of the lidar profile (P_2) above 41 km is discarded and the bottom portion of the vertical reference profile (P_1 in the figure) is padded with a missing value. This latter point is not a concern as the bins to be padded are all below the ground surface (assuming of course that we have accurate values of A_s and R_0, and that the spacecraft timing circuitry has done its job properly!) For the cases where z_0 is less than 41 km, which should not happen very often (these would correspond to places where the topography is below sea level, or the times of appreciable off-nadir pointing), the top portion of the reference profile is padded with molecular backscatter data and the end bins of the lidar shot (P_2 in the figure) will be discarded (as they may be below –1km, depending on the pointing angle).

3.2.1.2 Calculation of the Lidar Calibration Constant

Since the signal return which is used in the computation of C is from purely molecular scattering, and the atmospheric density at these altitudes is very low, the return signal is very weak. Therefore, one must first integrate the return signal through a layer 2 kilometers thick centered on the calibration height and then average over a sufficient time span to insure adequate signal to noise for the computation of C. Based on simulations and theoretical considerations, we believe that averaging the data for 10 to 20 minutes should provide ample signal to compute C (at least for the 532 channel). What we do not know is how stable C will be and whether it will change noticeably over an orbit. In theory, if all components of the lidar system are stable, then the value of C should not change. Of course in the real world, electrical and optical components that comprise this complex instrument do change their characteristics with time (theoretically, the 1064 calibration should be more stable than for the 532 channel). This is something that we will not know until after launch. Our approach used here is to calculate C continuously along the orbit using segments of data 10 minutes in length. There is reason to believe that the nighttime calculation would be more accurate and stable (because of the lack of background signal), however we will not know this for sure until we can analyze a time series of C values. Thus, in addition to calculating and storing C as part of GLA07, it is desirable to flag each C value as being calculated during night, day or indeterminate. This can easily be done by looking at the background during the time that C is being calculated. Recall that the average background for the calibration segment was output in the calibration pre-processing file output by GLA02 (section 3.1.1.3). Based on the magnitude of the background, we will classify each calibration as being produced from nighttime or daytime data. If the average background value for a given segment is greater than about 5 photons per microsecond, then it can be safely assumed that it is daytime. A background less than 1 photon per microsecond would indicate nighttime conditions and in between would be labeled indeterminate. Suggested values for the flag are –1 = night, 0 = indeterminate, and 1 = day.

As noted above, there may be considerable error in the calculation of C (from the atmosphere) for the 1064 channel. If this occurs and it is found that the laboratory calculation of C is not accurate, then we do have a backup plan for the computation of C for the 1064 channel. However, because of its complexity, it can not be implemented in the GLA07 processing. It would have to be done as special offline processing by the science team. In this event, the data would have to be re-

processed (GLA07 re-run) with the new, correct value of the 1064 calibration constant. Without specifying details, the procedure involves using calibrated 532 channel cloud returns to calibrate the 1064 channel. In theory, there is a range of backscatter cross section where the 532 channel is not in saturation, but the 1064 channel will produce a substantial signal above the 1064 noise floor. If the 532 cross section is known, then the 1064 cross section can be computed (or at least estimated) if the type of cloud producing the scattering is known. We anticipate using cirrus clouds for this, identifying them by their height and scattering characteristics.

A requirement for the calculation of C is a knowledge of the average molecular backscatter cross section through the calibration layer and the transmission (including ozone for the 532 channel) from the top of the atmosphere to the calibration height. The molecular backscatter cross section will be needed in other GLAS processing modules in the form of profiles with the same vertical resolution as the lidar data (76.8 m). Thus, they will be computed in GLA07 as complete profiles from 41 km altitude to the surface with a 76.8 vertical resolution. This requires knowing the atmospheric temperature and pressure at a vertical resolution of 76.8 meters (the lidar bin size). The pressure, temperature and relative humidity along the flight track will be calculated from the ancillary MET data which will be available to the GLAS ground processing system or from standard atmosphere tables (in the case of the 30 km calibration height). The MET data are reported at standard pressure levels which include temperature, relative humidity and the geopotential height. The geopotential height must first be converted to the equivalent geometric height and then the pressure (P(z)), temperature (T(z)) and relative humidity (R(z)) calculated for the bins (heights) between the standard pressure levels. This is accomplished with the hypsometric formula. From the calculated temperature and pressure profile, the molecular number density (N(z)) is calculated from the ideal gas law as:

(3.2.1) $$N(z) = P(z)/(kT_v(z))$$

where N(z) is in units of molecules per cubic centimeter, k is the Boltzmann constant for dry air in units of ergs per degree per molecule, P is the atmospheric pressure in units of ergs per cm^2, and T_v is the virtual temperature in degrees Kelvin. This equation is very similar to the equation to compute atmospheric density ($\rho(z)$), which is the same as 3.2.1 except that the Boltzmann constant is replaced by the ideal gas constant for dry air (R), which has a value of 0.0028769 m^2 s^{-2} $°K^{-1}$. Note that the I-SIPS code must compute $\rho(z)$ because it is needed for the computation of ozone transmission, in equation 3.2.7. The effect of moisture on atmospheric density is included through the use of the virtual temperature in equation 3.2.1, but these effects are generally negligible above the lower troposphere. T_v is computed from the relative humidity (obtained from the MET data) by first converting it to water vapor mixing ratio. To accomplish this, we need to first compute the saturation vapor pressure (e_s) which is a function of the atmospheric temperature (T) as:

(3.2.2) $$e_s = 0.6112e^{17.67T/(T-29.66)}$$

and from that compute the saturation mixing ratio (q_s):

(3.2.3) $$q_s = 0.622e_s/(P/10.0)$$

where P is the atmospheric pressure in millibars. The relative humidity is simply the actual atmospheric water vapor mixing ratio divided by the saturation mixing ratio times 100. Thus, the actual atmospheric water vapor mixing ratio is given by $q = rq_s/100.0$ where r is the relative humidity. And finally, the formula to compute the virtual temperature (T_v) is:

(3.2.4)
$$T_v = \frac{T}{1.0 - 3q/5}$$

Following Measures (1984), from the atmospheric molecular number profile, the molecular backscatter cross section ($\beta_m(z,\lambda)$) in units of $m^{-1}sr^{-1}$ is then:

(3.2.5)
$$\beta_m(z,\lambda) = 5.450N(z)(550.0/\lambda)^4 10^{-26}$$

where λ is the wavelength in nanometers (532 or 1064 nm in our case). The computation of the calibration constant then is:

(3.2.6)
$$C_\lambda = \overline{P'_\lambda(z_c)}/(\overline{\beta_m(z_c,\lambda)}T^2(\lambda))$$

where $\overline{P'_\lambda(z_c)}$ and $\overline{\beta(z_c,\lambda)}$

are the horizontal average (through the calibration latitude band) of the vertically integrated normalized lidar signal (output from GLA02) and molecular backscatter through the 2 km thick calibration layer, respectively. The length of the horizontal average will most likely be between 1/8 and ¼ of an orbit and is defined as input to GLA02. In equation 3.2.6, $T^2(\lambda)$ represents the two-way path transmission from the top of the atmosphere to the calibration height and is composed of Rayleigh and ozone components as: $T^2(\lambda) = T^2_m(\lambda)T^2_o(\lambda)$. In this discussion, we are assuming no .absorption due to aerosols. The ozone absorption is negligible at 1064 nm, but is large enough to consider for the 532 channel. The ozone transmission, $T^2_o(\lambda,z)$, is calculated using ozone mixing ratios obtained from a climatology provided by G. Labow (NASA-GSFC Code 916, unpublished data). The ozone mixing ratios (kg/kg) are obtained from lookup tables. The lookup tables will be grouped together into 10 degree latitude bands and month of year. The ozone profiles are gridded at the standard GLAS altitude resolution, with the first bin at 59.9796 km, stepping down by 0.0768 km to the last bin at number 795.

The ozone mass mixing ratios, $r_o(z)$, are first converted to column density per kilometer (atm-cm/km), $\varepsilon_o(z)$, using the following equation,

3.2.7
$$\varepsilon_o(z) = \frac{r_o(z)\rho_s(z)}{2.14148 \times 10^{-5}}$$

where z is the altitude in km, and $\rho_s(z)$ is the atmospheric density at z (obtained using the MET data already calculated). The next step is to calculate the ozone transmission term. $T^2_o(\lambda,z)$ is calculated using the following equation,

3.2.8
$$T^2o(\lambda,z) = \exp\left| -2 \bullet c_O(\lambda) \int_{glas-altitude}^{z} \varepsilon_o(z')\,dz' \right|$$

where $c_O(\lambda)$ is the Chappius ozone absorption coefficient in cm^{-1}. The ozone absorption coefficient is obtained at the correct wavelength from a table compiled in *Iqbal* [1984] using data from *Vigroux* [1953]. $c_O(\lambda)$ is 0.065 cm^{-1} at 532 nm and is zero at 1064 nm.

The $r_O(z)$ lookup table for the 0° to 10° N latitude band is displayed in Figure 3.2.2. Ozone column density profiles, $\varepsilon_O(z)$, were estimated for the month of July over both the equator and the south pole using standard density profiles [*McClatchey et al.*, 1971] and $r_O(z)$ from the lookup tables. The results are shown in Figure 3.2.3.
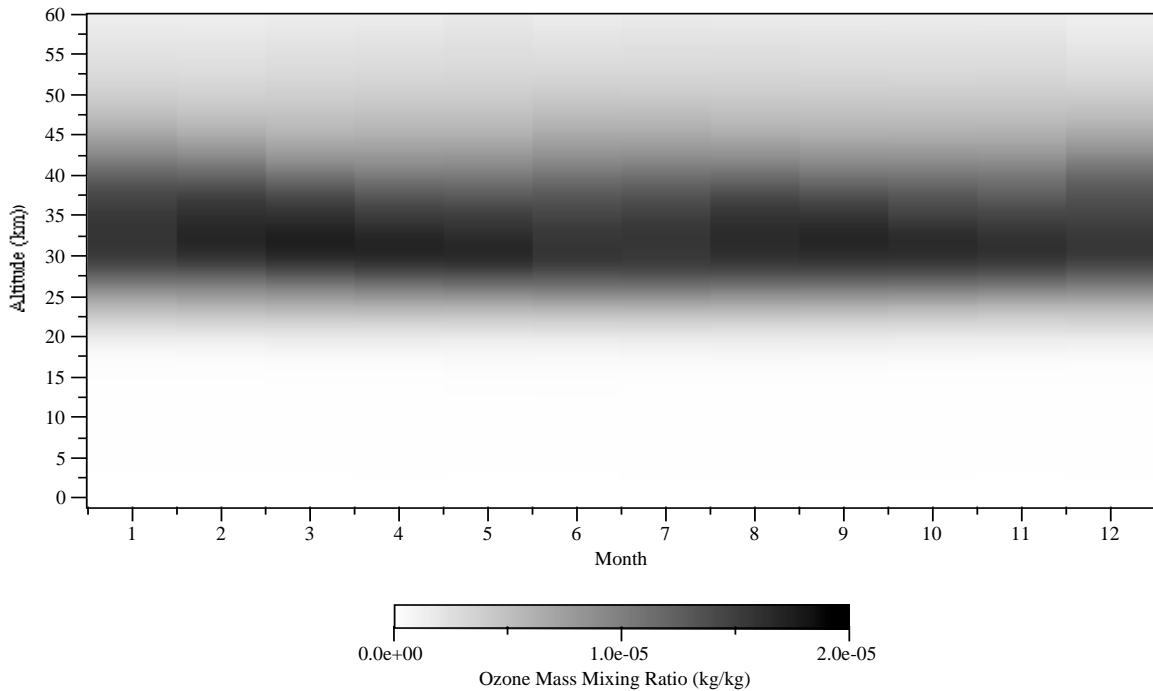
Figure 3.2.2 An example of the ozone mixing ratio as a function of altitude and month for the 0 to 10 degree north latitude band
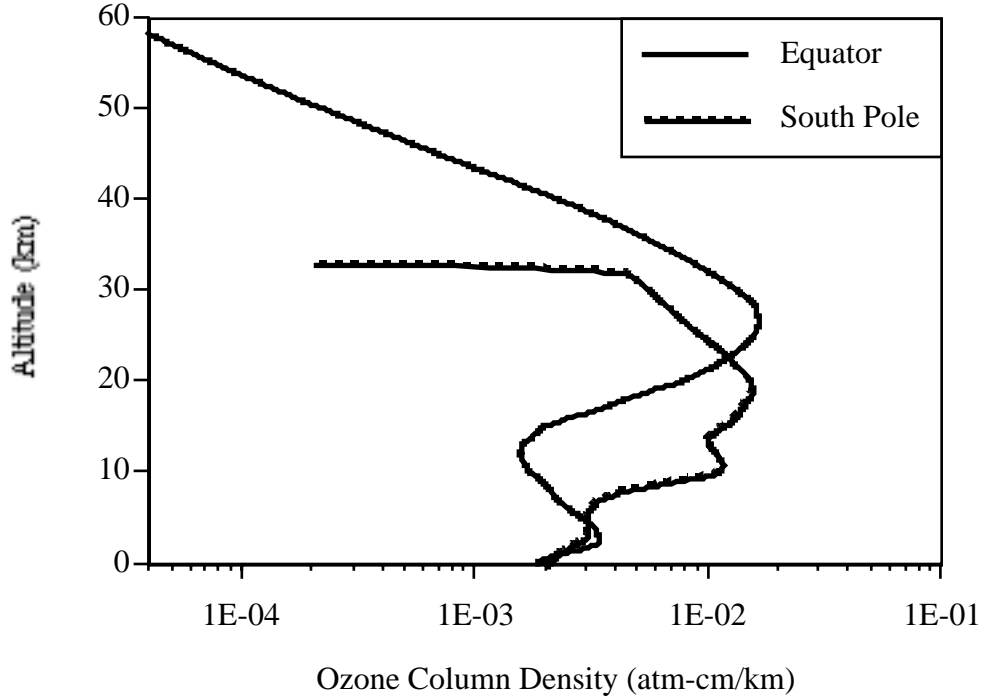
Figure 3.2.3 Ozone column density computed from equations 3.2.7 for the equator and south pole.

To calculate the molecular transmission, we first compute the molecular extinction profile ($\sigma_m(z,\lambda)$), by multiplying the molecular backscatter cross section by the molecular extinction to backscatter ratio, which is known theoretically to be $8\pi/3$.

$$(3.2.9) \qquad \sigma_m(z, \lambda) = 8\pi\beta_m(z, \lambda)/3$$

The molecular optical thickness from the top of the profile (ztop) to height z is equal to the integral of the molecular extinction profile as shown in equation 3.2.10.

$$(3.2.10) \qquad \tau_m(z, \lambda) = \int_{ztop}^{z} \sigma_m(z, \lambda)dz$$

and finally, the two-way molecular transmission (T^2_m) between ztop and any height z is:

$$(3.2.11) \qquad T_m^2(z, \lambda) = e^{-2\tau_m(z,\lambda)}$$

For the atmosphere, $T^2_m(z,\lambda)$ is very close to one for altitudes above 15 km, especially at 1064 nm (see figure 3.2.4). At 9 km, the two-way molecular transmission is about 0.95 at 532 nm and 0.99 at 1064 nm. Thus, we can assume that the two-way transmission is unity for the 1064 channel at the lower calibration height, but we must use the value of 0.95 for the 532 channel. Deviations from a purely molecular atmosphere (from aerosol above the calibration height) will lead to error in the assumed value of the two-way path transmission and thus to error in the calculated calibration constant (see section 3.2.2).

Transmission Profiles,Molecular
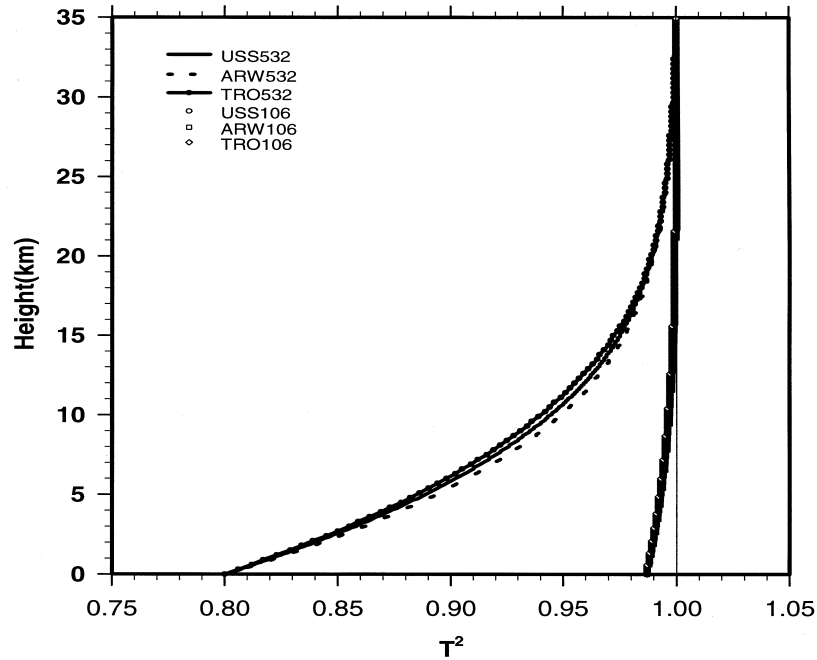
Figure 3.2.4. The two-way molecular transmission at 532 nm (left set of curves) and 1064 nm for various standard atmospheres.

In the actual implementation of the GLAS data processing system, profiles of attenuated molecular backscatter (the denominator in equation 3.2.5) will be generated on a continuous basis based on either interpolated MET data or standard atmosphere tables which correspond to the spacecraft location (i.e. tropics, mid-latitude, arctic, etc). As an example, figure 3.2.5 shows the attenuated molecular backscatter profiles (not including ozone absorption) for US Standard, Arctic-winter and Tropical atmospheres.

Molecular Attenuated Backscatter Coefficients
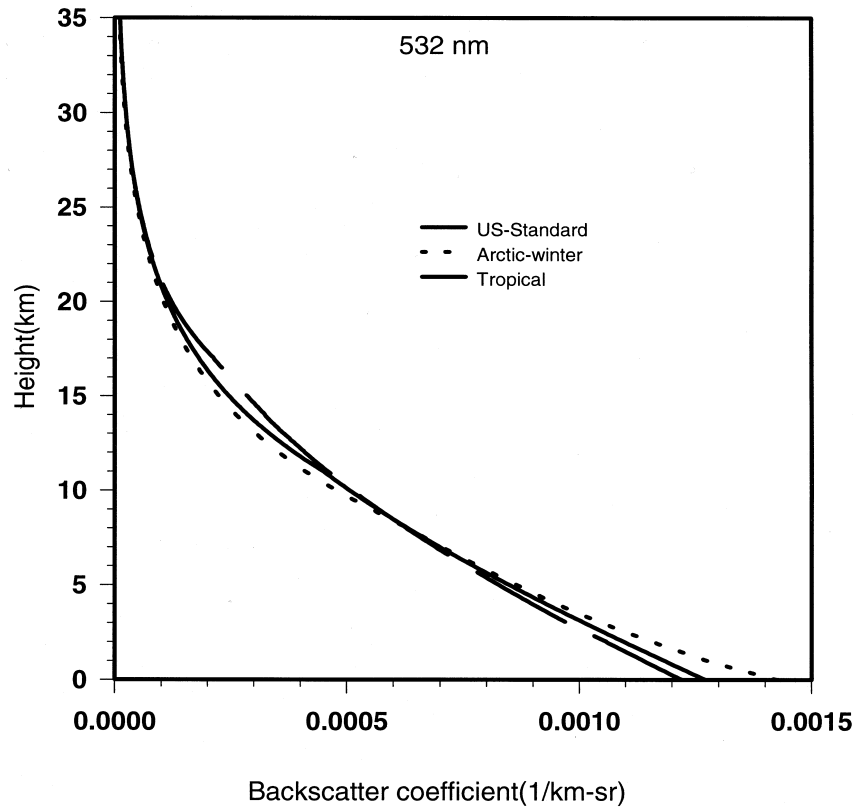
Figure 3.2.5. Profiles of the attenuated molecular backscatter cross section ($\beta_m T^2_m$) at 532 nm for three standard atmospheres. Note that the tropical atmosphere curve is denoted by the long dashed curve.

After we have computed the calibration constant at all of the points (about 8-10) along the orbit that were defined by the GLA02 processing, the next step is to define a calibration constant to use for each second. Two approaches are suggested here, but after we gain experience with the data, we might alter the method. For now, we will 1) calculate the average of all the calibration constants available for the current granule and use that one value for the entire granule or 2) linearly interpolate between points to obtain a unique calibration constant for each second of the granule. Note: the length of a granule for GLA02 and GLA07 is assumed to be *two* orbits. The value of a flag will determine which of the methods is used. Calflag = 1 means to linearly interpolate, and Calflag = 0 means to use the average calibration value.

Once the calibration constant is calculated, it must be applied to the data to obtain the calibrated, attenuated backscatter cross section ($\beta'_{532}(z)$ and $\beta'_{1064}(z)$) for the two channels as:

(3.2.12) $\qquad B'_{532}(z) = P'_{532}(z) / (C_{532} T^2_o(532, z)) \qquad\qquad FOR \quad SF(z) = 0$

$$(3.2.13) \qquad \beta'_{1064}(z) = P'_{1064}(z) / C_{1064}$$

Note that the ozone transmission in equation 3.2.12 is from the top of the atmosphere to height z. This is different than the ozone transmission used in equation 3.2.6, which is the ozone transmission from the top of the atmosphere to the calibration height (z_c). Note also that equation 3.2.12 is used only if the saturation flag (SF(z)) is zero, meaning that the 532 photon counting channel was not saturated (as determined in GLA02). If the data were saturated, then we estimate the 532 backscatter from the calibrated 1064 backscatter. While this procedure can give us a useable estimate of the 532 backscatter, it is not entirely accurate because the magnitude of the scaling depends on the scattering phase function of the scattering medium which is not known. However, a reasonably good approximation for the 532 cross section is to simply use the 1064 backscatter cross section as in 3.2.14. This approximation can be considered accurate to within 10 percent for both ice and water clouds. Note that the 532 channel will be saturated most frequently from water clouds which tend to have larger scattering cross sections than ice (cirrus) clouds. Theoretical simulations indicate that the 532 channel will not saturate from most naturally occurring aerosol plumes, but may saturate from dense smoke from large scale (biomass burning) fires.

$$(3.2.14) \qquad B'_{532}(z) = B'_{1064}(z) \qquad FOR \quad SF(z) > 0$$

The implicit assumption here is that we have correctly calibrated 1064 data and that multiple scattering (in the 1064 signal) is relatively small. The 1064 channel, with its much wider field of view, is much more prone to multiple scattering than the 532 channel. It is mainly the multiple scattering that limits the accuracy of 3.2.14. *We also want to implement in the code a flag which dictates whether or not this substitution (3.2.14) is to take place. If the flag is set to indicate that this is not to occur, then the 532 channel data is not replaced, but it left intact.*

The intended output product for GLA07 consists of 5 Hz full profiles of $\beta'_{532}(z)$ from –1 to 41 km and 40 Hz profiles from –1 to 10 km. The former requires averaging 8 shots from the lowest layer and the duplication of 8 profiles from the upper layer to form one continuous profile from 41 to –1 km. For the 1064 channel, the output will consist of 5 Hz profiles of $\beta'_{1064}(z)$ from –1 to 20 km and 40 Hz profiles from –1 to 10 km, again requiring the averaging of 8 profiles from the lowest layer to form the entire 20 km profile.

Output from GLA07 will include the saturation flag profiles (SF(z)) for the 532 channel output as 5 Hz full profiles from –1 to 40 km and 40 Hz profiles from –1 to 10 km. Since the former requires averaging of the lowest layer, SF(z) should be set to 1 (indicating saturation) if any of the 8 shots that make up the average was saturated. A detailed list of additional data output by GLA07 is listed in section 4.2.3.

3.2.2 Error Quantification

Here we try to identify the major sources of error in the calculation of calibrated attenuated backscatter. This essentially boils down to identifying the major source and magnitude of error in the calculation of C. For the 532 channel, C is computed from the atmospheric scattering at specific heights (Equation 3.2.3). The error in 3.2.3 comes from two major sources. The first is the assumption of a purely molecular atmosphere in calculating the two-way transmission from the top

of the atmosphere to the calibration height ($T^2(z_c)$). At the 35 km height this is ok, but the lower one goes, the higher the probability that some aerosol will be present. Normally, this is small since most of the aerosol is confined below 10 km. However, during episodic volcanic eruptions, a significant amount of aerosol can be injected into the lower stratosphere. Thus, the magnitude of this error will vary in space and time and is difficult to quantify. However, in most situations, this error will be negligible at the 35 km calibration height, and less than 5 percent for a 9 km calibration height. Further, at the lower calibration height, it will be necessary to identify and eliminate the occurrence of clouds in the data segment that is used to calculate C. While it is easy to find and eliminate dense clouds, it will be difficult to locate very thin cirrus or aerosol layers.

Another problem that can occur in the calculation of C is the error involved in computing the molecular backscatter cross section ($\beta_m(z_c,\lambda)$) at the calibration height. For instance, if the temperature and pressure used to compute $\beta_m(z_c,\lambda)$ were in error by 2 and 10 percent respectively (4.5 °K and 1.1 mb), then the molecular backscatter cross section would be in error by 10 percent. Thus, this error is likely to be of greater magnitude than the transmission error discussed above. A good way to quantify this is to plot β_m for various standard atmosphere models. Figure 3.2.5 shows a plot of the 532 nm molecular attenuated backscatter profile for the arctic winter atmosphere (solid line) and the tropical atmosphere, normalized by the molecular profile for the U.S. standard atmosphere. This shows that at about 16 km, β_m calculated from the standard atmosphere can differ as much as 18 percent from the β_m calculated from the tropical atmosphere model. Essentially, this is illustrating the effect that differences in temperature and pressure have on the magnitude of β_m. For most cases, we think that the accuracy of the MET data used to compute β_m will limit this error to within about 5 percent.

Ratios of Attenuated Backscatter Coefficient

Molecular, 532 nm
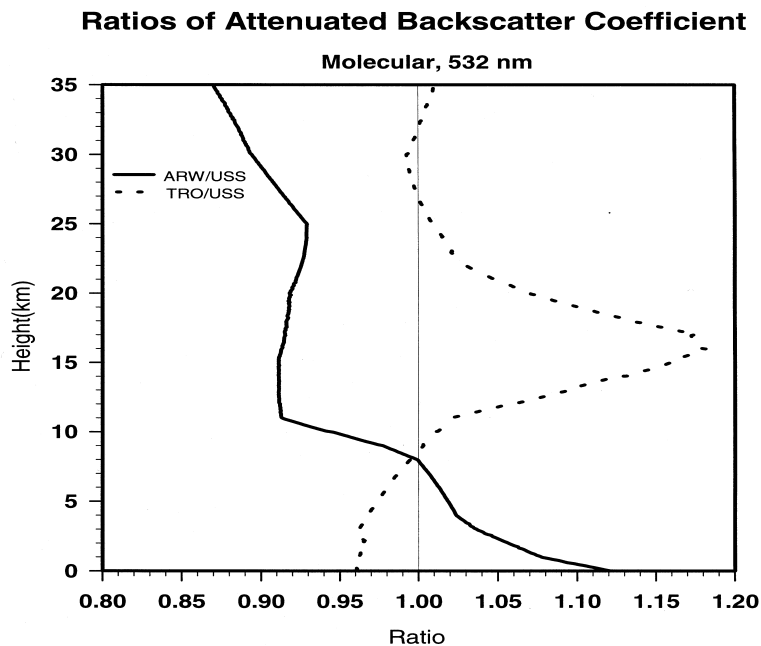
Figure 3.2.5. Ratio of the molecular backscatter profile computed from Arctic winter (solid) and tropical (dashed) atmosphere to the molecular profile computed from the U.S. standard atmosphere.

3.2.3　Confidence Flags

Confidence flags for GLA07 will include a measure of the variability of the calibration constant (for both channels) as a function of time as well as an objective measure of the quality of the attenuated backscatter profile. See section 4.2.4 for a full discussion.

3.3　Particle Layer Height and Earth's Surface Height (GLA09)

3.3.1　Theoretical Description

3.3.1.1 Cloud and Aerosol Layers Height

This section will present a description of the algorithms and techniques, designated GLA09, that will be used to find the locations of particulate layers. In GLA09, the GLAS atmospheric channel signal will be used to locate the vertical positions of horizontal surfaces of both cloud layers and aerosol layers. A generalized technique will be applied initially to locate boundaries of layers of both paritculate categories. Then, each detected layer will be determined to be cloud or aerosol using an objective discrimination algorithm. Those layers classified as aerosol will be compared to layers found using the GLA08 algorithm. Inconsistencies between the results of GLA08 and GLA09 will be resolved and a final determination of cloud or aerosol will be made for each layer.

A description of the algorithm to find the location of the earth's surface from the lidar return (ground signal) will also be given.

Cloud particles are those atmospheric constituents that are composed primarily of H_2O and that are formed by condensation of atmospheric water vapor around condensation nuclei. Cloud particles form in volumes where relative humidity is at or above 100%. Cloud particles can be either liquid or ice and both phases can exist together. Cloud particles can condense or evaporate quickly as a result of the surronding environment. Liquid droplets can exist in a supercooled state. Clouds are aggregations of these particles. The aggregations typically have a layered structure, as in stratus, or a towering structure, as with cumulus. The two types can exist together and often a cloud has characteristics of both structures. A given location may be cloud free, clear, or be occupied by one or more types of clouds. Often, the combination of cloud types is quite complicated. Liquid water droplets are approximately spherical in shape. The shapes of ice particles are controlled by the effects of temperature, humidity, and local dynamics upon the crystalline structure. Cloud particle sizes usually extend over a particle size spectrum.

We define aerosols as any particulate matter suspended in the atmosphere that is not considered to be cloud. The chemical composition of aerosols is quite varied. Sulfate, nitrate, salt, sand, smoke, and dust particles are common aerosol particles. Base aerosol particles tend to have a relatively long residence time compared to clouds since they are not the product of a change of phase of H_2O. Base aerosol particles can be hygroscopic in which case they can serve as cloud particle condensation nuclei. Aerosols exist in volumes where relative humidity ranges from 0% to 100%. In general, aerosol particle size spectrums have a smaller average size than cloud size spectrums. Aerosol and cloud particles coexist and often the distinction between the two is arbitrary.

The distinction between cloud and aerosol layers based upon lidar backscatter signals alone is quite problematic. Generalized lidar signal characteristics will be assigned to each category as a means to separate them in an objective scheme. It is expected that the categorization determination will be improved as experience is gained in analzing space borne lidar data. For our purposes, we consider the layer structure to consist of a specific number of layers at any location. Each of these layers is a region of particles defined by a top boundary and a lower boundary. The lower boundary of a fog layer or a planetary boundary layer is the surface of the earth. A boundary exists where the density of particles exceeds an arbitrary threshold, which serves to define clear air. A region between top and bottom boundaries of a layer contains cloud or aerosol particles that could have either homogeneous or inhomogeneous characteristics.

Because of the additive nature of scattering, cloud or aerosol atmospheric regions have greater volumetric backscatter coefficients than clear regions. In clear regions, radiative scattering stems entirely from air molecules; it is referred to as Rayleigh scattering. When particles are present, scattering is increased above Rayleigh scattering values. It is this enhancement in the scattering of photons in the lidar pulse that provides a signal that can be used to delineate particle layers in a lidar profile. Since absorption by water at the GLAS lidar wavelengths is negligible, the backscatter coefficient in particle rich regions always exceeds the Rayleigh backscatter coefficient. Because of this, a vertical profile of Rayleigh backscatter coefficient could be established as a baseline threshold to distinguish particle regions in a profile. This would be convenient since the profile can be readily computed when the air density is known. However, attenuation of the lidar pulse by intervening layers reduces the lidar backscatter signal from any given volume. Therefore, the Rayleigh backscatter coefficient profile can serve as only an upper limit of threshold.

Figure 3.3.1a) provides a conceptual view of a representative lidar profile of attenuated backscatter coefficient together with a profile of Rayleigh backscatter. The profile was fabricated by applying the basic lidar equation to an arbitrarily specified atmosphere and using the GLAS lidar system specifications to characterize the measured signal. Cloud boundaries are clearly evident from a visual inspection of the lidar profile. One's perception of the profile is such that the signals above and below a layer provide a threshold against which the protrusion of the cloud signal is compared. Even where the cloud density increases gradually, such as in the cirrus layer at about 8-km, the boundary can be discerned to within one or two sample elements. A profile characteristic that masks a weak cloud boundary is the random noise superimposed upon the basic signal. The signal from the second layer (from the top of the profile) of cirrus is diminished because of the attenuation of the first. The signal from the stratus layer at 1 km is very much lessened by attenuation. Also, notice how the (lidar) molecular signal is diminished by attenuation in the region between 8.0 and 10.5 km and below 6.0 km. Despite reduction of the signal due to noise and attenuation, the locations of cloud layers are evident. The task of an objective algorithm is to mimic what is perceived by eye. Figure 3.3.1 b) shows a simulated profile that has a layer with typical aerosol scattering characteristics between 14 km and 16 km.

An examination of cloud signatures in lidar profiles summarized above leads us to the assertion that an algorithm to find cloud boundaries in lidar profiles should use localized segments of small signal as a baseline in testing for cloud signals. By using the profile itself, rather than a threshold based upon some a priori determination, we can bypass the complications that arise from the many different atmospheric and background conditions that will be encountered by GLAS. Also, the

threshold can be made to be a function of altitude, which permits using values that are more attuned to the different types of cloud and aerosol layers at various heights. Such an algorithm can be designed to be an approximation of the results that would be attained from a visual inspection of a profile.

A positive attribute of an algorithm whose threshold is derived from the profile is that it can be implemented with very efficient computer code. The techniques required to find localized minimums are elementary. Only a small amount of coding is required and the solutions can be computed quite quickly. This will permit cloud boundaries to be found operationally at the highest resolution produced by the lidar. The following presents a detailed description of the algorithm
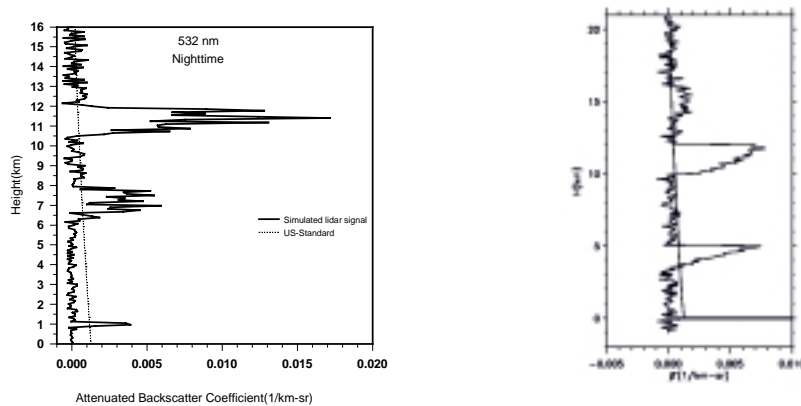
Figure 3.3.1. a) Simulated GLAS profile in a cloudy atmosphere. Two cirrus layers and one stratus are present. The optical depths are from top to bottom 0.5, 1.0, and 1.5; b) simulated profile that includes a layer with stratospheric aerosol scattering optical properties between 14 km and 16 km.

Cloud and aerosol layer boundaries will be found at four time resolutions. These are, from coarsest to finest, 0.25 Hz, 1 Hz, 5 Hz, and 40 Hz. To do this, the GLAS time series will be divided into a sequence of independent 4-second segments. These segments will be subdivided into four 1 second segments. Each of these will be divided into 5 segments and these will be divided into 8 segments, which will occur at the basic GLAS 40 Hz. frequency. Profiles of attenuated backscatter coefficients will be produced at 40 Hz and 5 Hz by GLA07 and serve as input into the cloud boundary algorithm. The 1 Hz and 0.25 Hz profiles will be produced by averaging the higher frequency data.

Boundary search operations will be applied to 0.25 Hz profiles first. Results at finer resolutions will be made only in vertical regions where layers were detected at a coarser resolution first. The reason for this procedure is that the smaller signal to noise characteristic at higher resolutions will tend to obscure any layers not detected at lower resolutions. This technique will fail to detect some cloud layers that are composed of horizontally sparse and rarefied patches. But such layers are presumed to be insignificant for climatological studies.

The basic layer boundary search technique will be the same for each of the four resolutions. Since the 0.25 Hz resolution profiles will be those first searched for the presence of cloud layers, we will focus first on those in our description of the search algorithm. The finer resolutions will use the results of coarse resolution searches to eliminate portions found to be cloud free.

Four one second attenuated backscatter coefficient profiles will be averaged together to produce a four-second averaged profile. A discussion of the potential difficulty caused by varying ground height among the four one second profiles will be given in a later section. The profile will be divided into a small number of segments. The optimum number will be found by applying the technique to simulated and proxy data sets to determine the means to obtain the best results. The number will likely be in the range of five to ten. The objective is that each segment has some samples that are in particle free portions of the profiles. A characteristic signal from particle free segments can reasonably serve as a layer signal threshold. In general, it will not be known, a priori, whether a segment has layer free samples. The difficulty is that rarefied layers are not easily discerned in a noisy profile. Each of the segments will be searched for its minimum value. Also, in order to characterize better each segment, the mean and variance of the sample values will be computed for each. In the cases where a segment has particle free regions, the minimum values will represent the attenuated signal from atmospheric molecules with negative random noise excursions superimposed. These will thus represent the absolute minimum that any layer-distinguishing threshold could be in each of the segments. A reasonable maximum threshold would be the computed molecular backscatter coefficient. Together, these values represent a range of values that could serve as layer signal threshold. To employ the molecular backscatter coefficient profile as the maximum threshhold value, a truncated lidar signal profile will generated. This profile will have the molecular profile as the upper limit of its value at any height.

To find an optimum threshold value within the threshold envelope, it is necessary to find a measure of random noise because the lower limit boundary of threshold values is strongly influenced by the magnitude of random noise. This magnitude can be represented by the standard deviation of the lidar signal in a layer-free profile segment. Based upon our experience, we can assert that the atmosphere is, in general, free from non-molecular, strong-scattering species in the 18-19 km layer. Therefore, the noise of the lidar signal there stems mostly from the molecular scattering signal and the background energy. The variance of the truncated lidar signal from this high region will be used as a measure of the random noise contained in the lidar signal.

Once a typical molecular signal variance has been computed, layer signal thresholds can be computed for each of the profile segments. In each segment, the threshold will be the sum of the minimum and a constant fraction of the square root of the variance. In some cases, the sum would exceed the computed molecular signal The value of the fraction will be determined from GLAS signal modeling studies but it will likely have a value in the range of 0.25-0.5. A profile of layer signal threshold will be then constructed by piecemeal, linear interpolation of the segment values. The interpolation would be done at GLAS vertical resolution. The interpolated profile will serve as a layer signal baseline upon which the presence of layer signals will be tested.

The threshold profile described above will have the following positive attributes: 1) threshold values will be computed from the profile itself and will automatically adjust to the current situation; 2) the threshold computed at given level will be influenced by the attenuation of the lidar signal by higher layers; 3) the technique will be valid for any time resolution. A negative attribute is that the

statistical nature of the computation of variance introduces some uncertainty into any particular result.

Once the profile of layer signal thresholds is established for a lidar signal, the layer boundaries are sought in the following manner. Starting at the top of the profile, the lidar profile is tested on a sample by sample basis. If a value is found to exceed the threshold, it is deemed a potential layer sample. If a specified number of potential consecutive layer samples are found, the segment is designated a layered region. The top of the layer is located at the height where the highest of the consecutive samples was found. The high-to-low testing continues under the stipulation that the profile is in a layered segment. The layer designation continues until several consecutive samples are found to be less than the layer threshold. In that situation, the profile is considered to be in a layer free region. The bottom of the layer is the point where the first of the consecutive particle-free values was found. The testing continues downward for the top of another layer. The profile will be so analyzed for layers to the DEM based location of the earth's surface.

The layer boundary analysis for a 0.25 Hz profile will be used as the basis for the equivalent analysis of the four 1 Hz profiles that it encompasses. The layers at which 1 Hz layer boundaries will be produced will be limited to those vertical intervals where layers are detected at 0.25 Hz. The reason for this design is that averaging to produce 0.25Hz profiles will result in samples with a large signal to noise characteristic, which will make it least likely to result in the fewest cases of incorrectly identifying layers. The 1 Hz data will have a smaller signal to noise ratio value. Limiting the results of the 1 Hz search to the layers as 0.25 Hz will minimize false layer results at 1 Hz. For practical reasons, the search for layers at 1 Hz will use entire 0-20 km profiles, but the layered regions found will be limited to those found at 0.25 Hz. The implication of these limitations is that any layers which are not substantial enough to produce a detectable signal at 0.25Hz are not considered to be significant at finer resolutions.

The results of the search for layers from 5 Hz. profiles will be limited by the results from the 1 Hz profiles in a manner equivalent to the limitations imposed upon 1 Hz by 0.25 Hz. The same search algorithm will be applied from 0-20 km but the resulting detected layers will have to be among the layers detected at 1 Hz. or they will be discarded in the output. The situation for 40 H. will be slightly different to accommodate to relatively small signal to noise at that frequency. Layer detection at 40 Hz will be limited to regions where one or more layers were detected in the 5 Hz profiles. If one or more layers are found in a 40 Hz profile, only the lowest one will be recorded. This procedure will allow detection of low cloud layers that typically have strong lidar signals and that have horizontal distributions that vary at relatively high frequencies.

There are difficulties that arise from the variable ground height that may exist along the distance interval over which the average profiles will be produced. GLAS will produce vertical profiles that will use the local DEM value as the reference and lower boundary. The DEM values will be updated every 1 second and so four DEM values will be used in the construction of the 20, 5 Hz profiles which will be used to produce a 0.25 Hz profile. For purposes of layer boundary detection, the value of the highest DEM boundary used within the 4-second interval will be considered the lowest altitude at which to search the profile for layers. Also, since the one-second period of the DEM updates will probably not be synchronized with the 1 Hz lidar profiles, the higher of the two DEM values spanned by the duration of the profile will be used as the lower boundary for the

search. Individual 5Hz and 40 Hz profiles will be contained within a single DEM interval, so this overlap problem will not exist.

A very important characteristic of downward looking lidar must be noted. As the laser pulse travels through the atmosphere, the scattering processes diminish its energy. In the case of a relatively small cumulative optical depth, the reflection of the pulse from the earth's surface has enough energy to be detected. If the cumulative optical thickness of the scatterers is large enough, the lidar signal will be reduced to the background level regardless of the magnitude of backscatter coefficients and no ground signal will be detected. No bottom boundary can be detected. Thus, when no return signal is detected from the earth's surface, the height of the bottom of the lowest layer is, in general, an invalid value with no relationship to the actual location. If a ground signal is detected, the uncertainty in the location of the bottom of the lowest layer increases as the ground signal's strength decreases.

3.3.1.2   *Objective Layer Disrimination Procedure*

The cloud and aerosol layer boundary detection algorithm will find top and bottoms of layers of both categories of particles. In order to assign a type to a layer, it will be necessary to test it to determine how well it matches characteristics ascribed to each category. A scoring of the testing will indicate the likelihood that a layer is either cloud or aerosol. It will be possible to categorize most layers with much confidence. However, some layers will have characteristics of both categories and the classification of these will be much less certain. In this section, we summarize the characteristics of each category and indicate the tests that will be done to discriminate between cloud and aerosol layers.

Table 3.3.1 lists layer attributes that can be detected with a lidar signal. Under the particle-type categories of cloud and aerosol is an indication of the relative values expected for each category.

	Aerosol	**Cloud**
Signal Magnitude(top)	**Smaller**	**Larger**
Signal Gradient(top)	**Smaller**	**Larger**
Altitude(top)	**Lower**	**Higher**
Horizontal Extent	**Wide spread**	**More localized**
Horizontal Uniformity	**More uniform**	**Less uniform**
Vertical Extent	**Larger**	**Smaller**
Vertical Uniformity	**More uniform**	**Less uniform**
Relative Humidity	**Lower**	**Higher**
Attenuation	**Lower**	**Higher**

Table 3.3.1. Comparative attributes of aerosol and cloud layers.

Each attribute is listed and briefly discussed below.
 a) Signal magnitude: The average and maximum signals in an aerosol layer tend to be less in an aerosol layers compared to cloud layers Cloud layers that have signal magnitudes of the same order as aerosol layers are typically cirrus layers that will be much higher in the troposphere than aerosol layers.
 b) Signal gradient at layer top: The top boundary of aerosol layers will tend to be less distinct. than tops of cloud layers.

c) Altitude: Cloud layers with small lidar signal characteristics will tend to be higher in the troposphere than aerosol layers

d) Horizontal extent: Elevated aerosol layers will tend cover larger areas. This is a weak distinquishing characteristic.

e) Horizontal uniformity: Elevated aerosol layers will tend to be more well mixed and therefore more uniform that cloud layers.

f) Vertical extent: Elevated aerosol layers will tend to have a larger detectable vertical extent than cloud layers at the altitude at which they are found.

g) Vertical uniformity: Elevated aerosol layers will be more uniform vertically.

h) Relative humidity: Measured relative humidities approaching 100% are necessary for the presence of a cloud layer. Elevated aerosol layers can exist at much lower relative humidites.

i) Attenuation: The vertical region where elevated aerosol layers exist is the lower troposphere. The clouds in this region generally have a volumetric backscatter cross section that is much larger than aerosol layers. Consequently, the optical depth of cloud layers will tend to be much higher than aerosol layers.

The actual values used for the discriminating criteria presented above will be determined from modeling studies and from studies of atmospheric lidar data taken by the NASA ER-2/CLS and other high altidude and ground based lidars. In general, low level layers that display weak and uniform lidar signal strength characteristics in a low relative humidity environment will be classified as aerosol layers. Most other layers will be considered cloud layers.

An example of the contrasting characteristics of cloud and aerosol layers is depicted in Figs. 3.3.2a and 3.3.3b. Table 3.3.2 shows results of rough computations of the discriminating criteria discussed above.
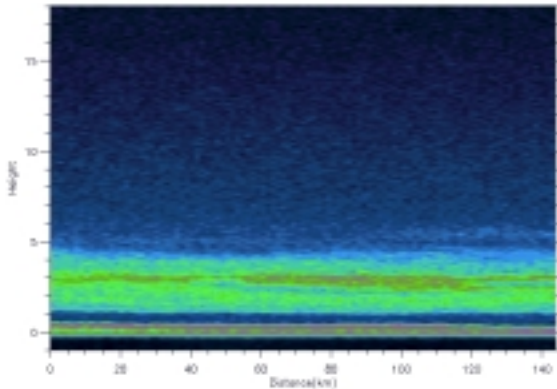
Figure 3.3.2 a) Satellite lidar signal cross-section showing a representative elevated aerosol layer.
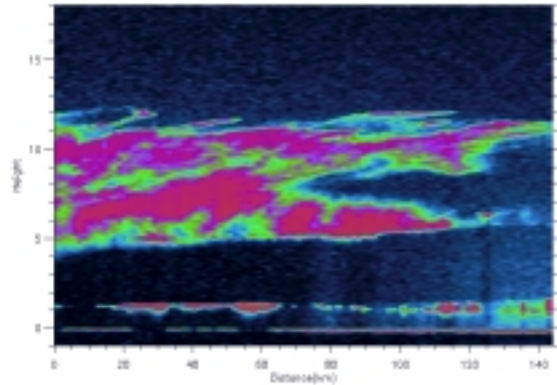
Figure 3.3.2 b) Satellite lidar signal cross-section showing a representative cirrus layer.

	Aerosol	Cloud
Signal Magnitude(top)	2.1×10^{-6}/m-sr	3.0×10^{-6}/m-sr
Signal Gradient(top)	-7.5×10^{-7}/m-sr/km	-1.5×10^{-6}/m-sr/km
Altitude(top)	~5 km	~11 km
Horizontal Extent	N/A	N/A
Horizontal Homogenity	0.25-0.35	0.2-1.0
Vertical Extent	~4 km	~6 km
Vertical Homogenity	0.12-0.30	0.4.0.8
Relative Humidity	~35%	>75%
Attenuation	0.3	0.6

Table 3.3.2. Computed discrimination criteria parameters for the aerosol
and cirrus layers shown in Figures 3.3.3 a) and b).

In an operational environment, difficulties in quantifying horizontal extent, horizontal homogenity, vertical extent, vertical homgenity, relative humidity, and attenuation probably precludes using these characteristics to distinquish between cloud and aerosol layers. Therefore, only the signal magnitude, signal gradient, and altitude of the top of each layer will be used in the layer discrimination procedure. The following description gives the details of the discrimination technique.

The discrimination algorithm is based upon thresholding process where the value of a single parameter serves to distinquish between the two categories of scatterers. For any paramater, there will likely exist a range of values that could indicate either cloud or aerosol. Therefore, it is reasonable to use a measured value of the parameter to find the probability that the layer belongs one of the categories, for instance, clouds . The arbitrary value of the parameter also determines the probability that a layer belonging to the other category, aerosols, is falsely assigned to the cloud category. The optimum value for the parameter is that which maximizes the probability that a cloud layer will be correctly identified while minimizing the probability that an aerosol layer is identified as a cloud. In this procedure, a correct selection of a layer as a cloud is considered a true positive and an incorrect selection of an aerosol layer as a cloud is a false positive.

The discrimination algorithm will be implemented in the following manner. The cloud detection algorithm will be applied to 0.25Hz data. Each detected layer will be assigned to an altitude category based upon the height of the top of the layer. For each layer, a parameter composed of the product of the layer's maximum signal and maximum vertical gradient magnitude will be computed. This product will serve as a discriminator for cloud and aerosol layers. Cloud layers will tend to have a significantly higher value. The value of the product will be compared to a threshold value previously determined for each altitude category. If the product exceeds the threshold, then the layer will be deemed a cloud layer. Otherwise, the layer is deemed an aerosol layer. The value of the threshold is arbitrary. It will be set at the lowest point where the probability of true positive of cloud designations is considered high enough when balanced against the probability of false designation of an aerosol as a cloud. All of the layers at higher frequencies associated with a layer designated cloud or aerosol will be considered to belong to the same category. Therefore, the cloud-aerosol discrimination will need to be applied only to 0.25 Hz data. The altiude category and discriminator threshold values will be stored in a table that will be read when the program is initialized. The values will be determined from statistical studies of existing ground-based and

airborne-based lidar system databases. The following diagram depicts the logical flow of the algorithm.

```
┌─────────────────────┐          ┌─────────────────────────────┐
│      0.25 Hz        │─────────▶│  Use cloud top to categorize │◀──┐
│   Detect Cloud      │          │        cloud altitude        │   │
└─────────────────────┘          └─────────────────────────────┘   │
                                              │                     │
                                              ▼                     │
┌─────────────────────┐          ┌─────────────────────────────┐   │
│      Compute         │◀─────────│ Compute maximum signal β'ₓ   │   │
│ P = β'ₓ x |(Δβ'/Δz)|ₓ │          │ Compute maximum vertical     │   │
│                      │          │  gradient magnitude |(Δβ'/Δz)|ₓ│  │
└─────────────────────┘          └─────────────────────────────┘   │
           │                                                        │
           ▼                                                        │
        ╱╲        YES                                               │
      ╱      ╲    ──────▶  ┌─────────────────┐                      │
     ╱ P > thr ╲           │   Deemed cloud  │                      │
     ╲ eshold  ╱           └─────────────────┘                      │
      ╲      ╱                      │                                │
        ╲╱                          ▼                                │
         │ NO              ┌─────────────────┐                       │
         ▼                 │ Set probability │                       │
┌─────────────────┐        │      flag       │                       │
│  Deemed aerosol │───────▶└─────────────────┘                       │
└─────────────────┘                 │                                │
                                    ▼                                │
┌─────────────────────┐    NO     ╱╲            YES                  │
│ Layer search at     │◀────────╱      ╲  ────────────────────────────┘
│ 1Hz, 5Hz, 40 Hz     │         ╲ Another╱
└─────────────────────┘          ╲ layer╱
                                   ╲╱
```

Layer discrimination algorithm

Below the flow chart, the boxes read:

- 0.25 Hz Detect Cloud
- Use cloud top to categorize cloud altitude
- Compute $P = \beta'_x \ \times \ |(\Delta\beta'/\Delta z)|_x$
- Compute maximum signal β'_x; Compute maximum vertical gradient magnitude $|(\Delta\beta'/\Delta z)|_x$
- $P > \text{threshold}$ — **YES** → Deemed cloud; **NO** → Deemed aerosol
- Set probability flag
- Another layer — **NO** → Layer search at 1Hz, 5Hz, 40 Hz; **YES** → (return to Use cloud top to categorize cloud altitude)

3.3.1.3 Corrections for false positive and certain false negative results

Random noise flucuations will result in layers being detected where no clouds and aerosol layers actually exist. False positive results of this type generally have the three distinguishing characteristics: 1) they have a very small vertical extent; 2) they have small horizontal extent; 3) they have a small total integrated signal. In order to minimize false positive results, the following tests will be incorporated into the algorithms at each testing resolution. The vertical depth of a layer will be compared to a minimum value. If the thickness is less than the minimum, the integrated

vertical signal will be computed and compared to a minimum. If the integrated signal falls below the minimum, the result will be considered negative. For 1Hz, 5 Hz, and 40 Hz resolutions, a test will be made for the existence of the layer in adjacent profiles. If the thin layer exists in less than a mimimum number of profiles, the result will be considered negative.

It is possible for the threshold method to fail to detect vertically thin but optically dense layers. These types of layers would result in a large lidar signal in a number of vertical samples less than the minimum necessary to be classified a layer. In such cases, no ground signal would be detected. Stratocumulus clouds could give such a signal. To detect such layers, an additional search of the signal profile will be made each time no ground signal is found. Starting at just above DEM level, the signal profile will be tested for large values. When a value is found to exceed a certain minimum, which will be much larger than the threshhold values, a cloud layer, which has a vertical thickness less than the threshhold algorithm minimum, will be put at that height

The values of the parameters used in these tests will be determined from modeling studies and from actual data as it becomes available.

3.3.1.4 Remedy for Day/Night Bias

Reflected solar energy is the source of two major components of total lidar signals from sunlit regions. These are constant offset signals, which are usually referred to as background, and random noise fluctuations, which are measured by the square root of the variance (root mean square, RMS) of random noise superposed upon the profile. Both components increase as the strength of reflected energy increases. The background component of a GLAS signal profile will be determined by averaging the signal in the portion of the profile where no laser signal is present (the background region of a profile). The background signal will be subtracted from the total to leave only the laser signal and random noise to comprise the total signal.

Our methodology to determine layer boundaries is based upon constructing a layer signal threshold profile where the value of the threshold is strongly dependent on the RMS value of signal random noise. A larger RMS value will lead to larger threshold values. As indicated above, the magnitude of the RMS noise will be larger, in general, during daylight observations than those in taken in darkness. The resultant threshold values become larger. This results in the layer detection technique being less sensitive to a given, small layer signal during daylight observations than during night observations. Layers with a certain level of weak signal will be detected in night observations but not in day observations. A day-night layer detection bias is the result of this procedure. Such a bias would hamper certain types of layer studies.

A solution to the day-night bias is to determine a threshold profile that is diurnally invariant and use this profile for all layer detection operations. A constant threshold profile would eliminate the differences caused by changing RMS magnitude of random noise. But, in order to eliminate false layer detection during daylight observations, such a threshold profile would have values that are greater than necessary for dark observations. For nighttime application, the method would be less sensitive than what is possible. Significant cloud and aerosol layers that could be resolved would go undetected.

In order to give both complete and unbiased layer boundary results, the GLAS algorithm will be applied twice. One application will use a threshold profile based upon the observed RMS noise of the backscatter profile (as discussed in section 3.3.1.1). The second application of the algorithm will use a threshold profile based upon a diurnally invariant threshold profile. The procedure is as follows. The boundary algorithm will be applied exactly as described in prior sections. This algorithm employs a threshold profile that uses the RMS magnitude of the profile noise as one of its components. Detection of cloud and aerosol layers in this manner will be the most sensitive for a given situation. Layer locations will be found and recorded at each of the temporal resolutions (0.25Hz to 40 Hz). After this operation is completed, the algorithm will be reapplied, this time using a threshold profile that incorporates an invariant noise component. The lidar signal will be compared to the threshold only in portions of the profile where layers were detected using the variable threshold profile. If the presence of a layer is indicated during this testing, it will be recorded in a true/false variable but its top and bottom boundaries will not be re-computed. This application will proceed through each of the resolutions. The result of the dual application of the layer boundary algorithm will be: a) a set of layer boundaries at each of the temporal resolutions, determined with the variable threshold profile; b) a set of corresponding true/false flags indicating whether each of the layers was detected using the diurnally invariant threshold profile.

Determination of the invariant RMS noise component will require appropriate GLAS simulation studies. A threshold profile must yield results where few significant layers are missed and where few false positive results occur. A trade-off between these two competing requirements always exists in finding a threshold. Modeling studies will permit the final determination of the threshold to be based upon the expected performance of the GLAS lidar and will permit an estimate to be made of the sensitivity and tolerance of the algorithm.

3.3.1.5 Polar Stratospheric Clouds (PSCs)

Polar stratospheric clouds are layers of particles that occur in Polar regions during winter seasons at the respective poles. These layers reside in the stratosphere from 15 to 30 km in altitude. The layers are composed of particles of various chemical compositions. These layers are more properly classified as aerosol layers than as H_2O cloud layers. They can reside above the cloud and aerosol -layer boundary algorithm upper limit (20km). Any PSC found as part of the layer detection algorithm will be classified an aerosol layer. They will be analyzed as part of the aerosol detection algorithm (see section 3.4.1.2).

3.3.1.6 Bottom of Lowest Layer

A short discussion concerning the ambiguity in the altitude of the bottom of the lowest detected cloud layer is given in the final paragraph in section 3.3.1.1. Two additional assertions can be made concerning this. First, if the ground signal is not detected, the bottom of the lowest detected layer is not determinable and additional layers may exist below the last layer. Second, the uncertainty in the location of the tops and bottoms of each detected layer increases as the cumulative optical thickness from the spacecraft increases. These uncertainties will be evaluated and quantified with the appropriate modeling and empirical studies of the expected GLAS signal.

3.3.1.8 Earth's Surface Height

The detection of the earth's surface (GLAS ground signal) presents a problem very similar to that of detection of layer boundaries. In fact, the algorithm is simplified because only one surface is to be found. Also, because the timing of the GLAS laser is synchronized with a 1 degree DEM of the earth's surface, the algorithm will have an approximate location available and the search can be limited to a small interval surrounding that height.

The characteristics of the ground signal in a GLAS profile are affected by the time resolution of the profile. Since the profile samples are much larger than the length of the laser pulse, the ground signal will be contained in only one or two samples at 40Hz resolution. However, the effective ground signal can broaden when more than one laser pulse is used to generate a profile. This broadening is caused by the variability of ground location over the horizontal extent that is used to generate the profile. If the terrain is rugged, the broadening would extend over 10 or more pixels for a 0.25 Hz profile, which would lead to a significant ambiguity in the meaning of ground location. Thus, a modified definition of ground signal is required of low resolution profiles.

Random noise can mask the ground signal. This is especially true for higher frequency profiles where signal attenuation reduces the pulse strength. This effect is generally less important when multiple shots are used to produce a profile.

The competition between higher precision results from high frequency profiles and higher reliability from lower frequency profiles leads to compromise algorithm design where the 5 Hz profiles will be used as the primary ground-location analysis frequency. The 5 Hz results will be averaged to produce ground locations at 1 Hz and 0.25 Hz. In addition, the location of the 40 Hz ground signal will be limited to an elevation interval close to that found for the encompassing 5 Hz profile.

The search for ground signal in a 5 Hz profile will proceed as follows. Since the GLAS laser is timed so that the final 13 samples of a profile occur after the level of the DEM elevation, the initial guess for the height of the earth's surface is at the 13th sample from the end of the profile. In such a case, the signal in the final 12-13 samples would be purely background with random noise superimposed. This permits a ground signal threshold to be computed from the signal in this segment. To do this, the mean, median, maximum, minimum, and variance of the final 20 samples will be computed. A threshold will be computed by adding the median and the square root of the variance multiplied by a factor that is a function of the current conditions. The value of the factor will be determined from simulation and proxy-data studies, which will reveal the optimum value to use in different circumstances. The values of the samples, beginning with the latest and proceeding to the earliest (bottom to top), will then be compared to the threshold. If a single value or several non-consecutive values exceed the threshold by a relatively large amount (perhaps three standard deviations for instance) then the earliest (lowest height) of these will be considered the ground signal. Otherwise, if there are one or more occurrences of one or two-only consecutive samples that exceed the threshold, then the lowest of these will be considered the ground signal. The higher sample of any ground signal pair will be selected as the ground signal. If no such results are found, then the ground signal will be considered undetectable for the profile. Once all of the 5 Hz ground signals within a 1 Hz or 0.25 Hz averaging segment are found, the detected ground signal heights of the 5Hz results will be averaged to produce the ground height for each of the lower frequencies.

Finally, this same ground signal detection algorithm will be applied to each of the 40 Hz profiles. The parameters that are derived from modeling studies will have different values than those for 5 Hz. The low signal to noise will result in a higher rate of falsely detecting ground signal.

3.3.2   Error Quantification

Multiple scattering is a potential source of large error in determining the boundaries of layers and the earth's surface from a space-borne lidar. The multiple-scattering process causes secondary photons to take deviated paths back to the lidar receiver where they are combined with the single-scattered signal of later samples. This causes the later sample to appear to have a larger signal than that based upon the density of the scatterers A possible result of this is that a layer's lower boundary is analyzed to be at a lower altitude than it actually is. Fortunately, the vertical resolution of the boundary analysis is, at best, 76 .8 m. Our experience with spaceborne lidar indicates that the multiple scattering effect is significant, at this resolution, only in dense low clouds. Since these clouds usually fully extinguish the laser pulse, no ground signal would be detected and the lower boundaries of these clouds would be unknown. Because of this, it is not expected that multiple scattering will have a significant effect on the quality of the results of the boundary algorithm for most clouds.

The quality of the results of a layer layer boundary algorithm can be divided into two components: a) true or false determination of the existence of layers; b) precisely locating the top and bottom of layers. Errors in component a), designated false positive or false negative, lead to inaccurate qualitative description of the atmospheric situation. Errors in the second component lead to imprecise computations of the optical and radiative parameters affected by layers.

Errors in the determination of layer boundaries from lidar profiles are largely controlled by the signal to noise ratios of small signals. The crucial objective of the boundary algorithm is to find a threshold small enough to detect signals from rarefied layers but large enough to reject random noise as layers. A large percentage of layers could be detected simply by using a single constant backscatter coefficient, based upon the computed molecular backscatter coefficient, as a threshold. If such a threshold were greater than the molecular value, the boundaries would be known to acceptable accuracy for many purposes. No false layers would result if the threshold were high enough. However, many significant rarefied, optically thin layers would be overlooked. If a threshold were too low, random noise would be often interpreted as layer signals. In both of these situations, the boundaries of identified layers would be uncertain. The occurrences of false negative results and false positive results are the competing detrimental effects in the selection of a proper threshold value.

The uncertainties associated with determination of layer boundary locations will be measured in terms of probabilities that boundary results are within specified confidence intervals. The magnitudes of these probabilities will be determined through studies of simulated profiles and proxy GLAS data. These studies will consist of application of the boundary algorithm to situations where the desired results are known. Comparison studies of the results of the output of the algorithm with the known situation will be conducted. Probabilities of deviations of the algorithm output from the truth will be computed from these studies and tabulated. Tables 2 and 3 illustrate two important types of confidence relationships that will be generated.

Probability of layer detection failure

	x1	x2	x3
T_1	P_{11}	P_{21}	P_{31}
T_2	P_{12}	P_{22}	P_{32}
T_3	P_{13}	P_{23}	P_{33}

Table 2. Probability that the GLAS layer boundary algorithm will fail to detect an actual layer. T_n represents threshold values, x_n represents the maximum backscatter coefficient in a layer and P_{mn} represents probability of failure.

Probability of layer boundary height error

	h_1	h_2	h_3
T_1	P_{11}	P_{21}	P_{31}
T_2	P_{12}	P_{22}	P_{32}
T_3	P_{13}	P_{23}	P_{33}

Table 3. Probability that an analyzed boundary height will deviate from the actual boundary height. T_n represents threshold values, Δh_m represents a magnitude of height deviation and P_{mn} represents probability of failure

Many types of relationships could be developed but those relating the layer/no layer result and the location of layer edges to selected threshold value are those that are most appropriate for the GLAS product output.

3.3.3 Confidence Flags

Based upon the studies referred to above, the following confidence parameters will be given for the layer boundary results of each profile.

a) for each layer detected: a flag to indicate a high, medium, or low confidence
b) for the top and bottom of each layer, a single number indicating a number of sample bins within which the boundary exists at a specified probability
c) for each profile, a single number representing the probability that an undetected layer exists
d) for a positive ground signal, a flag to indicate a high, medium, or low confidence
e) for a positive ground signal, the number of sample bins within which the actual ground height exists at a specified probability
f) for negative ground signal detection, a probability that a detectable ground signal actually exists but the algorithm fails to do this.

3.3.4   Sample of Results

The following figures a examples of results of the application of the layer boundary algorithm to simulated GLAS data derived from actual atmospheric conditions observed by the NASA ER-2

Cloud Lidar System. Figure 3.3.3 shows the analyzed layer heights of a single profile together with the the threshhold profile and molecular profile. Figure 3.3.4 shows an extended cross-section containing varied cloud conditions.
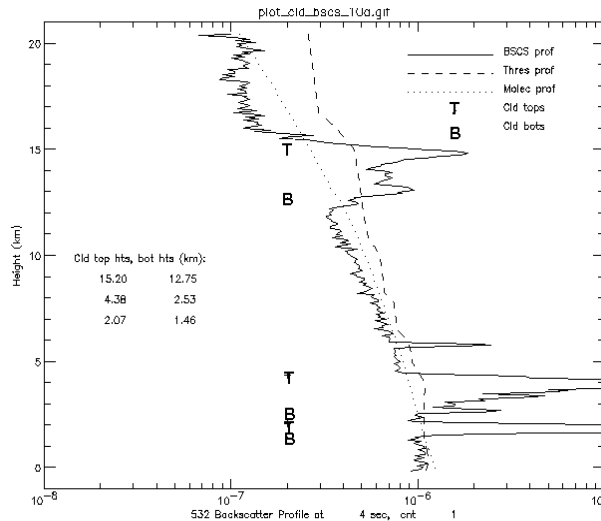
Figure 3.3.3. Simulated GLAS signal profile. Also shown are the molecular profile, the computed threshhold profile, and analyzed layer boundaries indicated with the symbols T and B.
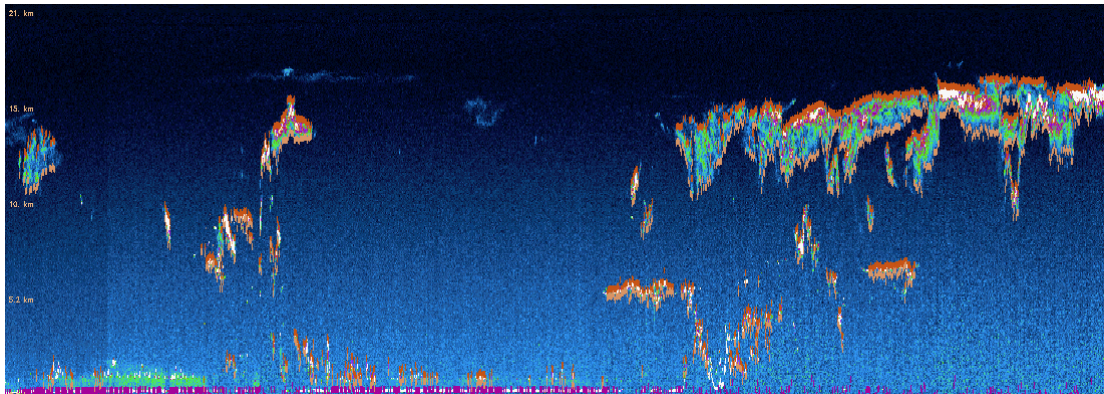
Figure 3.3.4. Analyzed layer heights on GLAS simulated data. Layer boundaries are indicated by brown symbols.

3.4   Planetary Boundary Layer and Elevated Aerosol Layer Height (GLA08)

The height of the Planetary Boundary Layer (PBL) is one of the most important parameters retrieved from the GLAS atmospheric lidar data. PBL height is related to the fluxes of heat and moisture at the surface and can be used to estimate the bulk water vapor content of the PBL (Palm et al, 1998). Because of the large aerosol gradient normally encountered at the top of the PBL, it is relatively easy to find the height of the PBL from high signal to noise (S/N) lidar data. The higher aerosol and moisture content of the PBL results in a much larger backscatter cross section, resulting in increased return signal. A strong inversion normally present at the PBL top traps the aerosol and moisture,

thereby maintaining the large gradient of moisture and aerosol at the PBL top. The ability to measure the height of the PBL with both ground based and airborne lidar is well documented. Algorithms used with both types of data basically search the lidar signal for the large gradient of aerosol scattering within certain pre-defined levels of the atmosphere. Comparison of the lidar derived PBL heights with coincident radiosonde or dropsonde data has verified the accuracy of these methods. (Boers et al, 1984, 1986; Melfi et al, 1986; Palm et al, 1998).

Airborne lidars have frequently been used to gather high resolution measurements of tropospheric clouds and PBL structure over large areas (Melfi et al, 1986; Boers et al, 1991). Most airborne lidar systems consist of relatively large and powerful lasers which fly in the lower or mid troposphere. Consequently, the signal to noise ratio is high which makes the task of retrieving PBL and aerosol layer height from the lidar data fairly easy. The Cloud and Aerosol Lidar System (CALS), developed at NASA Goddard Space Flight Center, is an exception since it flies in the lower stratosphere and utilizes a relatively low power laser. Through the analysis of data from CALS and more recently, simulated GLAS data, we have developed schemes to retrieve PBL height from data with very low S/N (Palm and Spinhirne, 1987; 1998). This technique is described in section 3.4.1.1.

Elevated aerosol layers (EAL) are not as ubiquitous as the planetary boundary layer, occurring only sporadically at various altitudes throughout the troposphere and lower stratosphere. Lidar is one of, if not the only remote sensing technique which can accurately resolve the height distribution of EALs. They are important because of their effect on the radiation balance and their contamination effect on many passive remote sensing measurements. The detection of EAL from lidar data is similar to that for the PBL height, but requires a somewhat different approach. Because of this, it will be addressed separately in section 3.4.1.2.

3.4.1 Theoretical Description

3.4.1.1 Planetary Boundary Layer

Retrieving PBL height from the GLAS data can be difficult especially if the PBL is relatively dry and aerosol free. Even under the best of conditions (optically dense PBL and after sunset) it is unlikely that the PBL top could be retrieved from GLAS data on a shot to shot basis. Averaging of lidar shots to increase S/N will undoubtedly be necessary. The degree of averaging will depend on the optical depth of the PBL and lighting conditions (background noise). Under typical conditions, we believe (based on data simulations) that the PBL top can be recovered after averaging between 5 and 10 lidar returns. GLA08 will be designed to detect the PBL height at two horizontal resolutions – high resolution (5 Hz or 8 shot average) which corresponds to 1.4 km, and low resolution (1/4 Hz or 160 shot average) which is about 30 km. There will undoubtedly be times when very little aerosol exists within the PBL, making the height determination very difficult or impossible at the high resolution. We believe that at the lower horizontal resolution, we should be able to detect the PBL top well over 90 percent of the time. There will also be times when ambiguities exist that tend to cloud the exact definition of PBL height (as defined by the lidar data). An example of this is when an elevated aerosol layer is riding directly on top of the PBL. In that case, it may be hard to discern the actual PBL top as distinct from the top of the elevated aerosol layer.

GLA08 will use the 5 Hz, 532 nm attenuated backscatter profiles which are output from GLA07 for the calculation of PBL height. The algorithm must be designed to remove bad lidar shots and spurious

noise spikes within shots. Failing to do so could result in noise spikes that are mistaken for PBL top. The filtering process can be done most efficiently by examining the quality flags that are output from GLA07.

The PBL height algorithm processes the data in roughly 150 km chunks, which corresponds to 20 seconds of data. The overall procedure is to first average 20 seconds of data to form one profile. That profile is searched below 7 km for the presence of the PBL and a ground return. If the PBL top is not found from this average profile, then it is assumed that the PBL top is not detectable for this segment of data and all the PBL heights for that time segment are set to zero. This would mean that the 100, 5 Hz (high resolution) and the 5, ¼ Hz (low resolution) PBL heights would all be set to zero. This is only expected to happen in cases where overlying clouds have attenuated the lidar beam, or in rare cases where the PBL is exceptionally devoid of aerosol. Now, there are certain criteria placed on the data within the 20 second data segment. First, if a cloud was detected for that shot (shot here means a single 5 Hz profile) via GLA09 above 5 km <u>and </u>the ground return was not detected, then that shot cannot be used in the 100 shot average. Further, if more than 50 percent of the shots fall into this category, then all the PBL heights for that segment are set to –1. If a time gap of greater than 5 seconds occurs, while forming the 20 second average, the 20 second average will have to be re-computed beginning after the time gap and all the PBL heights up to the time gap set to –2.

Assuming that a 20 second average is successfully formed and that an average PBL height is detected, the next step is to go back through the 20 seconds of data and form five, 4 second (20 shot) averages and search each for the PBL top, using the 20 second average PBL top as a guide to where to search for the low resolution top. Similarly, when a PBL top is found from the 4 second average, the 20 shots that make up that segment will be examined individually for the high resolution PBL top, using as a guide the location of the 4 second PBL top. The output from this step represents the high resolution, 5 Hz PBL height. Thus, the general idea of the algorithm is to locate the PBL top at low horizontal resolution and gradually increase the resolution in a three step process. The exact technique used to locate the PBL top at any given resolution is discussed below.

We need to identify the average ground bin (G_b) for the data segment under consideration. The position of the ground bin should not change substantially within a high resolution segment (5 Hz), but may change for a low resolution segment (4 seconds). For the 20 second average segment, the position of the ground bin could change substantially over mountainous terrain. The ground bin together with the last 20 second average PBL height in meters (H_{20}) gives us a reference from which to calculate various signal levels required by the algorithm. GLA09 will locate the ground bin from the 532 nm return signal. When available, this will be used by GLA08 for the ground bin. However, there will be times when clouds attenuate the signal and no ground return is found. In this case, a calculated value of the ground bin will be used. Next, we need to compute the average signal level within the boundary layer and above the PBL (within the troposphere). Let us call these average signals β_{pbl} and β_{trop}, respectively. We also need to find the maximum signal within the PBL. Let us denote this as β_{max}. The above filtering and averaging procedure should have eliminated all shots with no ground return and a cloud above 5 km. The reason that we do not want to eliminate all data with no ground return is that to do so would be to eliminate all cloud-capped boundary layer data. Instead, we want to eliminate all data with no ground return that was due to attenuation of the laser beam from mid and upper layer clouds, not from clouds that are associated with the PBL top.

We begin by applying a 3 point binomial filter to the attenuated backscatter data below 7 km to form a smoothed profile (β_s):

(3.4.1) $\qquad \beta_S(i) = S(1)\beta(i-1) + S(2)\beta(i) + S(3)\beta(i+1) \qquad$ for $G_b - 91 < I < G_b$

where I represents the lidar bin number, $G_b - 91$ represents the lidar bin corresponding to 7 km above the ground and S(j) is the binomial filter function with values: S(1) = 0.25, S(2) = 0.50, S(3) = 0.25.

To obtain the average signal within the PBL (β_{pbl}), compute the bin number that corresponds to half the average PBL height as k = H_{20}/(2.0*76.8). Then define the average PBL signal as:

(3.4.2) $\qquad \beta_{pbl} = (\beta_s(k-1) + \beta_s(k) + \beta_s(k+1)) / 3.0$

Similarly, to define the average signal above the PBL in the free troposphere (β_{trop}), we compute the bin number that corresponds to 500 meters above the average PBL height as l = (H_{20}+500)/76.8. Where l is constrained to be greater than $G_b - 91$. The average signal above the PBL is then:

(3.4.3) $\qquad \beta_{trop} = (\beta_s(l-1) + \beta_s(l) + \beta_s(l+1)) / 3.0$

Next, define a signal level (β_t):

(3.4.4) $\qquad \beta_t = \beta_{trop} + F_{pbl}(\beta_{pbl} - \beta_{trop})$

where F_{pbl} is a threshold factor between 0.0 and 1.0. In practice, the value of F_{pbl} may vary from about 0.4 to 0.7. A discussion of how to estimate the magnitude of F_{pbl} is given in section 4.3.1. Finally, we find the maximum signal between bins k and l. Call this β_{max}, occurring at bin m. The algorithm then searches from that point (bin m) upward until 2 consecutive bins have signal values less than β_t. The lidar bin corresponding to the top of the PBL is considered to be the first bin that is less than β_t. If we call this bin n, then the height in meters above ground of the PBL is:

(3.4.5) $\qquad H_{pbl} = (G_b - n)76.8$

An example of a typical GLAS return for a clear marine boundary layer is shown in figure 3.4.1. The increase in signal due to the trapped moisture and aerosol within the boundary layer occurs at about 900 m in this case. The various signal levels discussed above are labeled on the figure.
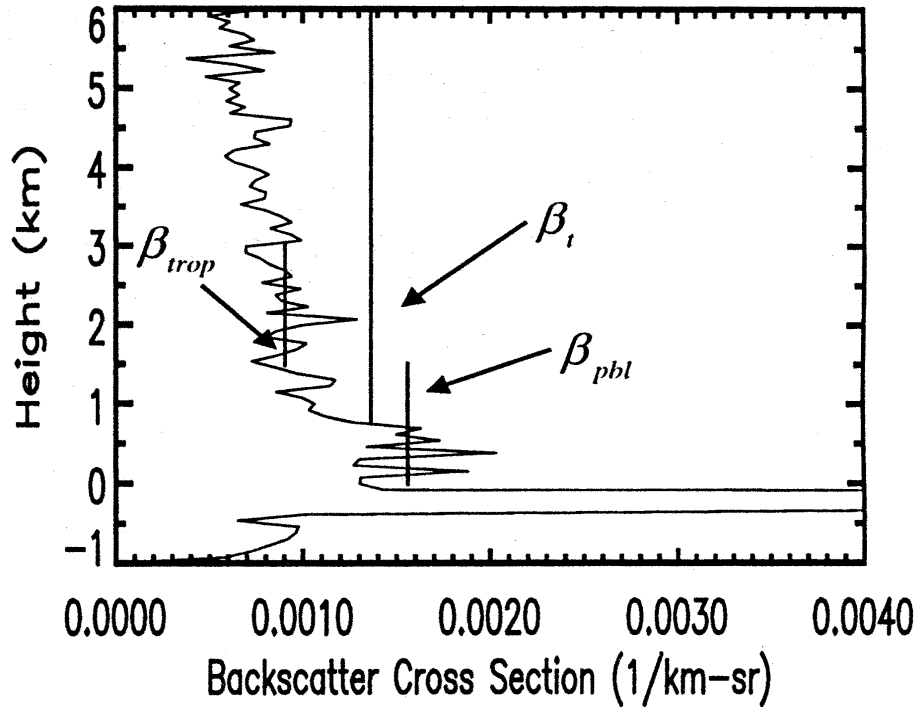
Figure 3.4.1. A nighttime simulated GLAS lidar return at 5 HZ showing the increase in signal associated with the marine boundary layer (below 1 km) and the various signal levels that would be computed by the algorithm from equations 3.4.2, 3.4.3 and 3.4.4 . The threshold value β_t was computed with $F_{pbl} = 0.5$.

Note that H_{20} is the average PBL height defined by the processing of the last 20 seconds of data. This means that when we begin processing or resume processing after a large data gap, the initial value of H_{20} must be assumed. While this is somewhat of a problem, it can be overcome by using the height of the maximum signal from the initial 20 second averaged profile as an estimate of H_{20}. The maximum signal would be computed based on the data form 7 km altitude to 2 bins above the ground bin.

After we have computed H_{20} from the 20 second average using the above procedure, we go back into that segment and form five, 4 second averages (20 shots). Each of these five profiles is searched for the PBL top in exactly the same way as described above, except for the following: the limits within which to search for the PBL top are more narrow. Now we use $n - 5$ and $n + 5$, which is a 750 m wide window centered on the 20 second average PBL height (H_{20}). After each of these segments have been processed to obtain the low resolution PBL height (H_4), the 20 shots which comprise them are individually searched for the PBL top in a similar manner, except we use a 600 m wide window centered on the low resolution height for that segment (H_4).

3.4.1.2 Elevated Aerosol Layer Height

The identification of elevated aerosol layers is a procedure similar to the detection of PBL height, but in this case, we do not know apiori where in the profile to look as we do for the PBL. Elevated aerosol layers can occur anywhere above the PBL and thus require searching nearly the entire profile. They are usually very tenuous and like the PBL will require a certain amount of profile averaging to detect.

45

Based on the results of GLAS simulations, we have decided to search for aerosol layers below 20 km at a 4 second resolution (30 km) and at 20 second resolution (150 km) above 20 km using the 532 nm attenuated backscatter profiles output from GLA07 at 5 Hz. The main reason for this is that most aerosol layers above 20 km will be very tenuous and the 20 second averaging will increase our chances of detecting them. Below 20 km, the aerosol layers are likely to be more dense and thus can (theoretically) be detected at the higher resolution.

Like the PBL height algorithm, the Elevated Aerosol Layer (EAL) algorithm will first average 20 seconds of data to form one profile. That profile is searched for the presence of layers. At this point, the layer could be a cloud or aerosol layer. We will not attempt to discriminate between cloud and aerosol until we examine the signal at the 4 second resolution. If an aerosol layer (or layers) are found at the 20 second resolution and they are below 20 km, then that 20 second segment is broken into five, 4 second averages and the aerosol layer height is determined at the higher resolution using the 20 second average height(s) as a guide. The bottom search limit for a given 20 second segment will be defined by the cloud height information generated by GLA09. The highest optically thick cloud height of the 100 shots defines the bottom search limit for the EAL algorithm. The term 'optically thick' means that the lidar signal has been totally extinguished by the cloud and there is no meaningful signal below the cloud. This information will be recorded in the GLA09 output. In the case of optically thin cirrus at 12 km above a thick stratus deck at 3 km, the search limit for the EAL algorithm would be 300 meters (4 bins) above the highest reported height of the stratus deck for that 20 second segment. In this case, when the EAL algorithm searches for aerosol layers, it must avoid the cirrus cloud. This can be done by defining a 'zone of exclusion' 500 meters above the highest cirrus cloud top height and extending down to 500 meters below the lowest cirrus cloud bottom (both cloud top and bottom are defined by GLA09). This approach will enable us to detect aerosol layers beneath optically thin cloud layers. If there were no clouds detected within the 100 shots, then the lower limit for the aerosol search is 1 km above the highest PBL top for that segment. If a time gap of greater than 10 seconds occurs, while forming the 20 second average, the 20 second average will have to be re-computed beginning after the time gap and all the high resolution aerosol layer heights up to the time gap set to 0. Unlike the PBL height algorithm, the EAL algorithm will need to find both the top and bottom of each aerosol layer. Above 20 km, the algorithm will search for a maximum of 3 layers at a horizontal resolution of 20 seconds (150 km). Below 20 km, a maximum of 5 layers are possible at a horizontal resolution of 4 seconds (30 km).

At this point, we want to take a moment to discuss Polar Stratospheric Clouds (PSC's). PSC's are extremely tenuous (optically thin) clouds that form at altitudes between about 10-25 km in the polar regions during winter. Very few observations of PSC's exist, especially for the Antarctic region. Because of their critical role in polar ozone depletion, they are of intense interest (McCormick et al, 1982, 1985). GLAS, with its polar orbit and extremely good spatial coverage of the polar regions, will provide a unique opportunity to measure the height, extent and coverage of PSC's for the first time. The magnitude of the return signal that GLAS is expected to receive from a typical PSC is very small. We expect the return signal will look more like that from an aerosol layer than from a normal cloud layer. This, together with the fact that GLA09 will search for clouds only below 22 km, makes it more appropriate to search for PSC's in the EAL algorithm (GLA08) than in the cloud detection algorithm (GLA09).

McCormick et al (1985) present observations of PSCs by satellite and aircraft lidar data which indicate that they occur mainly poleward of 65 degrees and only in very cold atmospheric temperatures less

than about –75 °C and that they usually occur between 10 and 30 km. Further, when temperatures are lower than –85 °C, PSCs occur virtually 100 percent of the time. When the EAL algorithm detects a layer that is above 10 km and the latitude is above 65 degrees and the temperature as estimated by the MET data is less than –70 °C, a flag will be set that indicates that this layer is likely a PSC. Additionally if the temperature at the height of the detected cloud layer is below –80 °C, and the latitude is above 65 degrees, then the flag will be set to another value indicating that there is a very high likelihood that the layer is a PSC.

We now move on to the details of the elevated aerosol layer algorithm. If $\beta_{20}(z)$ is the 20 second average attenuated backscatter profile, we first apply a 3 point binomial filter (S(j)) to form a smooth profile as:

$$(3.4.6) \qquad \beta_s(z) = S(1)\beta_{20}(z-1) + S(2)\beta_{20}(z) + S(3)\beta_{20}(z+1) \qquad \text{For } H_b < z < 40 \text{ km}$$

where H_b is the bottom search height as described above. We begin searching $\beta_s(z)$ at the 38 km level and work downward. The general scheme is to define a threshold level based on the local value of the signal and look for a signal consistently above that level. The threshold value is re-computed continuously (at every bin) as we search the profile from top to bottom to account for the increasing molecular signal as we move downward. To commence, let z be the current height of the search. Now compute the average signal representative of the 2km layer above the current height (z=38km):

$$(3.4.7) \qquad \overline{\beta_s}(z-1.384) = \sum_{h=z-0.384}^{z-2.384} \beta_s(h)/27$$

which represents an average over a 2 km thick layer centered at z-1.384 km. Notice that the vertical average does not begin at the current bin (at height z), but rather at height z-0.384 km, which is 5 bins. Next we form the threshold level ($L_t(z)$) for the aerosol layer top as:

$$(3.4.8) \qquad L_t(z) = \overline{\beta_s}(z-1.384) + F\sigma(z-1.384)$$

where $\sigma(z-1.384)$ is the standard deviation of the signal between z-0.384 and z-2.384 km, and F is a scaling factor most likely between 3 and 5. A constraint is placed on the magnitude of L_t. If L_t is greater than the attenuated molecular backscatter at height z times a factor, then set L_t equal to the attenuated molecular backscatter times the factor. In other words, if:

$$(3.4.9) \qquad L_t(z) > \beta_m(z)T_m^2(z)L_{\max} \qquad \text{then} \qquad L_t(z) = \beta_m(z)T_m^2(z)L_{\max}$$

where $L_{\max}$ is a constant factor in the range of 1.1 to 1.3 We begin the search at 38 km (bin 39) and search downward for the occurrence of 3 consecutive bins which have signal levels above L_t. Note that L_t is re-computed at each bin as we move down the profile. Let b1 represent the first bin of the three above the level L_t. The height (above mean sea level) of the top of the first aerosol layer is then:

$$(3.4.10) \qquad H1 = z_{top} - (0.0768)b1$$

where z_{top} is the height above mean sea level of the top of the profile (this should always be 41 km). As we search downward, for each step (bin) we must re-compute $L_t(z)$ as in equation 3.4.8. It is very important to do this, because of the increasing molecular signal as we go to lower altitudes.

Once the top of a layer is found, the bottom threshold (L_b) is formed based on L_t at the top of the layer and the change in molecular scattering from H1 to the current height (z):

$$(3.4.11) \qquad L_b(z) = L_t(H1) + (\beta_m(z) - \beta_m(H1))T_{fac}$$

where T_{fac} is a constant between 0.8 and 0.95 which is designed to take into account the signal attenuation due to the aerosol above the current height. Testing with LITE data has shown that a value of 0.90 for T_{fac} works well. Initially, of course, $L_b = L_t$, but as you progress downward, L_b becomes greater than L_t. For thick aerosol layers, L_b can be considerably greater than L_t (see figure 3.4.2). The bottom threshold level will be computed for each bin below bin b1 and compared with the signal level at that bin. The bottom of the aerosol layer is defined as that height (H2) where the third of 3 consecutive bins (b2) are less than L_b.

$$(3.4.12) \quad H2 = z_{top} - (0.0768)b2$$

Once we have found the bottom of a layer, the search then continues downward in the profile looking for the next aerosol layer in the same manner as the first. There is one problem, however. We are not able to calculate L_t like we did before when we are within 2.384 km of the bottom of a layer (since doing so would include data from within the layer and contaminate the threshold). Thus, while we are within this range, we define L_t as the following:

$$(3.4.13) \qquad L_t(z) = L_b(H2)0.95 + (\beta_m(z) - \beta_m(H2))T_{fac}$$

where T_{fac} here is about 0.80. After we have searched down past 2.384 km below the aerosol layer bottom (H2), then equation 3.4.8 is again used to compute L_t from the 2 km of data above the current height as before.

plot_aer_bscs_10a.gif

BSCS prof
Top thres prof
Bot thres prof
+   up aer tops
·   up aer bots
◇   lo aer tops
△   lo aer bots

Height (km)

up aer top hts, up bot hts (km):
2146435.07 2146435.07
2146435.07 2146435.07
2146435.07 2146435.07

lo aer top hts, lo bot hts (km):
14.05   12.44
4.99   0.25
2146435.07 2146435.07
2146435.07 2146435.07
2146435.07 2146435.07

10^{-10} 10^{-9} 10^{-8} 10^{-7} 10^{-6} 10^{-5}
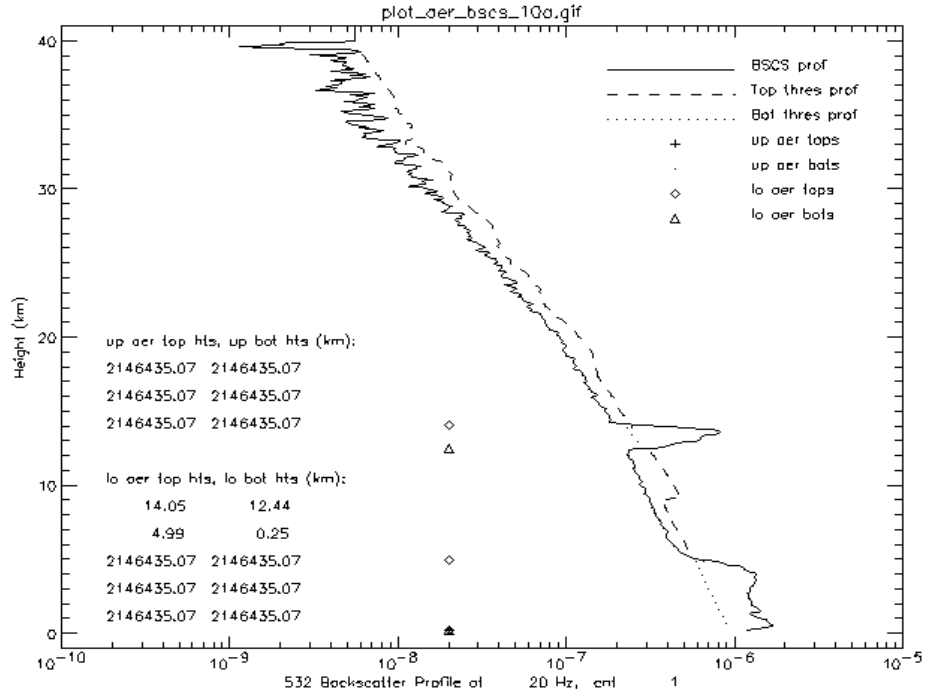
532 Backscatter Profile of   20 Hz, cnt   1

Figure 3.4.2. An example of a 20 second average signal from the LITE space-borne lidar system (solid line) containing two aerosol layers (14 and 5 km). The top threshold (L_t) computed from equation 3.4.8 is shown as the dashed line, and the bottom threshold (L_b) computed from equation 3.4.11 is the dotted line.

The 41 to 20 km region is searched for a maximum of 3 aerosol layers, though a large portion of the data will be devoid of aerosol layers in this region. The search continues below 20 km until it reaches the bottom height defined by the highest optically thick cloud within that 20 second segment. If there were no clouds in the segment, then the highest PBL height for that segment is used instead. If a layer top is found, but no layer bottom was found before reaching the bottom search limit, then the bottom of the layer is set to the bottom search limit. This situation should only occur when an elevated aerosol layer is sitting directly on top of the PBL. If layers were found below 20 km, then five, 4 second averages are formed and the 5 profiles are searched for the aerosol layer height using the 20 second average layer height as a guide. If a layer top is found above 20 km, but the layer bottom is located below 20 km, it is considered to be a layer above 20 km.

After all layers have been found in the 20 second average profile, we then examine those below 20 km at the higher 4 second resolution. Before we can do so, however, we must make sure that the layer that has been found in the 20 second average profile is not a cloud. To do this, we use the output of GLA09. If C_t is the bin corresponding to a 4 second cloud top output by GLA09 and C_b is the bin corresponding to the bottom of the same cloud layer, define a window as $C_t - 10$ and $C_b + 10$. If the 20 second aerosol layer top is within this window, then this layer is not aerosol, but is the cloud detected by GLA09.

If b1 and b2 represent the bin numbers corresponding to the top and bottom of an aerosol layer below 20 km (found from the 20 second average profile), respectively, then to search for the high resolution

(4 second) top and bottom of the layer we first form the vertically smoothed 4 second average profile ($\beta_s(z)$) as:

(3.4.14) $\qquad \beta_s(z) = S(1)\beta_4(z-1) + S(2)\beta_4(z) + S(3)\beta_4(z+1)$ For z < 20 km

where β_4 is the 4 second average attenuated backscatter profile and S is the 3 point binomial filter defined in section 3.4.1.1. The search then proceeds much in the same way as for the PBL height. Average signal levels are computed about 1 km above b1 and from b1 to b2 which represent the scattering levels above and within the aerosol layer, respectively as:

(3.4.15) $\qquad \beta_{abv} = \sum_{j=b1-15}^{b1-12} \beta_s(j)/4.0$

(3.4.16) $\qquad \beta_{aer} = \sum_{j=b1}^{b2} \beta_s(j)/(b2 - b1 + 1)$

where the subscript 'abv' refers to the signal level in the free atmosphere above the aerosol layer. Next, a threshold level (β_a) is defined based on β_{abv} and β_{aer} as:

(3.4.17) $\qquad \beta_a = \beta_{abv} + F2(\beta_{aer} - \beta_{abv})$

where, as with the PBL, F2 is a scaling factor with a magnitude of about 0.3 to 0.5. A maximum limit is placed on the allowed value of β_a If β_a is grater than the molecular attenuated value at the height of the height of the 20 second aerosol layer top, then β_a is set to the molecular value times a constant. In other words, if:

(3.4.18) $\qquad \beta_a > \beta_m(z)T_m^2(z)L_{max}$ then $\qquad \beta_a = \beta_m(z)T_m^2(z)L_{max}$

where L_{MAX} has a value in the range 1.10 to 1.30 and z corresponds to the height of the 20 second aerosol layer top. With this threshold level thus defined, the 4 second average profile is searched downward in a narrow window from b1-12 to b1+12 for 2 consecutive bins with signal values greater than the threshold level β_a. The first of the two consecutive bins above this level is the bin number corresponding to the top of the layer. The bottom of the layer is found in exactly the same way, except we search backwards, up the profile in a narrow window 24 bins wide. The signal threshold is defined using an average signal below the layer (β_{bel}) and the average signal within the layer (β_{aer}).

(3.4.19) $\qquad \beta_{bel} = \sum_{j=b2+15}^{b2+12} \beta_s(j)/4.0$

(3.4.20) $\qquad \beta_a = \beta_{bel} + F2(\beta_{aer} - \beta_{bel})$

where F2 has the same value as in Equation 3.4.17. A maximum limit is also placed on β_a as in equation 3.4.18, but now z corresponds to the height of the 20 second aerosol layer bottom. The search begins at bin b2+12 and continues to bin b2-12, searching upwards again looking for 2

consecutive bins with a signal value greater than β_a. The first of the two bins above the threshold level (β_a) defines the bottom of the layer. The above process is repeated for each of the five, 4 second average profiles yielding the high resolution elevated aerosol layer heights for the 20 second data segment.

3.4.2 Error Quantification

The accuracy of PBL or elevated aerosol layer height retrieval is governed by a number of factors. These are:

1.)   Signal to noise ratio of the data.
2.)   Accuracy of satellite altitude and time of laser fire in the absence of a detectable ground return.
3.)   Sampling frequency (bandwidth, which determines the vertical resolution of the data).
4.)   Number of lidar shots averaged together (horizontal resolution)
5.)   Optical depth of the PBL

Factor one encompasses numbers 4 and 5 as the signal to noise ratio increases with the square root of the number of shots averaged and the optical depth of the layer. Thus, the ability and overall accuracy with which we can detect the PBL top at low resolution (30 km, or 160 shot average) is going to be much better than high resolution (1.4 km, or 8 shot average). Since the sampling frequency is every 76.8 meters in the vertical, under the best of conditions, with high signal to noise levels, the PBL or aerosol layer can be resolved to a vertical accuracy of +/- 76.8 meters. As signal to noise values decrease (corresponding to either higher horizontal resolution or smaller aerosol backscatter) the retrieval accuracy will diminish. The magnitude of this effect must be determined by applying the algorithm to simulated GLAS data. For the horizontal resolution we hope to obtain with the GLAS measurements (1.4 km), 76.8 meter vertical accuracy is too optimistic. We estimate that for the high horizontal resolution, the PBL top can be retrieved to within 150 meters. However, under typical conditions we estimate that we can obtain average PBL and aerosol layer height to within 76.8 meters at low resolution (30 km).

PBL height is normally defined thermodynamically based on a rapid increase of potential temperature with height (temperature inversion) and a simultaneous decrease in relative humidity. A number of studies have shown that a rapid decrease in backscatter cross section also occurs at the inversion height, allowing lidar to provide a consistent and accurate measure of PBL height. Thus, we expect that the technique described here will usually yield the thermodynamic height of the PBL, but there are times when this might not be true. For example, elevated aerosol layers can lay directly on top of the boundary layer or there are cases where the boundary layer is growing into a residual boundary layer from the previous day. In these instances, the gradient of scattering at the PBL top might be relatively small and difficult to detect. Instead of yielding the PBL height, the algorithm might pick up the height of the elevated aerosol layer or residual boundary layer. Unfortunately, these types of errors are unavoidable when processing lidar data autonomously, without human interaction.

GLA08 calculates the height of the PBL or elevated aerosol layer with respect to the ground return bin. If the ground return has not been detected from the data (from GLA07 or GLA09 processing), then clouds are assumed to be present. In this case, the algorithm will rely on either the last ground return bin found or a calculated ground return bin based on the onboard DEM value used for that shot. The

onboard DEM is accurate to about 200 meters. Thus, when there are clouds obscuring the ground return, there could be a 200 meter error in the determination of aerosol or PBL layer top.

It should be noted that the vertical resolution of the data combined with the technique used to find the PBL height place an upper and lower bound on the height of the PBL which can be detected by the PBL algorithm. It is estimated that the algorithm will have trouble detecting boundary layers which are less than about 150 m thick. Boundary layers this thin are relatively infrequent but do occur at times near the center of subtropical high pressure ridges over the oceans (and possibly elsewhere). Similarly, the algorithm as coded will not detect boundary layers that are higher than 7 km. As far as we know, the highest boundary layers occur over the Sahara desert and normally range from 4 to 6 km in height.

3.4.3   Confidence Flags

Confidence flags for both the PBL height and elevated aerosol layer height can be constructed out of the difference between the average signal levels outside of the layer and inside the layer (ΔSI). These levels are computed by the respective algorithms as detailed in sections 3.4.1.1 and 3.4.1.2. Basically, the confidence in our height determination increases as ΔSI increases. If β_{aer} and β_{abv} represent the average signal levels inside and above an aerosol layer (or boundary layer) respectively, then we can form the ratio:

$$(3.4.21) \qquad \alpha = (\beta_{aer} - \beta_{abv}) / \beta_{abv} = \Delta SI / \beta_{abv}$$

If the value of α is less than or equal to zero, then there is no confidence in the resulting height. As α increases, so does the confidence in the corresponding height measurement. It should suffice to compute and store α for the confidence levels of both the PBL height and elevated aerosol layer height.

Another measure of confidence that could be used is the standard deviation of the heights for a given segment. Normally, for segments less than a few hundred kilometers, the PBL heights should have a standard deviation on the order of 200 to 400 meters. Any significant deviation outside of this range may indicate trouble with the algorithm. This approach could also be used for the elevated aerosols, except that the standard deviation is expected to be somewhat less, perhaps 50 to 200 meters.

3.5 Optical Properties of Cloud and Aerosol Layers

Before we examine the equations that will be used to retrieve optical properties of clouds and aerosols from the GLAS atmospheric data, we will present a short description of the physical processes which govern the light-particle interactions and the notable difficulties in using these.

First, we note that the primary atmospheric observation channel of GLAS will be at 532 nm. Gas absorption processes are negligible compared to scattering processes at that wavelength and so they will be omitted in the derivation of the particulate optical depths given herein. Ozone absorption, although small, will be factored out prior to the optical properties algorithm by calculating ozone transmission profiles from ozone climatological databases then dividing the lidar signal profile (attenuated backscatter) by the ozone transmission (See section 3.2).

The observed or effective optical depth of a horizontal layer of particles between the orbiting lidar and a given altitude is the logarithm of the ratio of a laser's initial normalized pulse energy to its energy at that altitude. Thus, the basic physical effect which permits finding the cloud and aerosol layers' optical depths is the diminution of the lidar pulse energy as it is scattered or absorbed by the atmospheric constituents. As the laser pulse travels from the instrument, its photons interact with and are scattered (redirected) by the molecular and aerosol particles of the atmosphere. The lidar detector measures those photons which are redirected into a small solid angle centered at 180 degrees (backscattered) into its receiver. The number of laser pulse photons received in a short time interval from a given atmospheric volume are recorded. This quantity is the lidar signal strength. It is proportional to the densities of particles in that volume and the combined scattering characteristics of the particles. These scattering characteristics are strongly affected by the shape of the scattering particles and the size of the particles relative to the wavelength of the laser light. A given scattering volume may contain zero (in a vacuum) to several scattering species each of which has its own density, size distribution, and scattering characteristics.

A major challenge in optical analysis of lidar signals from cirrus clouds is that these clouds are composed of particles whose shapes and size distributions are not readily discernible by any remote sensing techniques. This forces us to incorporate some crucial assumptions in order to obtain quantified results. The validity of these strongly rely upon former experience with cirrus lidar observations (Spinhirne et al., 1990,1996).

In particular, when attempting to obtain cloud optical depth from a spacecraft lidar, two assumptions are required regarding the scattering characteristics of the cloud. One of these assumptions is that the multiple scattering effect can be reliably quantified. The multiple scattering effect is the modification from the true optical depth caused by the increase in detected signal strength due to the portion of the detected signal which has experienced more than one scattering interaction. It is primarily the result of photons that are deflected only slightly during the scattering process. This is referred to as forward scattering and it serves to decrease the perceived optical depth. Ice particles typically have a very pronounced forward scattering component which will cause the multiple scattering effect to be quite significant. Multiple scatter is also a factor for aerosols, though much smaller. From calculations (Spinhirne, 1982), it is estimated that aerosol multiple scattered signals will have less than an 8 percent effect for even the most hazy conditions. Details of the procedure to handle multiple scattering are discussed in section 3.6. The other assumption is that the value of the extinction to backscatter ratio is known. The extinction to

backscatter ratio is the total scattered energy divided by the amount of backscattered energy. For a given scattering layer, it is assumed to be constant. Sometimes, under favorable circumstances, this ratio can be estimated from remotely sensed data, but computations based upon satellite observations often will require externally computed values. These are discussed in sections 3.5.1.1 and 4.5.1. The values of both of these parameters are determined by the details of the volumetric scattering phase function that quantifies the scattering effect as a function of scattering angle.

3.5.1 Theoretical Descriptions

3.5.1.1 Transmittance Solution to the Lidar Equation and Calculation of Backscatter Profiles (GLA10)

The goal of the optical properties analysis of the GLAS lidar signal is to obtain particulate extinction cross section profiles (σ_p) and particulate layer optical depths (τ_p), involving clouds, aerosols, and polar stratospheric clouds (PSC's). The discussion given below essentially restates a derivation given many times in the literature. For example, see Spinhirne (1980,1996), Elouragini (1995), and Marenco (1997). The derivation of the multiple scattering factor (η) will be handled in its own section (3.6). At this point one needs to note that transmittance, extinction, and optical depths obtained directly from the solution of the lidar equation are actually the apparent or effective values (Platt, 1979) without multiple scattering effects factored out and are denoted with the superscript prime.

The working lidar equation for a spaceborne and nadir pointing lidar has been stated previously and can be rewritten in the following form:

$$(3.5.1) \quad P_n(z) = \beta(z)T'^2(z).$$

The left side of the equation is the calibrated normalized lidar signal of attenuated backscatter coefficient corrected for ozone attenuation. The total (particulate and molecular) volumetric backscatter coefficient at distance z is denoted by $\beta(z)$ and the two-way particulate and molecular transmission factor from z to the spacecraft altitude is given by $T'^2(z)$, expressed as $\exp[-2(\tau_m(z) + \tau'_p(z))]$. Optical depth is represented by the symbol τ, while the subscripts m and p designate molecular and particulate contributions, respectively. Furthermore, the influence of the multiple scattering effect (η) on the particulate optical depth is described by:

$$(3.5.2) \quad \tau'_p(z) = \ \sigma'_p(z)dz = \ \eta(z)\sigma_p(z)dz \cong \overline{\eta} \ \ \sigma_p(z)dz ,$$

where σ_p is particulate extinction.

Since the molecular contribution to the total backscatter and transmission can be computed from theory, it is advantageous to separate the scattering terms into components which represent the molecular and particulate contributions independently.
With $\quad \beta = \beta_p + \beta_m \quad$ and $\quad T'^2 = T'^2_p T^2_m$

the lidar equation becomes:

(3.5.3) $P_n = \beta_p T_p'^2 T_m^2 + \beta_m T_p'^2 T_m^2$.

The following relationships must now be defined:

(3.5.4) $T_p'^2 = e^{-2 \int \sigma_p' dz}$ and $S_p' = \dfrac{\sigma_p'}{\beta_p}$ (assumed a constant for each layer), and

(3.5.5) $T_m^2 = e^{-2 \int \sigma_m dz}$ and $S_m = \dfrac{\sigma_m}{\beta_m}$,

where S_p' and S_m are the effective particulate and molecular extinction to backscatter ratios, respectively. $T_m^2(z)$ can be calculated accurately given the vertical temperature and pressure structure of the atmosphere from MET data or appropriate standard atmosphere data and the fact that S_m is known to be $8\pi/3$ throughout the vertical profile. The purpose of this derivation is to solve the equation for the vertical profiles of β_p. The true particulate optical depth and extinction profiles can be then be computed from the values of S_p, β_p, and η.

From these relationships, we see that:

(3.5.6) $\dfrac{d(T_p'^2)}{dz} = T_p'^2 \left(-2S_p' \right) \beta_p$

We can use this relationship to substitute for β_p in (3.5.3) to arrive at:

(3.5.7) $P_n = -\left(\dfrac{1}{2S_p'} \right) T_m^2 \dfrac{d\left(T_p'^2\right)}{dz} + \beta_m T_m^2 T_p'^2$ or

$\dfrac{d\left(T_p'^2\right)}{dz} - 2S_p' \beta_m T_p'^2 = -\dfrac{2S_p' P_n}{T_m^2}$

By specifying z as the independent variable and $T_p'^2$ as the dependent variable, this is a first order linear ordinary differential equation; it is a special form of the Bernoulli equation. The solution can be found by using the common integrating factor method where the integrating factor is

$F = e^{-2X \int \sigma_m dz}$, and $X \equiv \dfrac{S_p'}{S_m}$. The general solution is:

(3.5.8) $T_m^{2X} T_p'^2 = -2S_p' \int T_m^{2(X-1)} P_n dz + K$

where the integrand is defined only where particulates are present and K is a constant of integration.

For convenience, we define the coordinate z as the <u>vertical</u> distance from the spacecraft, increasing downward. At this point we must now allow for the effect of the lidar pointing off-nadir at a zenith angle of θ. If we visualize the situation where the lidar pulse encounters layers of particulates after traveling through the molecular atmosphere from the spacecraft, we can define the boundary condition at the top of any layer, $I_B(z_t)$, as:

$$(3.5.9) \quad I_B(z_t) = T_p'^{2\sec\theta}(z_t)T_m^{2X\sec\theta}(z_t),$$

where z_t is the distance to the top of the layer. If the layer is the first layer encountered, the $T_p'^{2\sec\theta}(z_t)$ term can be estimated as 1.00. The calculation of $I_B(z_t)$ for multiple layers is covered in detail in Section 4.5.2.

So in general, the two-way particulate transmission within the particulate layer, whether cloud or aerosol, given a lidar zenith angle of θ is

$$(3.5.10) \quad T_p'^{2\sec\theta}(z) = \frac{I_B(z_t) - 2S_p'\sec\theta \int\limits_{z_t}^{z} T_m^{2(X-1)\sec\theta}P_n dz'}{T_m^{2X\sec\theta}(z)}.$$

This forward inversion processing continues throughout each particulate layer until $T'^{\sec\theta}_p(z) < T_L$ or the signal from the earth's surface is detected. T_L is a limit defined through error consideration (see section 3.5.2). Extensive automated use of this algorithm has been incorporated into the Global Backscatter Experiment (GLOBE) with aircraft lidar and into the Atmospheric Radiation Measurement (ARM) program with the ground-based Micro pulse lidar (MPL) with good results (Hlavka, 1998). Backward inversion processing, where the boundary conditions are known at the base of the layer, will optionally be used for low noise and high optical depth situations. Details of the backward inversion algorithm can be found in section 4.5.2 including equations 4.5.4, 4.5.5, 4.5.6, and 4.5.7.

An important ingredient of this transmission solution is the factor S_p'. When the particulate layer being analyzed is determined to meet the appropriate criteria for underlying signal analysis, an algorithm to calculate an estimate of S_p' will be called. If S_p' is found to be within tolerances, it will be used in equation (3.5.10). Appropriate criteria would be 1) layer is optically thin with either a lower layer or earth's surface sensed and 2) enough clear air (no aerosols) exits below the layer to determine signal loss through the layer. The clear air zone must be at least a minimum thickness (around 1 km) and analysis is usually restricted to 3 km thickness. Ice clouds above 5 km are the most likely candidates. Under these conditions, an estimate of $T_p'^{2\sec\theta}(z_b)$ (and thus an estimate of effective optical depth for the layer) can be found using the following equation, where z_b is the distance to the bottom of the layer and z_c is the distance to the end of the clear air analysis zone:

$$(3.5.11)\quad T_p'^{2\sec\theta}(z_b) = \frac{\displaystyle\int_{z_b}^{z_c} P_n(z)\,dz}{T_m^{2\sec\theta}(z_b)\displaystyle\int_{z_b}^{z_c} \beta_m(z)T_m^{2\sec\theta}(z)\,dz}\ .$$

This method is called the integrated ratio technique. Simulations show this method is more stable under noisy conditions compared to other methods such as the log signal difference technique (see section 3.5.2). By defining $I_B(z_b) = T_p'^{2\sec\theta}(z_b)T_m^{2X\sec\theta}(z_b)$, S_p' can then be calculated through an iterative solution from the following equation:

$$(3.5.12)\quad S_p' = \frac{I_B(z_t) - I_B(z_b)}{2\sec\theta\displaystyle\int_{z_t}^{z_b} P_n(z)T_m^{2(X-1)\sec\theta}(z)\,dz}\ .$$

The iterative process is started with an initial guess of S_p' as it relates to the X parameter, with the next iteration using the calculated value until the solution converges to a set tolerance. A version of this routine has worked well during automated MPL processing of aerosols using the calibrated signal to resolve the layer optical depth similar to the loss of signal in a cloud (Spinhirne, 1999). This routine should also function for PSCs and enhanced upper tropospheric aerosol layers. Later versions of this ATBD will look into the feasibility of expanding the integrated ratio technique by combining two close layers if they are the same layer type and the bottom layer meets the criteria. An average S_p' can then be calculated to represent both layers.

For atmospheric layers where S_p' cannot be calculated, a value will be assigned for each layer based on pre-defined look up matrices of S_p and η, distinguishing between different cloud and aerosol regimes. Because the calculation of S_p' requires a clear air zone below the layer, all Planetary Boundary Layers (PBL) will <u>have</u> to default to the pre-defined matrices. Details of the decision matrices for S_p look up tables are presented in section 4.5.1. S_p' will be determined as:

$$(3.5.13)\quad S_p' = \eta\, S_p,$$

where η, the multiple scattering factor, is separately estimated from appropriate look up selection distinguishing between apparent cloud or aerosol type, layer top and bottom heights, effective optical depth estimate, and particle size (see section 3.6). Initial determination of S_p for clouds will be driven by cloud temperature. The underlying surface signal attenuation is an additional factor to improve retrievals.

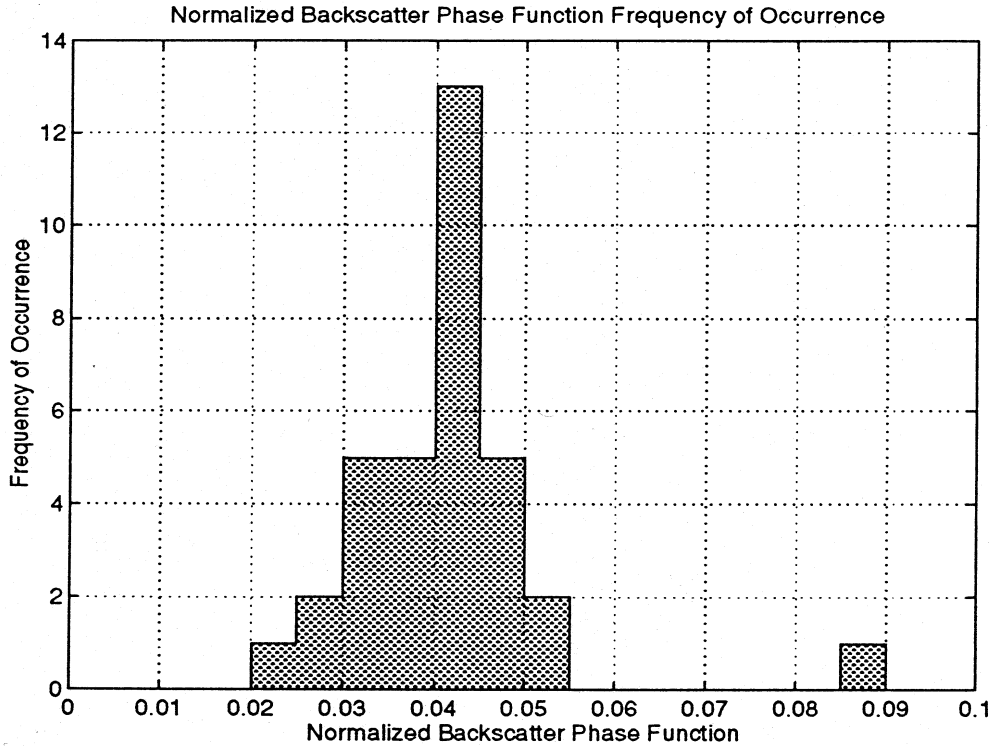**Normalized Backscatter Phase Function Frequency of Occurrence**

Figure 3.5.1 Phase function ($1/S_p$) for Midlatitude Cirrus Observations

A lidar study of mid-latitude cirrus (Eloranta, 1999) indicates that although S_p can vary by 30 or more, by far the highest frequency of occurrence is near 24 sr (refer to figure 3.5.1). Water clouds have a much lower variation. Determination of S_p for polar stratospheric clouds will be handled as a special subset of the aerosol look up table because they have more of an aerosol origin than a water origin and will be processed at the aerosol time resolution. Determination of S_p for regular aerosol will be driven by geographic location, layer height, relative humidity, and possibly surface signal attenuation analysis and wavelength ratios of solar reflectance at 532 and 1064 nm, with geographic location the most important factor. Geographic location can be channeled into three main aerosol regimes: continental, desert, and maritime (Ackermann, 1998) with functions relating the influence of relative humidity. Analysis of the GLOBE data set of 1990 suggests that, on average, aerosol S_p equals 28±5 sr for all height levels, even though there were distinct boundary layer and upper tropospheric layers with different sources. An example is shown in figure 3.5.2.

Note that if $T_m^2(z) \equiv 1$, which means that molecular scattering is negligible at all processing levels, the transmission equation for nadir pointing lidar reduces to:

$$(3.5.14) \quad T_p'^2(z) = 1 - 2S_p' \int_{z_t}^{z} P_n dz',$$

which many times is sufficient for cirrus cloud analysis using a 1064 nm channel.

58
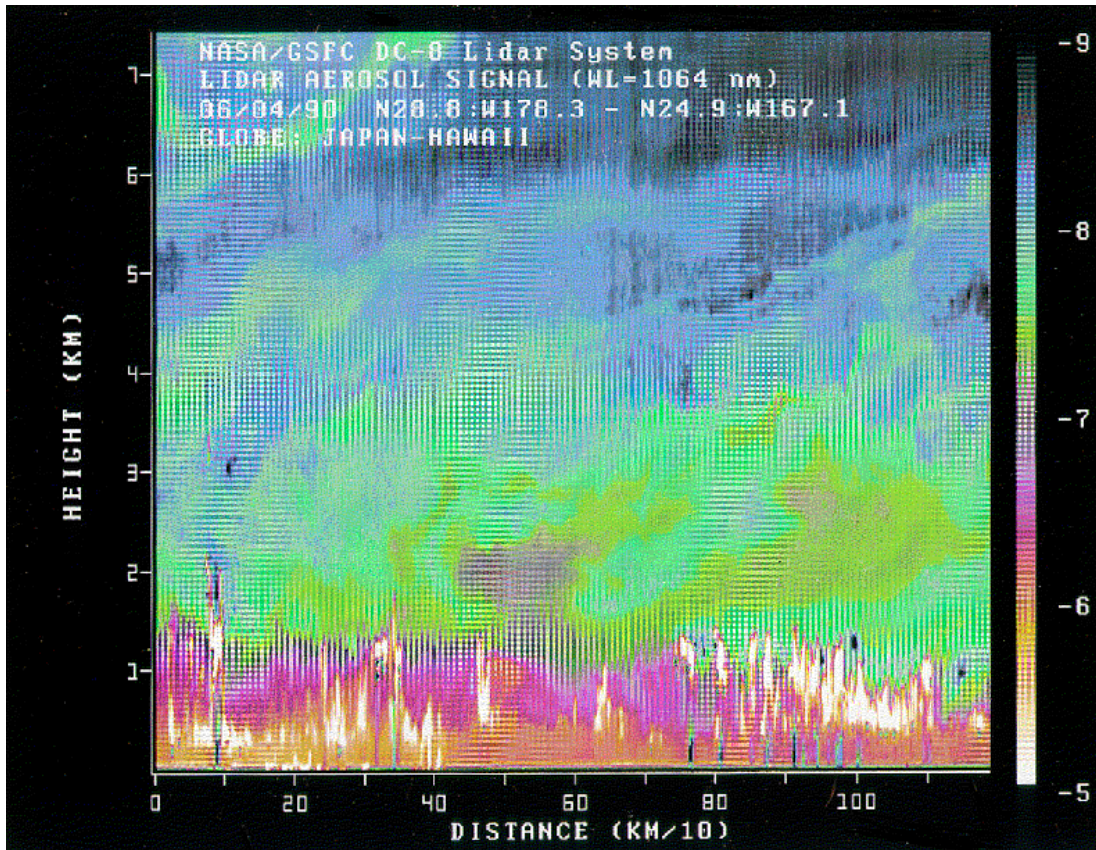
Figure 3.5.2 Despite complicated vertical structure, the GLOBE project showed that S_p did not vary appreciably in the vertical.

Finally, in order to obtain the relative density for aerosol and cloud scattering, it is useful to solve the lidar return signal for the actual particulate backscatter cross section without attenuation. To solve for this backscatter cross section profile, use results from (3.5.10) as input to (3.5.3) by rearranging:

$$(3.5.15) \quad \beta_p(z) = \frac{P_n(z)}{T_m^{2\sec\theta}(z) T_p'^{2\sec\theta}(z)} - \beta_m(z).$$

3.5.1.2 Aerosol Extinction Cross Section

Once the particulate effective transmission and backscatter profiles for each aerosol layer sensed have been calculated, it is a straightforward procedure to determine the aerosol extinction cross section profiles. Extinction cross section for particulates (σ_p) is defined as the total scattered energy at height z or the change in optical depth with height:

$$(3.5.16) \quad \sigma_p(z) = \frac{d\tau_p(z)}{dz} \text{ , where}$$

59

τ_p is the particulate optical depth at distance z and is defined in Section 3.5.1.4. However, since the backscatter cross section profile has, at this point, already been calculated, the aerosol extinction to backscatter ratio (S_p), earlier obtained through table look up or its relationship with S'_p, could also be easily used to obtain the extinction profile for visible wavelengths:

$$(3.5.17) \quad \sigma_p(z) = S_p \beta_p(z)$$

Note that multiple scattering has already been accounted for in the calculation of S_p.

3.5.1.3 Cloud Extinction Cross Section

As discussed in section 3.5.1.1, the calculation of the extinction cross section of clouds from backscatter lidar data requires knowledge of the 180 degree scattering phase function, or extinction to backscatter cross section, (S_p) and a correction, in the case of space born lidar especially, for multiple scattering (η). In all cases an extinction solution, or correction, for cloud lidar can only be applied for a limited range of optical thickness. Our experience with ER-2 remote sensing indicates an upper limit of approximately 1.5 effective optical depth. Signal to noise issues and others will be a factor for other systems, and modeling and testing with simulated GLAS data will determine the applicable limit. In order to determine the effective attenuation, neglecting first multiple scattering, most generally previous work has made the assumption of a constant phase function within cloud layers. With this assumption it is well know that integration of the observed attenuated backscatter cross section for optically thick clouds is equal to half the backscatter to extinction cross section

$$(3.5.18) \qquad B'(z)dz \quad k/2\eta \text{ as } \tau \quad \infty$$

By identifying the limiting integral value, a solution for the effective backscatter to extinction value is known. For cirrus, Platt (1979) and others have used infrared emittance to determine asymptotic values. For nadir observations, Spinhirne and Hart (1990) have shown that the disappearance of the surface signal below the cloud can be used to identify the asymptotic value. For real time processing however there are limitations. The assumption must be made that near by thin clouds are in character with dense clouds. Also signal noise and the complexity of real cloud formations can be expected to introduce significant error, based on ER-2 experience. The noise effects and appropriate application routines can be examined from modeling. A more basic limitation is that the multiple scattering correction to the derived effective extinction is already a large uncertainty term, and complex algorithm development for the effective attenuation may not be warranted.

Another approach to obtaining the extinction cross sections, which is the one we prefer for automated processing, is to start with assumed 180 degree scattering phase functions. For water cloud this is accepted as a good assumption where 17.8 (sr) is widely applicable (Spinhirne et al., 1989; Pinnick et al., 1983). For cirrus, modeling has not shown such an universal value, give the complexity and variation of cirrus shape and size. However experimental measurements have shown, likely because most cirrus are complexes of many different crystal types, that cirrus phase functions values tend to peak statistically toward characteristic values (E. Eloranta, personal communication; Spinhirne et al.,1996). With further work it will be possible to tailor values to

geographic location and cloud temperature or height. When the profile is determined to be appropriate for direct S'_p analysis, an algorithm to calculate an estimate of S'_p will be called and the calculated value will be compared to the table. Similarly, modeling for the multiple scattering correction, discussed in a later section, will lead to look up tables for the correction based on the cloud location and temperature.

Given a 180 degree phase function value, we use equation (3.5.17) to get the vertical profile of visible extinction cross section, σ_p of a cirrus cloud from top to the upper limit of the effectiveness of an attenuation correction. Please note that multiple scattering has already been accounted for in the calculation of β_p and S_p.

Any conversion of the visible extinction coefficients in clouds to thermal infrared absorption coefficients will rely on the assumption that the ratio of these two parameters is constant through the vertical extent of a cloud layer. A profile of lidar derived backscatter coefficients can be converted to absorption coefficients by a direct multiplication. The value of this constant absorption ratio, q, can be approximated from the results of theoretical studies. The investigation into cloud infrared absorption conversion will be investigated as a level 3 product.

3.5.1.4 Cloud and Aerosol Layer Optical Depth (GLA11)

A fundamental use of the spaceborne lidar is to detect and quantify the layers of optically dilute clouds that often reside in the mid to high troposphere where the temperatures are cold . These temperatures result in low water vapor density. Because the total amount of water must be conserved, when clouds form, the particle density will likewise be low. Clouds which form at lower altitudes are generally denser because of the greater availability of water. In such clouds, the useful geometrical penetration of the lidar signal is limited because of laser pulse attenuation.

The clouds of interest are generally classified as cirrus clouds. They are usually composed primarily of ice crystals with some coexistent supercooled water droplets. Analysis of PSC's are also of strong interest. Both these clouds often have a sufficiently small optical depth that a meaningful lidar signal can be detected at the bottom of the cloud layer. In these cases, a total layer optical depth can be derived by the lidar. Sometimes, two or more layers exist and the optical depth of each layer can be determined.

The lidar signal can also be used to estimate the optical depth of the layer of non-cloud aerosols which reside in the planetary boundary layer. These aerosols can be composed of a variety of substances that are trapped by the temperature inversion which tends to exist at the top of the boundary layer. In some cases elevated haze layers of significant density are also found higher in the troposphere or stratosphere which have appreciable optical thickness. Examples include volcanic dust layers, smoke layers, and dust layers caused by periodic continental dust storms. The boundaries of any of these layers that are significant would be located by using the backscatter discontinuity algorithm of Section 3.4.

The solution to the lidar equation to obtain particulate <u>effective</u> optical depths (τ'_p) at any range z from a nadir pointing spaceborne lidar is by definition a straightforward relationship with the particulate effective transmission calculated in (3.5.10):

(3.5.19) $\qquad \tau'_p(z) = -\left(\dfrac{1}{2}\right) \ln\left[T''^2_p(z)\right]$ or $T''^2_p(z) = e^{-2\tau'_p(z)}$.

This solution will achieve best results in terms of the magnitude of error when applied to situations where the optical depth is relatively small. To evaluate and quantify this declaration we examine the relationships from which τ'_p is computed from cirrus data:

We neglect molecular scattering within the cloud such that

(3.5.20) $\qquad T''^2_p(z) = 1 - S'_p 2\gamma(z)$ $\qquad$ where $\gamma(z) = \displaystyle\int_{z_t}^{z} P_n dz'$

We see that $T''^2_p(z)$ approaches zero as 2γ approaches $1/S'_p$. Random noise excursions superimposed upon the detected signal can cause the computed value of $T''^2_p(z)$ to become less than 0 as the integral to evaluate gamma is numerically computed from the lidar signal. In this situation, τ'_p becomes undefined. Also, differentiation of (3.5.19) and (3.5.20) shows

(3.5.21) $\qquad d\tau'_p = \dfrac{S'_p d\gamma}{T''^2_p}$

This means that a given excursion $d\gamma$ causes an error in τ'_p in inverse proportion to the value of T''^2_p ; that is, the magnitude of the error becomes larger as the effective transmittance become small and the effective optical thickness becomes relatively large. Based upon experience gained from aircraft lidar studies (Spinhirne, 1990), computational errors in cloud optical depth for GLAS due to random noise remain tolerable until the value of T''^2_p reaches 0.12-0.20 or τ'_p =1.1-0.8. Where the clouds are more optically thick, the lidar cannot give meaningful results. We will discuss the details of computational uncertainty more fully in section 3.5.2.

The specific method we will be using to calculate the particulate <u>layer</u> optical depth stems from the same transmission solution to the lidar equation, put uses the relationship of the extinction cross section profile in the layer (described in sections 3.5.1.2 and 3.5.1.3) to optical depth. The final optical depth products from these calculations will be the optical depth (τ_l) for each of the particulate layers meeting the analysis criteria:

(3.5.22) $\quad \tau_l = \displaystyle\int_{z_t}^{z_b} \sigma_p(z)dz$,

where z_b and z_t are the bottom and top locations of the particulate layer, respectively and multiple scattering has already been factored out.

The vertical coordinate limits on the integration in the transmittance equation in (3.5.10) will be determined by the cloud and aerosol boundary algorithms described in Sections 3.3 and 3.4. In

practice, the integration will be carried out starting at the first particulate layer top. Although the whole molecular transmission vertical profile starting at the top of the atmosphere and ending at the bottom of the lowest particulate layer sensed will have to be calculated, the particulate transmission vertical profile will be calculated only inside cloud and aerosol layers. The boundary condition (equation 3.5.9) at the top of any secondary layer will involve the particulate transmission squared at the bottom of the layer above and the molecular transmission squared at the top of the current secondary layer.

The attenuation of the pulse energy due to molecular scattering in the intervening clear air layers is small in the mid to high troposphere where the optically thin clouds reside. The magnitude of the molecular scattering is a significant fraction of the aerosol scattering since the gaseous atmosphere is relatively dense at the low altitudes of the boundary layer and the optical density of the aerosol particles are typically much lower than that found in even cirrus clouds.

Optical parameters would be obtained either empirically or from prior studies for aerosol layers. In practice, three necessary conditions for determination of the boundary layer or elevated haze optical depth will be that: 1) the top of the layer is detected, 2) there is no obscuring cloud layer present, and 3) the earth's surface or a lower particulate layer has been found by the lidar. Evidently, the most prominent source of uncertainty will be how closely the actual aerosols which are being observed match the characteristics of the assumed aerosol type. Re-processing from level 3 extinction-to-backscatter investigations will help reduce these uncertainties.

3.5.2 Error Quantification

The most important optical measurements derived from the lidar measured backscatter profiles are the total effective optical thickness and transmission of particulate layers which are fully penetrated by the laser pulse. We will inspect here the effect that various uncertainties have on the uncertainty of the derived values of these physical quantities.

To begin, we will use the relationships

(3.5.23) $\qquad T_p'^2(z_b) = 1 - 2S_p'\gamma(z_b)$ (ignoring the molecular component),

(3.5.24) $\qquad \tau_p'(z_b) = -\dfrac{1}{2}\ln\!\left[T_p'^2(z_b)\right]$, and define the parameter

(3.5.25) $\qquad \alpha = S_p'\gamma(z_b)$, where $0 < \alpha < 0.5$ and $\gamma = \int P_n dz$

The subscript p denotes particulate and α will represent actual value of the product which the measurements are attempting to attain. Because practical computations become unstable for relatively optically thick clouds, the useful limits of lidar measurements are exceeded as the value of α goes above 0.475.

Differentiation gives us,

(3.5.26) $dT_p'^2 = -2\gamma dS_p' - 2S_p' d\gamma = -2\left(\alpha \dfrac{dS_p'}{S_p'} + d\alpha\right)$ and $d\tau_p' = -\dfrac{1}{2T_p'^2} dT_p'^2$

If we let dS_p' and $d\alpha$ represent deviations from the correct values of the respective parameters, then we can assess the effects that such deviations will have on the derived values of these parameters. To simplify this assessment, we will estimate the effects of each deviation independently.

$dS_p'/Sp' = 0.25$
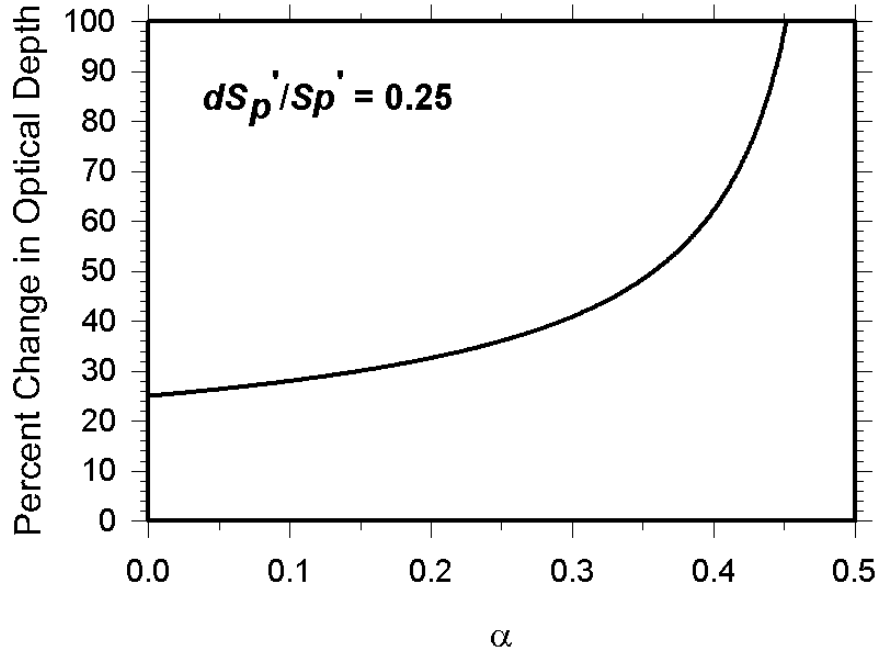
Figure 3.5.3 Computed sensitivity in optical depth from error in S_p'

Figure 3.5.3 shows an example of expected error if $d\alpha \equiv 0$. The plot in the figure summarizes the percent change produced in the computed values of τ_p' by an error of 25 percent in the estimate of S_p'. The importance of such errors is determined by what the purpose of the computed values are.

The plot in figure 3.5.4 illustrates expected magnitude of deviation in the computed optical depth as a function of α when $dS_p' \equiv 0$ and there is a typical 5 percent error in the magnitude of the integrated backscatter. We see that the magnitude of the error in the optical thickness becomes very large as the limit in meaningful measurements is approached at $\alpha \approx 0.475$. For larger errors in the evaluated magnitude of α, the uncertainty in τ_p' is even larger. A fact that reduces the detrimental effect revealed by these relationships is that, for a given evaluation of optical depth from a lidar profile, the random fluctuation contribution to $d\gamma$ will become smaller as more samples are used to compute the result. This means that for layers of a given optical depth, the

error in the optical thickness will be less for layers of greater geometrical depth. These are typically the types of layers of cirrus and aerosols which are the greatest interest to climatological studies.

Figure 3.5.4 Sensitvity in optical depth from errors in integrated backscatter

The accuracy of the retrieved backscatter lidar signals relies heavily on the signal to noise ratio of the data. The signal to noise ratio rises and falls with the following:
        1) inverse of the strength of the background signal,
        2) strength of cloud or aerosol return, and
        3) horizontal smoothing of lidar shots.
Tests using simulated backscatter data developed from GLAS instrument specifications as of January 1, 2000 were run to estimate the accuracy of lidar signal techniques for extracting the extinction to backscatter ratio directly from the signal return of elevated layers and to estimate the accuracy of optical depth retrievals as per the operational algorithm. These tests were performed using three different background lighting conditions: 1) no background, 2) daytime over dark ocean, and 3) daytime over bright cloud. Figure 3.5.5 shows simulation results comparing a layer with no background noise with the same layer after bright daytime noise was applied. Resultant retrievals using 1 second averaging (simulating cloud processing) show the drop in accuracy in S_p and τ calculations with increased background noise. For these simulations, η was set to 1.0.

The effect of noise on GLAS optical properties retrievals

SIMULATED GLAS BACKSCATTER PROFILE
NO NOISE CASE, 1 SEC

SIMULATED GLAS BACKSCATTER PROFILE
DAY, BRIGHT CLOUD CASE, 1 SEC
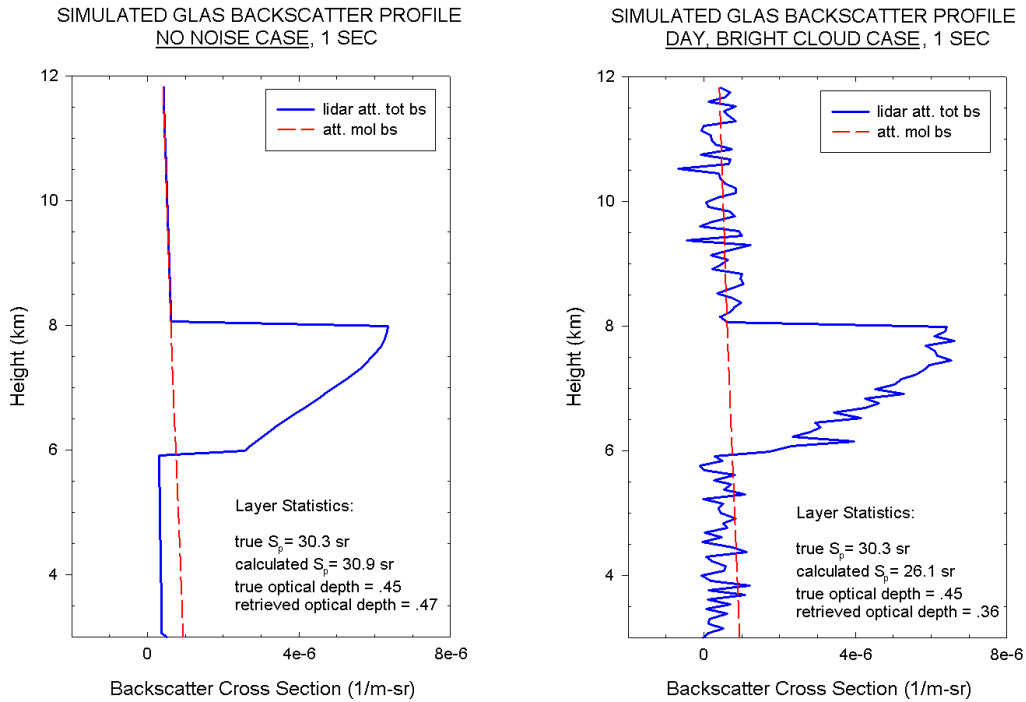
Figure 3.5.5 Simulations showing the effect of noise on GLAS optical properties retrievals from a single layer of optical depth 0.45

Figure 3.5.6 compares the log signal difference technique and the integrated ratio technique for overall accuracy in calculating S_p from the lidar backscatter signal inside elevated layers. In general, although the log signal difference technique is slightly more accurate during no noise situations, the integrated ratio technique, our current algorithm, is much more stable during noisy signals with acceptable error. Errors for both 4 second (aerosol) and 1 second (cloud) are shown. Figure 3.5.7 displays simulated error results for optical depth retrievals also as a function of noise using the current protocode algorithm. The simulations show that on average for single layer conditions of moderate optical depth, output error will be near 4 to 5 percent for low noise situations but rise during noisy conditions to 20 percent for clouds. Aerosol errors remain much more stable with increasing noise. These simulations can be thought of as a "best case" scenario since multiple layers, low optical depth situations, high optical depth situations, and the addition of multiple scattering all tend to increase the error.

66
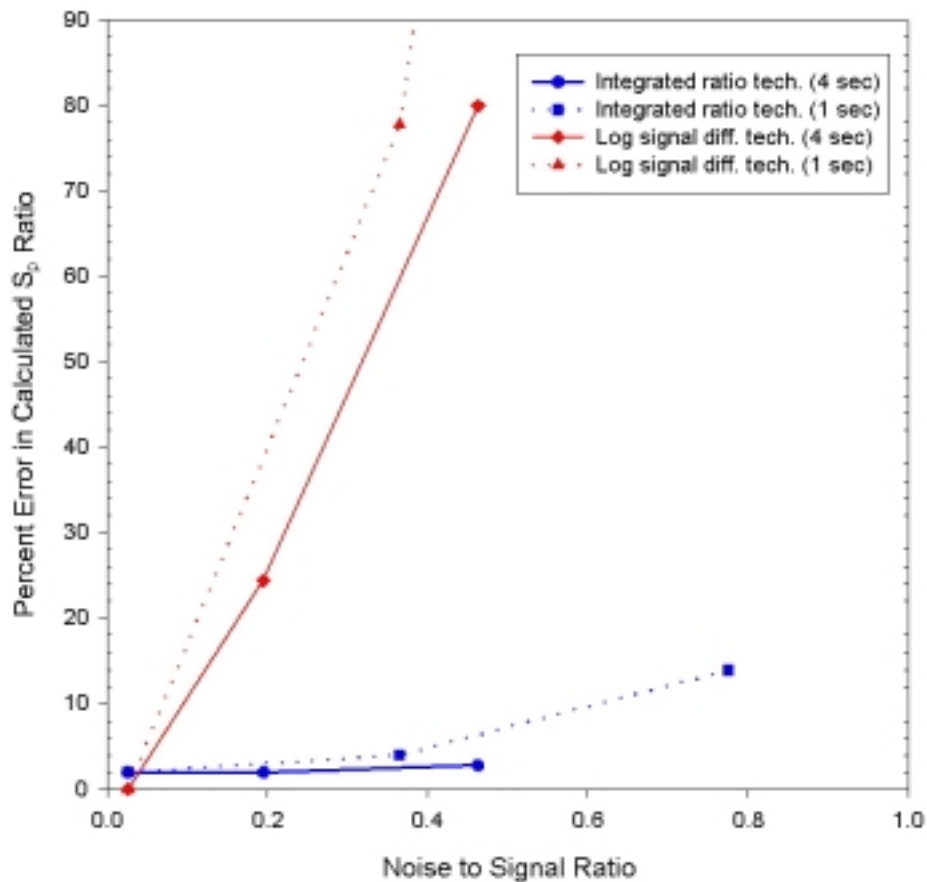
Figure 3.5.6 Accuracy of lidar techniques for extracting extinction to backscatter ratio (S_p) from the signal profile as a function of noise using GLAS simulated backscatter profiles for a single layer of optical depth 0.45

Errors in the transmittance solution due to lidar signal degradation and atmospheric molecular misrepresentation are discussed further in Section 3.2.2.

Real time error analysis will accompany the optical properties processing. Representative error profiles of the signal for the various time resolutions will be developed from the standard deviation profiles superimposed on the original signal. Optical processing of the error profiles will allow for the calculation of error bars for calculated S_p, retrieved optical depth, and backscatter and extinction profiles. Details of the methodology can be found in sections 4.5.1, 4.5.2, and 4.5.4.

The graphs in this section represent an initial analysis into quantifying errors in optical products from the GLAS atmosphere channel. Error analysis is on-going and will result in more detailed projections with further protocode testing using simulated lidar returns. Because the particulate transmission is restricted to a value of T_L and above ($.35 < T_L < .45$) to keep the integration stable, effective accumulative particulate optical depth is restricted to ≈ 0.9 or below, and true optical depth is restricted to roughly 3.0, depending on the value of η. With cloud profiles averaged to 1

second or 7.5 km and aerosol profiles averaged to 4 seconds or 30 km, we believe optical depths can be calculated to within an error of 50% in the troposphere.
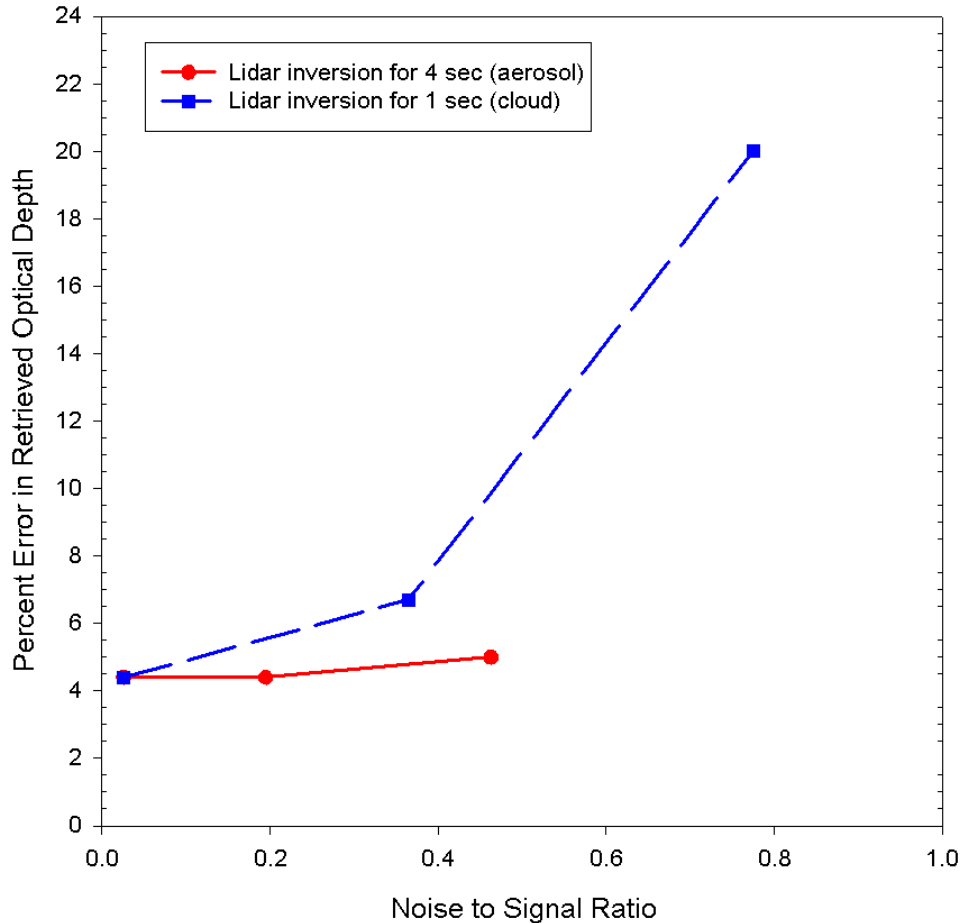
Figure 3.5.7 Accuracy of lidar inverson retrievals for layer optical depth as a function of noise using GLAS simulated backscatter profiles

3.5.3 Confidence Flags

Confidence flags for GLA10 and GLA11 will include a measure of quality for the following parameters per layer: aerosol backscatter cross section, cloud backscatter cross section, aerosol extinction cross section, cloud extinction cross section, cloud optical depth, elevated aerosol optical depth, and boundary layer optical depth. Polar stratospheric clouds are incorporated into the aerosol analysis. The quality rankings, ranging from 0 to 15, will come directly from the magnitude of error bars created from the real time error analysis described in Section 3.5.2. Use flags will accompany the quality flags. The optical depth and extinction use flags are designed to contain atmospheric layer type information, such as water versus ice cloud, or maritime versus continental aerosol, or tropospheric versus stratospheric aerosol. This information will be passed to the use flags from the S ratio default decision matrices. The backscatter use flag will contain information on signal saturation conditions per layer. See Section 4.5.4 for a further discussion on quality control.

3.6 Multiple Scattering Correction

The multiple scatter factor is a complex function of particle scattering phase function and the vertical distribution of the scattering plus the field of view and the height of the lidar receiver. A procedure for the correction of the GLAS lidar signal for multiple scattering from cirrus and other optically thin clouds is presented in this section. Two methods have been developed for calculations of GLAS multiple scattering using cloud and aerosol models. One is a precise Monte Carlo radiative transfer model, and the second is a computational fast analytic approximation. However, a precise radiative transfer calculation to account for the effects of the multiple scattered contribution is not practical for real time analysis, and approximation by semi-empirical methods is necessary. For initial level 2 processing, the value of the multiple scattering factor may be decision matrixed into a look up table based on parameterized calculations. The best method to ultimately correct for multiple scattering is a subject in development but a preliminary acceptable procedure can be described.

3.6.1   Theoretical description

The component of the lidar signal from multiple scattering arises chiefly due to the strong forward scatter component, or diffraction peak, where the forward scattered photons stay within the receiver FOV. The width of the forward scattering is strongly dependent on particle size and may be approximated by

$$\theta^2_s \approx \lambda^2/\pi^2 r^2$$

where θ_s is the width of the forward diffraction peak containing one-half of the scattered photons and r represents the particle radius. If none of the forward scattered photons were lost from the FOV of the receiver, higher order scattering is neglected, the transmission term in the lidar equation can be written as $e^{-2(\tau-1/2\tau)}$. This is equivalent to $e^{-2\eta\tau}$ where $\eta=0.5$. In actuality neither assumptions just mentioned will necessarily hold. Only for the cases where the ratio of the diameter of the receiver FOV foot print at the top of a scattering layer is sufficiently large, and width of the forward peak sufficiently narrow will the approximation be close. However for space borne lidar the FOV footprint is large compared to terrestrial systems, approximately 100 m diameter, and for cloud scattering, especially cirrus, the narrow forward peak is expected. Under these situations prior work with ground based and airborne lidar indicate that the constant η value near 0.5 is an acceptable approximation. A constant value of η can be assumed and variation in the value from 0.5 determined for a first order correction of higher order scattering and loss of photons from the receiver FOV. For aerosol, or extended ranges due to multiple cloud layers, a constant η factor or values near 0.5 will not hold. In any case, values of η as a function of layer heights and propagation depth, and parameterized cloud and aerosol particle models, can be calculated as a basis for look up tables for real time processing.

Given the GLAS 532 nm channel specifications, Monte Carlo calculation show that the multiple scattering effect is expected to be significant (on the order of $\eta=0.5$) in cloud situations, but is less than 20 percent (with $\eta=.83$) in the worst aerosol situations.

To account for the multiple scattering effect, we assert then the transmittance and optical depths obtained from the solution to the lidar equation are apparent or effective values. For lidar cirrus studies Platt (1981) proposed an extension of the single-scattering lidar equation to account for multiple scattering by introducing the parameter η introduced before:

$$(3.6.1) \quad \tau'_p(z) = \int_{z_t}^{z} \sigma_p(z')\eta(z')dz' = \int_{z_t}^{z} S_p\beta_p(z')\eta(z')dz' \quad \text{and}$$

$$(3.6.2) \quad T'_p = e^{-\tau'_p}$$

The parameter η is the multiple scattering correction factor where $0 < \eta \leq 1$. The superscript prime is used to denote the effective value. Modeling studies have indicated that usefully accurate results can be obtained if a constant value of η is used within the integrations for typical cirrus layers. We use this to obtain:

$$(3.6.3) \quad \tau'_p(z) = S'_p \int_{z_t}^{z} \beta_p(z')dz'$$

where $S'_p = \overline{S_p \eta}$ is denoted the effective extinction to backscatter ratio.

The multiple scattering factor is accurately calculated by Monte Carlo methods or approximated by analytic methods (Duda et al., 1999). As mention above, the η coefficient as a constant value is inaccurate to apply toward some aerosol or cloud layers. However, for the case of cirrus clouds (or other clouds) where the cloud particle sizes are much larger than the wavelength of the lidar, η is shown to be a property of the forward diffraction phase function and can be computed analytically. The question to be answered by a parameterization is the appropriate η factor.

From diffraction theory, the width of the diffraction peak may be alternatively defined as 1.21 λ/d, where λ is the lidar wavelength and d is the particle diameter. Using this definition of the diffraction peak width, the portion of the energy scattered in the peak can be calculated for ice spheres from Mie theory. The results are presented for the 0.532 nm channel in Figure 3.6.1 as a function of particle radius. For monodisperse spheres, the scattering in the diffraction peak oscillates. The central line in Figure 3.6.1 represents the diffraction peak scattering for a broad size distribution of particles, in which the size averaging tends to smooth out the oscillations.

Diffraction peak scattering probability
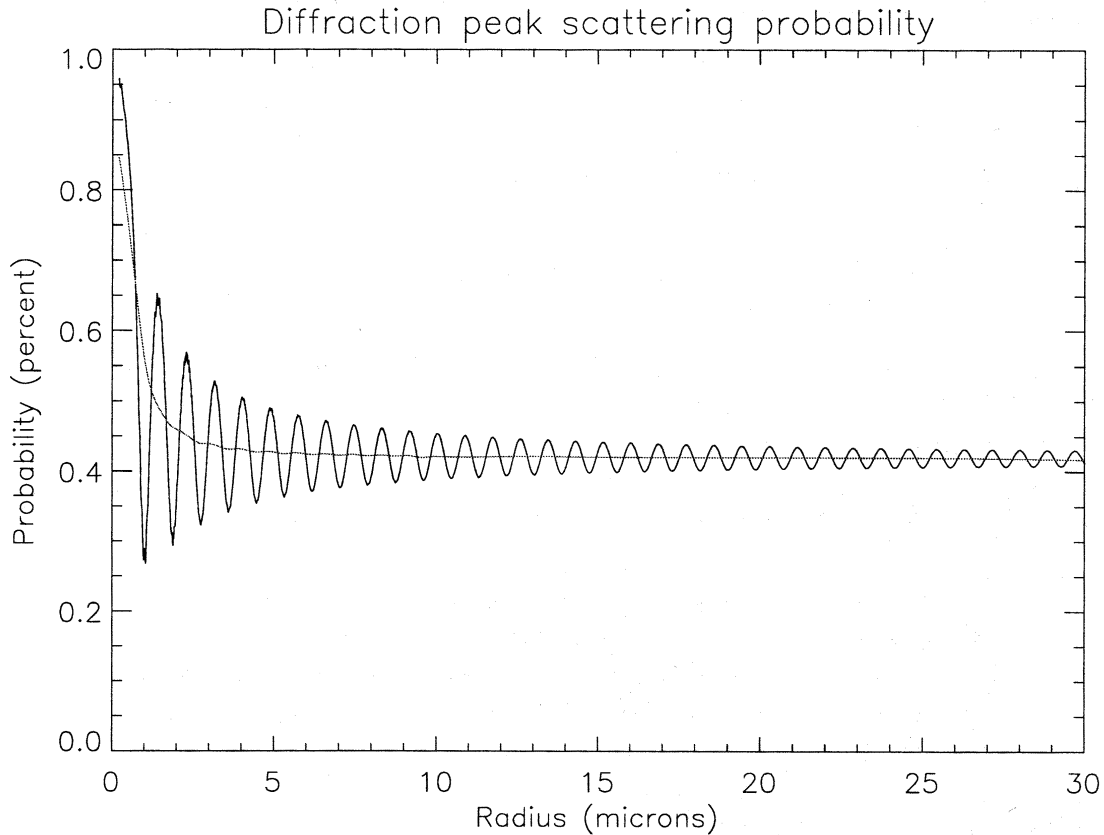
Figure 3.6.1 The portion of the energy scattered in the diffraction peak as a function of particle radius for ice spheres. For large particles, the portion approaches 0.42.

As the particle size increases, the fraction of the energy scattered into the diffraction peak approaches 0.42. Nicolas et al. introduce a similar model where the amount of energy scattered within the forward peak $(1 - \eta)$ is given as

$$(3.6.11) \quad 1-\eta = \frac{0.5}{\omega} + R,$$

where ω is the single-scattering albedo and R is a measure for nonspherical particles that describes the fraction of light refracted into the forward direction through opposite parallel faces.

From the methods and results as described above plus other available knowledge appropriate values to apply in calculations can be obtained. Also values of η for cirrus analysis can be parameterized based on the height of the cirrus layers and observed depth. As an example of the effectiveness of approximations, values of η beneath cirrus are shown as determined from accurate Monte Carlo calculations in figure 3.6.2. For a given depth below the cloud the η value is seen to be independent of optical depth as required. In addition the value immediately below the cloud has an η of approximately 0.4. The increase for depths below cloud base more than 2 km greater are not dramatic.
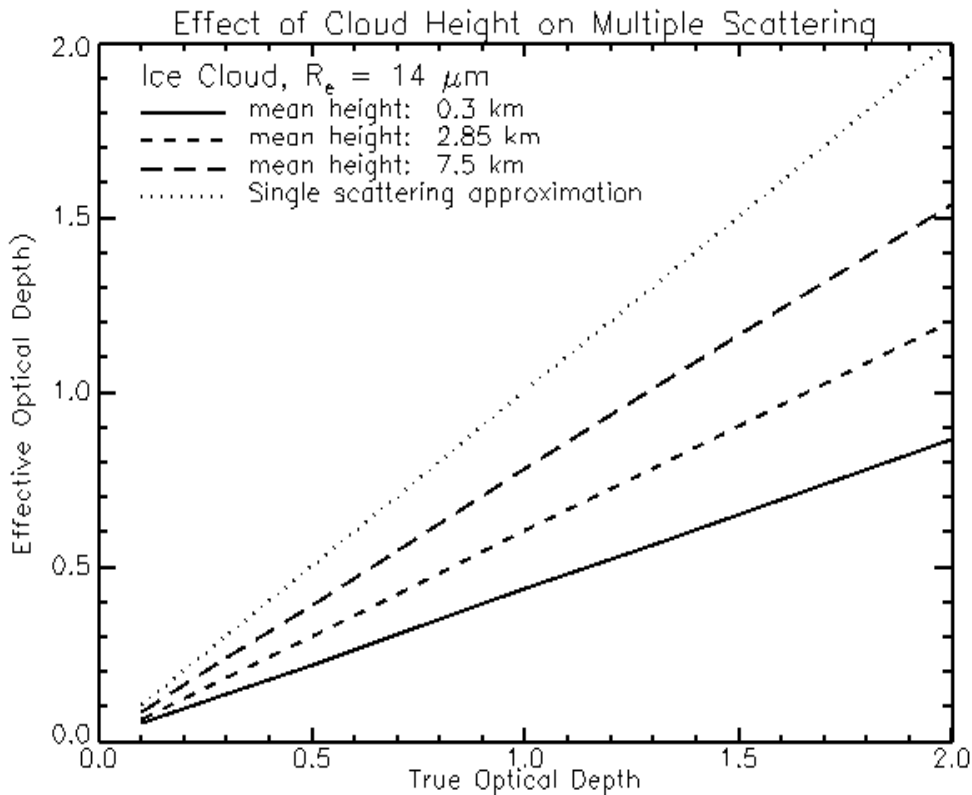
Figure 3.6.2 Cloud height plays an important role in determining multiple scattering from ice clouds. The results of Monte Carlo calculations of the apparent optical depth at the surface as a function of the true optical depth for differing cloud layers is shown. The lower the cloud, the lower the ratio of effective to true optical depth, or η.

A cloud classification based on cloud temperature, geographic location, cloud height, and integrated backscatter in the layer will be used to parameterize a systematic cloud multiple scattering factor look up table. The table will be generated by systematic Monte Carlo calculations supplemented by analytic models and is discussed in detail in section 3.6.2, below.

For aerosol, there is typically not the sharp forward scattering peak as there are for clouds and their larger particles. The approximation for a constant η with depth is not expected to hold as well as for clouds. However the initial Monte Carlo calculations or GLAS parameters for the aerosol multiple scattering indicate that the multiple scattered component of the lidar signal is no more than 20%. Also most generally the more optically thick aerosol are concentrated in thin layers at the surface. The approximation of a constant η for aerosol will be tested. It is expected that the errors will not be a dominant uncertainty for optical depth retrievals. A scene classification based on geographic location, integrated backscatter in the layer, and aerosol height distribution plus a systematic aerosol multiple scattering calculation look up table will be used for an η factor. For a layer labeled as PSC, a special subset of the aerosol look up table will be used. Errors in η extracted from look up tables based on modeled results have yet to be formulated due to the design work still in progress.

3.6.2 The Multiple Scattering Algorithm

The multiple scattering algorithm will compute both the multiple scattering factor (η) used to correct the optical depth and extinction retrievals as discussed in the above section, and the range-to-surface delay. The latter is not used by the atmospheric processing routines, but is output on the GLA11 product for use by the altimetry processing group. The multiple scattering algorithm does very little in the way of computation. It merely obtains values of η and range-to-surface delay from pre-calculated lookup tables corresponding to the inputs described below.

The multiple scattering factor (η) depends on the extent to which photons in the laser pulse have their trajectories altered by scattering events. This in turn is a function of the microphysical and physical properties of the cloud and aerosol layers in which the scattering occurs. Specifically, the effect of scattering depends on (a) particle sizes within the scattering layer, (b) the layer optical depth, (c) the proximity of the scattering layer to the surface (for the range-to-surface delay only), and (d) the physical thickness of the layer. It is important to understand that each of these factors is examined here independently, and the actual multiple scattering factor and scattering-induced range-to-surface delay are a result of both competing and additive effects from these various sources.

The following inputs are used in the algorithm

   a. Day of year
   b. Layer type
   c. Layer Top Height
   d. Layer Bottom Height
   e. Layer Average Temperature
   f. Estimated Effective Optical Depth of the Layer
   g. Latitude and Longitude of Observation
   h. Height of surface from DEM

As mentioned above, most of these inputs are used to index into lookup tables that contain corresponding values of the multiple scattering correction factor and the range-to-surface delay. A combination of Monte Carlo and analytical calculations will be performed prior to launch to obtain the values of η and range-to-surface delay in the lookup tables. The tables are explained in greater detail in section 3.6.2.1 below, but first we discuss the major inputs to the multiple scattering algorithm and note their effects on the multiple-scattering factor and the range-to-surface delay. As each input is considered, the others are neglected; e.g., when optical depth is examined, variations in layer thickness, particle size, etc. are not considered. It must therefore be borne in mind that the relationships outlined here will likely differ from those seen in observations of scattering layers, where the effects of each input is enhanced or diminished by those from others.

1. *Layer optical depth*

This quantity is directly input to the algorithm. Increases in the optical depth of the scattering layer make more surfaces available for scattering, thereby increasing the potential for photons to be removed from the emitted direction. All other things being equal, therefore, optical thick layers

(both clouds and aerosols) will scatter away more photons than thin layers. The layer optical depth is important for both η and the range-to-surface delay.

2. *Proximity of the scattering layer to the surface*

This input quantity is obtained from the bottom of the layer, and from knowledge of the surface elevation obtained from a pre-determined lookup table (DEM) over all longitudes and latitudes. It is important for the calculation of the range-to-surface delay and in the computation of η.

When a photon is scattered high in the atmosphere, it travels further along the scattered direction prior to reaching the surface, than it would if the scattering event occurred nearer to the surface. Very near the surface, most scattered photons, regardless of the angle at which they are scattered away from the emitted direction, will likely remain within the view of the receiver. Higher in the atmosphere, the range of scattering angles at which photons will still remain within the field of view is more limited, and only those scattering events that occur at small enough angles to retain the photon within the instrument's field of view contribute to the magnitude of the multiple scattering factor and range-to-surface delay.

3. *Layer physical thickness*

This input quantity is determined from the layer bottom and layer top heights. The geometric thickness of the scattering layer is important for both the range-to-surface delay and η.

The physical thickness of the cloud impacts scattering-induced delay in much the same way that the height of the cloud above the surface does. As we saw above, all other things being equal, scattering events closer to the surface are more likely to contribute to the scattering factor. This understanding can be extended to the physical thickness of the cloud as follows. If all scattering surfaces are concentrated in a narrow region at the base of the layer, i.e. if the cloud (or aerosol) is physically thin, this is equivalent to stating that the scattering occurs nearer the surface. If, on the other hand, the scattering surfaces are distributed over a large physical thickness of the cloud, some scattering events take place near the surface, whereas others occur at larger distances from it. Scattering events from the higher elevations within the layer are likely to direct the photons away from the field of view of the receiver, and cause little multiple scattering effects recorded by the receiver.

4. *Cloud particle effective radius*

This input quantity is obtained from a look-up table computed as a function of latitude, longitude, layer height, and month using information from satellite studies of clouds and aerosols across the globe. Figure 3.6.1 shows how the diffraction peak of scattering varies with particle size; along with oscillating values for mono-dispersed spheres, the curve for a broad distribution of particle sizes is also shown. As particle sizes become larger, a decreasing fraction of the emitted energy is forward scattered; this reduces the number of photons that remain within the footprint of the receiving instrument. At some threshold value of particle radius, around 15-20 microns, this relationship is bounded, and a fixed fraction of the emitted energy then remains within the forward scattered portion, and further increases in particle size do not cause any changes. Thus, both the

atmospheric multiple scattering effect (η) and the range-to-surface delay depend on the particle size.

The I-SIPS software will retrieve particle size from this lookup table, which will be generated and supplied by the science team. Here we define the size of the table and how the particle size will be obtained from the table. There will be 18 latitudes, 18 longitudes, 12 months and 3 heights for a total of 11664 entries. Thus, the particle size lookup table will be a 4 dimensional array as: P (18,18,12,3). Accessing the appropriate bin will be a matter of computing the necessary indices from the spacecraft position (latitude/longitude) and the layer height and associated month (from the clock data). If I, J, K and L are the four indices of the particle size array, then:

I = (90-latitude) / 10 + 1
J = longitude / 20 + 1
K = julian day / 30 +1, where julian day is the day of the year

And L is calculated as shown in table 3.6.1.

Table 3.6.1. Calculation of the 4th index of the
particle radius lookup table as a function of layer height.

L	Layer Height (km)
1	<3.0
2	3.0 – 6.0
3	> 6.0

3.6.2.1 Multiple scattering factor (η) tables

Monte Carlo calculations will be made by the science team to generate tables of the multiple scattering correction factor (η) and the range-to-surface delay. The details of how these tables are generated are not presented here. The I-SIPS software merely generates the proper indices (based on the inputs) from which to retrieve the information from the tables. The multiple scattering correction factor will be a function of optical depth, particle size, height above ground, and the physical thickness of the scattering layer. Much like the particle size table described above, these tables will be accessed by computing the array index from the appropriate input parameter. Specifically, the multiple scattering factor table will have four dimensions: $\eta(\tau,r,d,h)$, where τ is the layer optical depth, r is the particle size, d is the geometric depth of the layer, and h is the height of the layer. The dimension of this table will be (12,11,7,8). If I, J, K, and L are the 4 indices of the array, their values are defined from the inputs as shown in tables 3.6.2, 3.6.3 and 3.6.4 and 3.6.5.

Table 3.6.2. Layer optical depth, the first index of the multiple scattering correction table.

I	Layer Optical Depth
1	<0.02
2	0.02 - 0.05
3	0.05 – 0.10
4	0.10 – 0.20
5	0.20 – 0.35
6	0.35 – 0.60
7	0.60 – 0.90
8	0.90 –1.20
9	1.20 – 1.60
10	1.60 – 2.00
11	2.00 – 2.50
12	> 2.5

Table 3.6.3. Particle size, the second index of the multiple scattering correction table.

J	Particle Size (μm)	J	Particle Size (μm)
1	1.0	9	30
2	2.0	10	50
3	3.0	11	>50
4	5.0		
5	7.0		
6	10		
7	14		
8	20		

It should be noted that for particle sizes less than 0.1μm, the value of η at J=1 is used, and that for particle sizes greater than 50μm, the value of η at J=11 is used.

Table 3.6.4. Layer physical thickness, the third index of the multiple scattering correction table.

K	Layer Geometric Depth (km)
1	< 0.200
2	0.200 – 0.500
3	0.500 – 1.0
4	1.0 – 2.0
5	2.0 – 3.5
6	3.5 – 6.0
7	> 6.0

The last index (L) is calculated from table 3.6.5, which shows the index as a function of the height of the bottom of the scattering layer above the local surface. This must be calculated by subtracting the DEM value for the given latitude/longitude from the retrieved layer bottom height.

Table 3.6.5. Layer bottom height, the fourth index of the
Multiple scattering correction table.

L	Layer Bottom Height (km)
1	< 0.20
2	0.20 – 0.50
3	0.50 – 1.0
4	1.0 – 2.0
5	2.0 – 4.0
6	4.0 – 8.0
7	8.0 – 12
8	>12

Once all the indices are calculated, the multiple scattering correction factor (η) is retrieved from the table.

3.6.2.2 Likely Range-to-Surface Delay

The range-to-surface delay is extremely important for the proper assessment of the accuracy of the altimetry product. Monte Carlo calculations can be used to assess this error based on the layer effective optical depth, particle size, layer geometric depth and the height of the layer above the surface. The last two of these can be accurately characterized by the lidar channel, as can the optical depth, but to a lesser degree of precision. As with the calculation of η, the greatest uncertainty in the assessment of the range-to-surface error is the uncertainty of the particle sizes that comprise the scattering layer. As for the calculations of η, the estimated particle size will be obtained from the lookup table generated by the lidar science team and described in section 3.6.2, above. There will undoubtedly be errors associated with the assumed particle sizes for a given layer. However, some knowledge is put into the selection of particle size and we will call the results of this process the likely range-to-surface error. In the following section, we present a method to compute the maximum range-to-surface error. These two approaches will provide the altimetry group the most information on the multiple scattering effect on surface ranging that can be derived from the lidar channel. The multiple scattering algorithm will try to quantify the uncertainty in the estimated range delay and will include it in the output products in GLA11.

The range-to-surface delay table will be generated independently from the η table using Monte Carlo methods based on the lidar system parameters for the 1064 (altimetry) channel. It will be a four dimensional array with dimensions: (I=12,J=11,K=7,L=8). The I, J, K, and L indices are calculated from tables 3.6.2, 3.6.3, 3.6.4, and 3.6.5 respectively.

3.6.2.3 Multiple Scattering Warning Flag

The multiple scattering warning flag (F) is based on the total column optical depth (aerosol plus cloud) calculated in GLA11. It is intended as a way to quickly obtain information about the potential severity of multiple scattering with regards to the range-to-surface calculated by the altimetry processing software. It will be output on the GLA11 product for use by the altimetry group. A more rigorous and quantitative determination of the effect of multiple scattering on the range-to-surface is also included on the GLA11 product and is described above in section 3.6.2.2. The multiple scattering warning flag will have values ranging from 0-14, based on the total column optical depth as detailed in table 3.6.6.

Table 3.6.6. Calculation of the multiple scattering Warning flag

Optical Depth	Multiple Scattering Warning Flag
< 0.01	0
0.01 – 0.03	1
0.03 – 0.06	2
0.06 – 0.10	3
0.10 – 0.15	4
0.15 – 0.225	5
0.225 – 0.30	6
0.30 – 0.40	7
0.40 – 0.50	8
0.50 – 0.67	9
0.67 – 0.90	10
0.90 – 1.20	11
1.20 – 1.60	12
1.60 – 2.00	13
> 2.00	14

A warning flag value of 15 will signify "invalid".

In summary, the algorithm will produce following quantities which will be written out to the GLA11 data product:

     I.   Multiple scattering factor (ranges from 0 to 1)
     II.   Surface range delay estimate (millimeters)
     III.   Surface range delay uncertainty estimate (millimeters)
     IV.   Multiple Scattering Effect Warning Flag (ranges from 0 to 15)
     V.   Particle sizes estimated and used in the scattering calculation

3.6.2.4 Maximum Range-to-Surface Delay

As mentioned above, the greatest uncertainty in determining the effects of multiple scattering arises from uncertain values of global particle size distributions. Using data from regional experiments, cloud and aerosol particle sizes are obtained in a fairly coarse grid, both spatially and

temporally. In many regions of the world, such approximation is nonetheless the best that is possible. Particle sizes measured at a coastal Antarctic station, such as Palmer, for example, must be attributed to much of the coast of that continent. Broad latitudinal and longitudinal grids are defined within which the particle sizes are estimated from such regional studies.

An alternate approach to understanding the effect of multiple scattering on the range-to-surface, however, exists. By this method, described below, it is possible to estimate the largest likely error in observations that will result from multiple scattering, even when particle sizes are unknown. In effect, this yields an upper limit to the uncertainty (due to multiple scattering) in the GLAS altimetry measurements. *Though the approach is described here, the actual implementation will be done in the altimetry processing code. We will provide the altimetry team with a pre-calculated lookup table which they will use to asses the maximum range-to-surface error.* The following discussion is based on work performed by Ed Eloranta at the University of Wisconsin.

Photon delays caused by scattering are dependent on both particle size and cloud altitude. Because particle sizes are not known, prudent estimation of ranging errors requires the assumption of worst case particle sizes at each altitude. The largest multiple scattering delays occur for particle sizes between 1 and 20 microns. Since particle sizes in this range are common in the atmosphere, the safest way to compute error bars describing the effects of multiple scattering would be to assume that clouds always contained particle sizes producing the maximum delay. In this way we are assured that this is a maximum upper limit on the ranging error due to multiple scattering. In addition, if the particle size at each altitude is selected to produce the largest delay, the delay is not a strong function of altitude, especially for small optical depths.

Let us define the 1/e half width of the received surface return pulse (in the absence of atmospheric scattering) as: $\delta_p = \sqrt{\delta_0^2 + \delta_s^2}$ where δ_0 is the 1/e half width of the emitted laser pulse and δ_s is the standard deviation of the surface roughness elements. An increase in surface roughness produces effects which are indistinguishable from those caused by lengthening the laser pulse (δ_0). As we know, atmospheric multiple scattering tends to broaden the received surface return waveform. Surface roughness and slope will have a similar effect. Surface roughness broadens both the directly reflected pulse and the multiply scattered return symmetrically and thus has no effect on the *centroid* estimate of altitude. However, because increased surface roughness produces a longer directly reflected pulse with a flatter peak, adding the temporal skewed atmospheric scattering will shift the center position of the *Gaussian* fit.
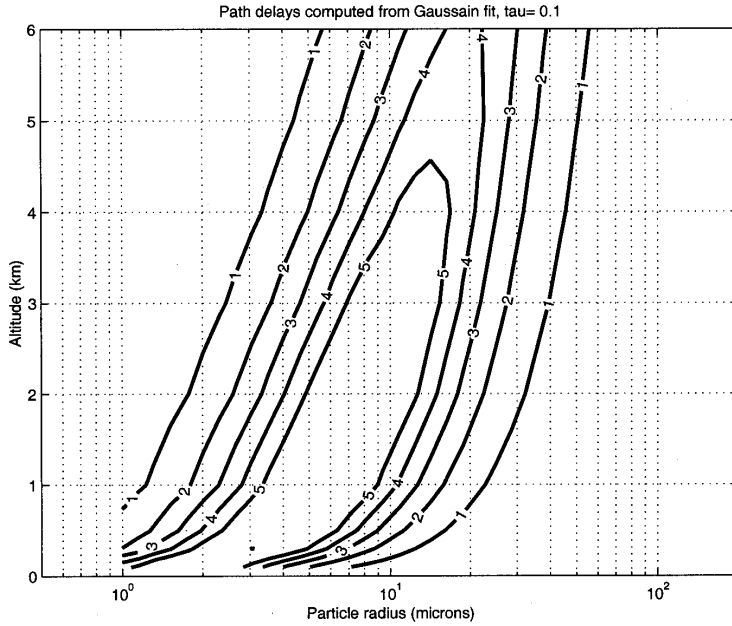
Figure 3.6.1. Path delay (cm) computed from Gaussian fit with δ_p = 2 and τ = 0.1.

An examination of figure 3.6.1 shows that while the particle radius that produces the worst delay changes with altitude, the maximum value of the photon delay is nearly constant with altitude. This simplifies the error calculation because the worst case error becomes a function of the total optical depth and it is not necessary to know the vertical profile of the scattering cross section. Using this observation, it is possible to generate a plot of the worst case errors as a function of surface roughness and optical depth which may then serve as a basis for assignment of realistic multiple scattering error bounds for the GLAS altitude measurements.
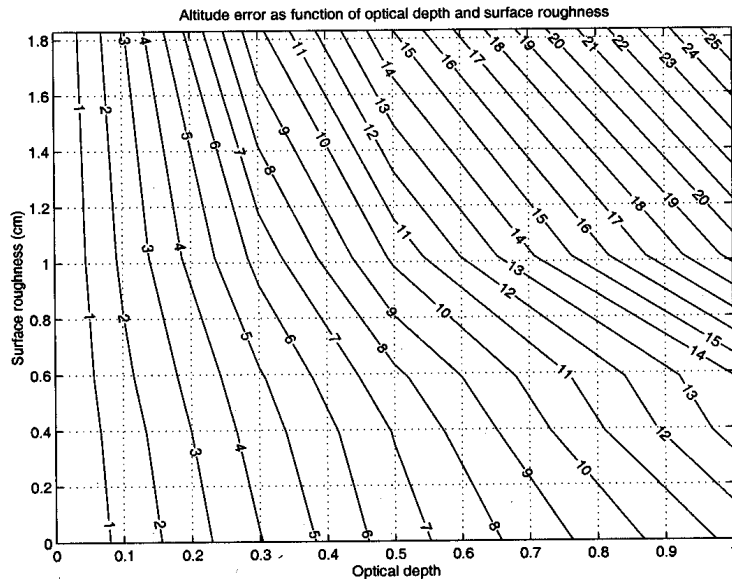
Figure 3.6.2. Contour plot of altitude error as a function of optical depth and surface roughness. Note that the y axis is actually in units of meters, not cm.

80

Figure 3.6.2 shows the maximum ranging error as a function of atmospheric optical depth and surface roughness. The figure provides a means of assigning an upper bound to the scattering induced error in the GLAS altimetry measurements. The optical depth is estimated from the 532 nm lidar channel. The width of the received pulse determined from a Gaussian fit to the received waveform would be used as an upper limit on the value δ_p. The lidar science group will do the necessary calculation to prepare a two dimensional table that will have optical depth as one index and δ_p as the other as shown in table 3.6.7 below. The contents of the two dimensional array will be the maximum delay for each δ_p, optical depth pair. The values may be linearly interpolated from the given points to obtain the delay for specific values of optical depth and δ_p. We will supply this to the altimetry software group and they can use their measured surface pulse width and our total optical depth (output on GLA11) to index into the table to retrieve the maximum delay.

Table 3.6.7 The calculation of the I,J indices of the maximum range-to-surface delay table

δ_p (m)	I Index	Optical Depth	J Index
0.20	1	0.05	1
0.40	2	0.10	2
0.60	3	0.20	3
0.80	4	0.30	4
1.0	5	0.40	5
1.5	6	0.50	6
2.0	7	0.60	7
2.5	8	0.70	8
3.5	9	0.80	9
4.0	10	0.90	10
5.0	11	1.0	11
6.0	12	1.2	12
7.0	13	1.4	13
8.0	14	1.6	14
9.0	15	1.8	15
10.0	16	2.0	16

4 Practical Application

This section address the practical issues related to coding, implementing and running the algorithms. These topics include the type and source of input data required to run the algorithm, execution time, program flow considerations (execution order), and examples of output where appropriate. Each algorithm will be addressed separately, and in the same order they were presented in section 3.

4.1 Normalized Lidar Signal

4.1.1 Required Input Data

In addition to the raw lidar return signal for each channel, the normalized lidar signal (GLA02) algorithm will require the laser energy (reported at 40 Hz) and the two background measurements. Also required are the dead time correction table for the 532 photon counting channel, the 1064 amplifier gain and attenuation settings, the 1064 voltage offset and the factor relating digital counts to volts. While not explicitly used in the algorithm, the 532 channel etalon filter settings should be supplied, as it may be needed in subsequent processing (GLA07). The first data bin of the 532 channel is supposed to be 41 km above local DEM. In order to compute the range (R) used in equations 3.1.1 and 3.1.2, we need to know the range from the spacecraft to the top bin of the lidar profile. While not required, it is assumed that Global Positioning System (GPS) time and position (latitude and longitude) will be provided in the input data stream.

4.1.2 Algorithm Implementation

This algorithm is relatively easy to implement and does not require a large amount of CPU time. A version of this routine has been coded in the C programming language and run with simulated GLAS data on a Silicon Graphics Indigo II workstation (R10000 processor). Results indicate that to process an orbit of data would take about 1 minute of CPU time. There will be 3 main loops for the processing of the 3 distinct data layers (2 layers for the 1064 channel). The data in the upper two layers for the 532 channel must be normalized by the number of shots summed in that layer before being used in equations 3.1.1 and 3.1.2 (as will the top layer of the 1064 channel). The bottom layer of both channels do not need normalization as they are single (un-summed) shots. Note that the laser energy must be computed at 5 Hz for the 1064 and 532 channels in order to compute P' from the 8 shot summed data (the 10 to 20 km layer). For the 532 channel, the laser energy at 1 Hz must also be computed in order to use equation 3.1.1 in the upper layer. Similarly, the background must be computed at 5 and 1 Hz in order to process the data in the 10 to 20 km layer and the 20 to 40 km layer (532 only), respectively. These calculations should take place as the 40 Hz data are being processed, using the 40 Hz laser energy and background values.

The saturation flag applies only to the 532 channel and will take the form of profiles, each bin of which will have a one-to-one correspondence with the data bins of the 532 channel. It will be a one byte value, where zero indicates that the 532 channel is not saturated and 1 denotes detector saturation. Whether a 532 bin is saturated will be determined from the magnitude of the 532 signal in that bin. The level at which saturation occurs will be determined during calibration procedures in the laboratory.

The predicted height of first cloud top will be calculated at 5 Hz using the raw 532 channel data, which means that an 8 shot average of the data from the lowest layer must be computed. This would be tacked on to the corresponding normalized 8 shot sum form the middle layer to form a profile from –1 to 20 km (at 5 Hz). A search would then begin as described in section 3.1 to find the first bin which exceeds a cloud threshold level, which will be about 2-3 photons per bin (after background subtraction). The bin number that exceeded the threshold will be stored and the height will be calculated as described in section 3.1.1. The 5 Hz profile that is used to find the height of the first cloud top is not saved as output. It is discarded.

As noted in section 3.1.1.3, GLA02 will also be computing averages of the normalized signal at the calibration heights. A crucial part of this process (for the lower calibration height) will be cloud screening the data so that no shots that have clouds in them will be included in the average. The cloud search described above will be used for this purpose. If a cloud is found anywhere above 7 km, then that second of data is not used for the computation of the signal average.

After the normalized signal for the 3 layers is computed using 3.1 and 3.2, it must be scaled to fit in a 4 byte signed integer. A signed integer is required because P' can be negative (due to the subtraction of the background value). The fairly large dynamic range of the computed signals warrants the use of a four byte integer. The scaling can be accomplished by applying a simple multiplicative scaling factor.

.

4.1.3   Interpreting the Output

The output from GLA02 consists of calculated parameters as well as passed-through quantities which are not calculated or used by the algorithm, but which will be used in the creation of level 2 data products. A list of all GLA02 output follows:

1. P at 532 nm for 3 layers: -1 to 10 km (40 Hz), 10 to 20 km (5 Hz), and 20 to 40 km (1 Hz)
2. P at 1064 nm for 2 layers: -1 to 10 km (40 Hz) and 10 to 20 km (5 Hz)
3. .532 nm saturation flag for the 3 layers: -1 to 10 km (40 Hz), 10 to 20 km (5 Hz), and 20 to 40 km (1 Hz)
4. Range from spacecraft to top of data
5. Predicted height of first cloud top (5 Hz)
6. Ground return flag (bin number) and maximum ground signal
7. 532 background (40, 5 and 1 Hz) and 1064 background (40 and 5 Hz)
8. 532 laser energy (40, 5 and 1 Hz)
9. 1064 laser energy (40 and 5 Hz)
10. 532 laser energy quality flag (40 Hz)
11. 1064 laser energy quality flag (40 Hz)
12. 532 integrated return from 40 to 20 km (1 Hz)
13. 532 quality flag (1 Hz) – based on 11 above
14. 1064 nm programmable attenuation setting (1 Hz)
15. 532 nm etalon filter parameters (1 Hz)
16. GPS time (1 Hz)

Items 1 through 8 have been thoroughly discussed in section 3.1. The 532 and 1064 channel laser energy quality flags (9 and 10) are discussed in section 4.1.5 below, as is the 532 integrated return and associated quality flag (11 and 12). The 1064 programmable attenuation setting (13) is used to compute the normalized signal (Equation 3.1.2) and should be reported in the GLA02 input data stream. The 532 nm etalon filter parameters are as yet unspecified but should provide a measure of how well tuned the etalon was to the laser frequency. The etalon filter parameters are not used in GLA02, but may be needed in subsequent processing.

4.1.4   Quality Control

At this early stage of data processing quality control should be directed at assessing the health of the instrument and the fundamental soundness of the lidar return signal. The health of the laser can be assessed by monitoring the laser energy. For each channel, a quality flag should be set for every shot (40 Hz) which characterizes the laser as follows:

1 = full laser energy (within 90 percent of expected max value)
2= marginal laser energy (between 90 and 70 percent of expected max value)
3 = deficient laser energy (less than 70 percent of expected max energy)

Used in conjunction with the above flags, the boresite can be assessed by integrating the 532 return signal from 41 to 20 km altitude (I_s). This could be done using raw photon counts after the background (computed from equation 3.1.3) is subtracted out. A quality flag should be set much like for the laser energy flag above, depending on the magnitude of the integrated return. Based on simulations, the expected number of integrated photons (the summation of 268 bins) per second from this region of the atmosphere is about 1900. For the 532 channel a quality flag can be formulated as follows:

1= excellent signal strength ($I_s > 1800$)
2= good signal strength ($1400 < I_s < 1800$)
3= marginal signal strength ($1000 < I_s < 1400$)
4= poor signal strength ($500 < I_s < 1000$)
5= bad data ($I_s < 500$)

These limits are based on simulations and may be adjusted up or down after actual data are acquired.

4.2   Attenuated Backscatter Cross Section

4.2.1 Required Input Data

This algorithm requires the output from GLA02, the normalized lidar signal and associated output as described in section 4.1.3. In addition to this, the GLA07 algorithm requires MET data in order to compute the molecular backscatter cross section at the various calibration heights (see equations 3.2.1 to 3.2.5). Realizing that MET data will most likely not be available at all times, it is important to also provide the standard model atmosphere as a backup source to obtain the required temperature and pressure profiles. The standard atmosphere actually consists of 5 models defined roughly by latitude and season as follows: Mid latitude and arctic for both summer and winter and tropical (5 standard atmosphere models in all). Additional required input includes the precision orbit determination (POD) data which includes latitude, longitude, spacecraft altitude and pointing angle. In order to transform the data height coordinate from above local DEM to above mean sea level, we need to know the spacecraft altitude (above mean sea level) and the range from the spacecraft to the top of the lidar profile. Also, to correct for vertical errors introduced by off-nadir pointing, the pointing angle is required. These issues are discussed fully in section 3.2.1.1.

4.2.2 Algorithm Implementation

The main function of this algorithm is to compute and apply the lidar calibration constant to the data to form a continuous 5 Hz profile of attenuated backscatter cross section from 41 to –1 km for the 532 channel, and from 20 to –1 km for the 1064 channel (the altitude is with respect to mean sea level). In addition, 40 Hz profiles from 10 to –1 km will also be generated for both channels. The calibration constant (C) will be computed from the signal average file generated by GLA02 and described in section 3.1.1.3. This is done immediately by GLA07, before anything else is done. This process will generate a calibration constant to be used for each second of the granule via interpolation between points or simply an average of all the calibration values.

The ability to compute accurate C values for the 1064 channel is in doubt. The algorithm will perform the calculations for the 1064 channel as described in section 3.2.1.2, but, at least initially, the laboratory calculated 1064 calibration constant will be used in equation 3.2.6. If subsequent analysis indicates that the 1064 C calculated from the flight data is good, then it may be used. Thus, for the 1064 channel, a flag should be built in which tells the software to use the laboratory C value or the C calculated from the atmospheric data.

The calculation of the lidar calibration constant requires the construction of accurate molecular backscatter profiles through the calibration layer(s). Since the entire (0 to 41km altitude) molecular backscatter profiles will be required by other GLAS atmospheric data product modules, it makes sense to compute them here. When this is done from MET data or from standard atmosphere data, it will be required to interpolate between the standard pressure levels to a vertical resolution equivalent to the lidar profile (76.8 m) as discussed in section 3.2.1.2. Since the molecular scattering depends only on atmospheric density, it makes sense to first compute the density from the temperature, relative humidity and pressure at the geometric heights corresponding to the standard pressure levels and then use the hypsometric formula to compute the density between the standard heights. This will result in a smooth density profile with 76.8 meter vertical resolution.

The output consists of 5 Hz full profiles (-1 to 41 km for 532 and –1 to 20 km for 1064) and 40 Hz profiles of only the lowest layer (-1 to 10km) for both channels. In order to form the 532 full profile, 8 shots of the lowest layer are averaged and the corresponding 8 shot sum (after being normalized) of the middle layer (10 to 20 km) is placed above that, with the normalized 40 shot sum profile (20 to 41 km) above that. The same 20 to 41 km profile is used repeatedly for each of the 8 shots for a given second. The result is a 5 Hz full profile from –1 to 41 km with respect to mean sea level. For the 1064 channel, 8 shots of the lowest layer are averaged and combined with the normalized 8 shot sum of the middle layer to form one 5 Hz profile from –1 to 20 km. Note also that the 532 saturation flag full profile (5 Hz, -1 to 41 km) must also be formed. In this case, instead of averaging in the lowest layer, we sum up the saturation flag for the eight shots yielding a number between 0 and 8. This is then combined with the saturation flag from the middle layer and the saturation flag profile from the upper layer (which is repeated 8 times).

The algorithm is not computationally intensive. A version has been coded in the C programming language and run with simulated GLAS data on a Silicon Graphics Indigo II workstation (R10000 processor). Results indicate that to process an orbit of data would take about ½ minute of CPU time.

4.2.3   Interpreting the Output

The output of GLA07 consists of profiles of calibrated attenuated backscatter cross section and the calibration constants for both channels. The 532 channel will consist of 5 Hz, -1 to 41 km (548 bins) and 40 Hz, -1 to 10.3 km (148 bins) profiles which have had saturated bins replaced with estimated cross section provided by the 1064 channel (if a flag indicates that this should occur). The 1064 channel output will consist of 5 Hz profiles from –1 to 20.5 km, and 40 Hz profiles from –1 to 10.3 km. An example of one 5 Hz profile (532 nm) output from the algorithm is shown in figure 4.2.1. This calibrated, attenuated backscatter profile was created by running a prototype GLA07 algorithm on simulated GLAS data produced by the GLAS Atmospheric Lidar Simulator (GALS).
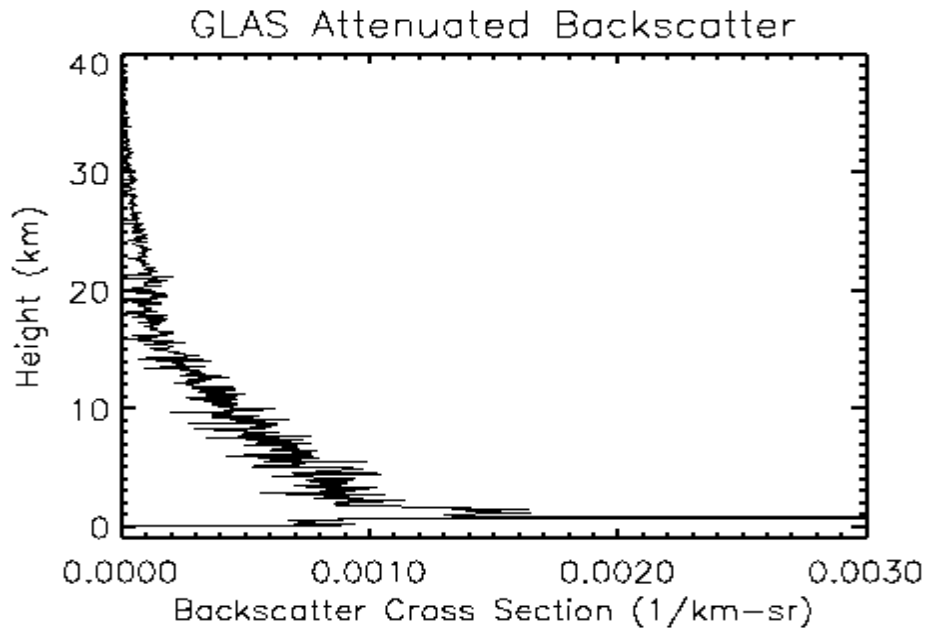
Figure 4.2.1. An example of a 5 Hz attenuated backscatter profile from 40 to –1 km which is output from the GLA07 algorithm. The profile was made by running a prototype version of the GLA07 algorithm on simulated nighttime GLAS data produced by the GLAS Amospheric Lidar Simulator (GALS).

Comparison of the above plot and figure 3.2.4 shows that the profile closely follows the molecular return until the top of the PBL is reached (at about 1.5 km height). Scattering within the PBL is much larger than the molecular scattering level due to the high concentration of aerosol there. Also seen in the figure is the large ground return signal which is truncated by the compressed scale. It is in reality several orders of magnitude larger than shown.

In figure 4.2.2, we have assembled many such profiles together and presented them in image form. This is probably the most informative way to display the data because it contains so much information. At a glance, one can see the various cloud layers, the boundary layer height and structure and any elevated aerosol layers that might be present.

Figure 4.2.2. 532 nm attenuated backscatter cross section displayed in color image form. The image is comprised of 2000 separate 5 Hz profiles like the one shown in figure 4.2.1.

In addition to the backscatter profiles, the calculated calibration constants for both channels at the two heights are output as are the actual calib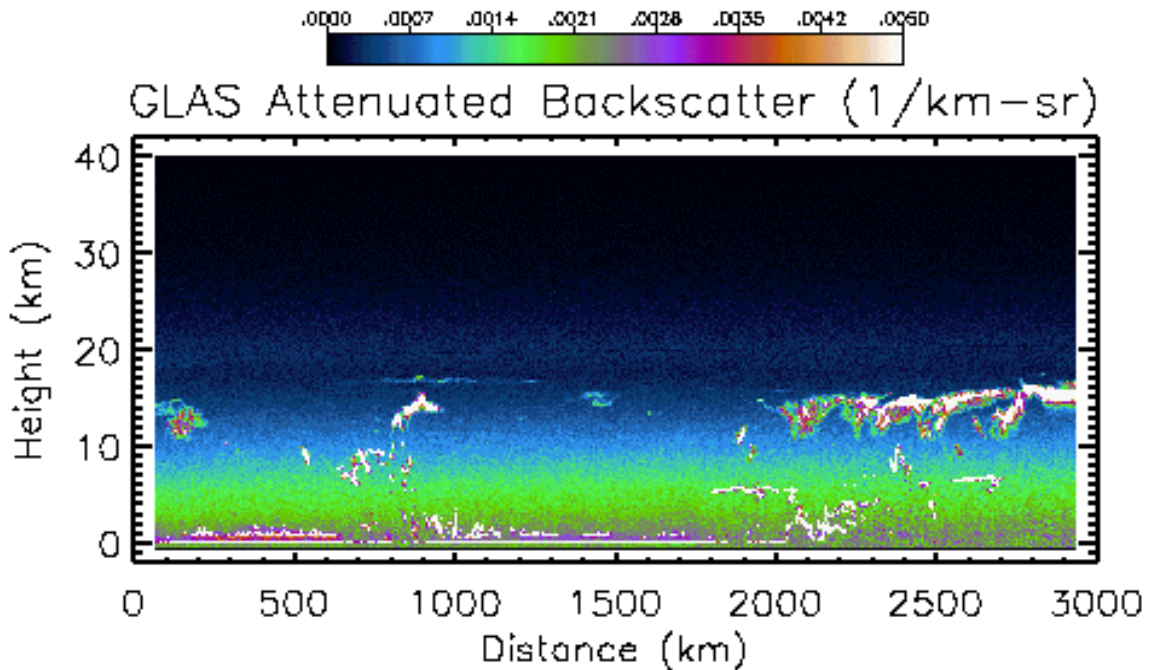ration values used in equations 3.2.12 and 3.2.13. Remember that the program is designed to use either the calculated value, a previously calculated C value or the laboratory calibration constant. With each calibration point a flag will be generated which characterizes the background condition (day, night or undetermined) which existed during the calculation of that C value. The 532 saturation flag profiles will be output at 5 Hz for –1 to 41 km and 40Hz for –1 to 10 km as described in section 4.2.2.

The profiles of attenuated backscatter cross section, which are the main output from GLA07, will consist of 548 bins, each 76.8 meters wide and stretch from 41 km to –1 km above mean sea level. The process of shifting the bins to compensate for the varying topography will mean that some of the data will be cut off on top and some will be buffered with a missing data value at the end of the 548 bin profile. For example, if data are being acquired over a region which is 5 km above mean sea level (as determined from the onboard DEM), the resulting acquired 532 nm profile will actually cover the region 46 to 4 km above mean sea level. The profile which will be output from GLA07 will truncate the 5 km of data above 41 km, and fill the region of the profile below 4 km with a missing data value (-999 is suggested). The same is true of the 1064 channel, except it extends to only 20 km above mean sea level. Note that there will be a small percentage of time where the data are cut off at the bottom of the profile and padded at the top. This would occur when the DEM value is less than mean sea level. A complete list of the output for GLA07 follows:

1. 532 nm attenuated backscatter cross section, 41 to –1 km above mean sea level at 5 Hz

2. 532 nm attenuated backscatter cross section, 10 to –1 km above mean sea level at 40 Hz
3. 1064 nm attenuated backscatter cross section, 20 to –1 km above mean sea level at 5 Hz
4. 1064 nm attenuated backscatter cross section, 10 to –1 km above mean sea level at 40 Hz
5. 532 nm saturation flag profiles, 41 to –1 km above mean sea level at 5 Hz and 10 to –1 km at 40 Hz.
6. 532 nm calibration constants – upper (C_{30}), lower (C_l) , and the actual C value that was used in equation 3.2.12
7. 1064 nm calibration constants – C_l , and the actual C value that was used in equation 3.2.13
8. Calibration constant day/night flag (see discussion, section 3.2.1.2)
9. Calibration constant quality flag (see discussion section 4.2.5, below)
10. Ground return bin as determined from POD and DEM
11. Predicted height of first cloud top, 5 Hz
12. Ground return flag (bin number) and maximum ground signal
13. 532 nm background at 40 and 5 Hz
14. 1064 nm background at 40 and 5 Hz
15. 532 laser energy at 40 and 5 Hz
16. 1064 laser energy at 40 and 5 Hz
17. 532 laser energy quality flag at 40 Hz
18. 1064 laser energy quality flag
19. 532 nm integrated return from 40 to 20 km at 1 Hz
20. 532 quality flag (1 Hz) based on 17 and 19 above
21. 1064 programmable gain amplifier setting (1 Hz)
22. 532 nm etalon filter parameters (1 Hz)
23. GPS time (1 Hz)
24. Precision Orbit Determination (POD) data (1 Hz)
25. Attitude information (pointing angle)
26. Onboard Digital Elevation Model (DEM) value used (1 Hz)

Items 1 through 10 are calculated by GLA07. The remaining output is either from the output of GLA02 or another input source.

4.2.4   Quality Control

Quality control should be implemented during the calculation of the calibration constant by checking the data quality flags that were generated by GLA02. Specifically, the laser energy flag and the integrated (20 to 40 km) return flag should be used to eliminate bad shots. Based on these flags, a bad shot counter should be kept during the calculation of C. If the number of bad shots exceeds say 5 percent of the total number of shots expected to be processed for a given calibration cycle (there are about 27,000 shots per 1/8 orbit), then the C value calculated for this calibration cycle should be flagged as questionable. Also time continuity must be checked during the calculation of C to check for large time gaps in the data that might adversely affect the calculation of the calibration constant. If a time gap greater than 30 or 40 seconds is encountered (total time for 1/8 orbit is about 675 seconds), the calibration constant should similarly be flagged as questionable.

The quality of the calibration constant can be assessed by looking at its variability with time and the difference between the constants calculated at the two different heights. The 532 nm attenuated

backscatter cross section profiles can be checked by normalizing them by the attenuated molecular profile. This should produce a profile that ranges between 0.9 and about 10.0. This test could only be applied to data with a ground return as the values below thick clouds will approach zero.

A test that could be applied to all the data would be to integrate the attenuated backscatter (β') from 40 to 20 km and divide by the integrated attenuated molecular backscatter ($\beta_m T_m^2$) to form a ratio that should be very close to unity. A major deviation from one would indicate a problem.

4.3   Cloud Layer Height and Earth's Surface Height (GLA09)

The implementation of the algorithms to find vertical cloud layer boundaries and the height of the earth's surface (ground height) will require only modest resources in terms of coding and execution time. The processing will be done on a time series of 4-second segments. Each of these will be composed of matrices of values consisting of on the order of 10000 points. Only elementary arithmetic computational and logical functions and testing will be done on these to produce the output. The output will consist of tables of values, numbering in the range of 500-1000.

4.3.1   Required Input Data

The vertical boundaries of the horizontal surfaces of cloud layers and the earth's surface will be found by testing profiles of attenuated backscatter coefficients (backscatter cross-section) against thresholds developed from the profiles themselves. The profiles will be those developed in GLA07. Only the profiles from the 532nm channel will be needed. The following list summarizes the required input for each 4-second granule.
a) 160 40 Hz attenuated backscatter coefficient profiles, -1-10 km, from GLA07;
b) 20 5Hz attenuated backscatter coefficient profiles, -1-40km,
c) 4 sets of 1-second DEM values corresponding to the 4-second processing interval, with each set containing the mean, maximum and minimum values of the height of the earth's surface in the local 1-degree square grid
d) one current atmospheric profile, 0-22km, containing pressure, temperature, height. and relative humidity.

4.3.2   Algorithm Implementation

Cloud and aerosol layer boundary searches will be limited to the lowest 22 km above ground level. For each 4-second interval, the computations proceed in the following manner.

The input profiles are acquired. These consist of 160 40Hz profiles and 20 5Hz profiles. Each of the 40Hz profiles extend from -1 to 10 km. The total number of samples therefore is
 {[10-(-1)] km/ 0.0768 km}= 143 samples/profile;
143 samples/profile x 160 profiles=22880 samples.
Each 5 Hz profile extends from -1 to 40 km; thus, each has 533 samples. So, the total number of 5 Hz samples is
(533 samples/profile) x 20 profiles = 10660 samples. The total number of backscatter coefficient samples required for each 4-second interval is 22880+10660=33540. This value represents the most significant demand on computer memory storage for this algorithm.

The first task will be to detect and position the signal from the earth's surface (ground signal). As mentioned in Section 3.3.1.2, the ground height for the 1Hz and 0.25 Hz profiles will be the average of the ground height from the appropriate 5 Hz profiles. The details of the ground procedure are found in that section. Since the algorithm requires that cloud boundaries be found at the 4-second resolution first, a 4-second average profile will be found by averaging the 5 Hz profiles. The averaging will extend from -1 km to 22 km. When a layer is found at the 4 second resolution, it will be then be characterized as either cloud or aerosol using a set of discrimination criteria described in section 3.3.1.2. If it is aerosol, no further searches are done at the higher resolutions. If it is determined to be a cloud, the one-second profiles will be analyzed after the processing of the 4-second profiles is complete.

The 4-second average profile will be divided into n_s segments. These will not necessarily be of uniform length. In each of these segments, a minimum value will be found. A measure of the random noise associated with the molecular signal will be computed. For observations taken in sunlight, the standard deviation of the background signal will be used. This value will be found by using values in the final 13 samples of the profile, which occur after the laser pulse is extinguished by the ground. The lack of a significant background signal in night observations requires that the variability be estimated from 18-19 km. portion of the profile. The atmosphere at that altitude will be free from strong non-molecular scattering constituents. Therefore, the variability of the signal found there will be representative of the variability found in the particulate free portions of the entire profile. A constant fraction of this variability will be added to each of the segment minimums. The optimum value for the fraction will be determined from modeling studies. A threshold profile, extending from 0-22 km, will be formed by linear interpolation and extrapolation of the segment points.

Layer boundaries can now be found from the 4-second profile. Starting at the first sample, which represents the highest point, each profile value will be compared to the threshold profile. The presence of layer will be designated false. When a certain number of consecutive samples are found to be greater in value than the threshold, a top-of-layer will be located where the first sample exceeded the threshold. The presence of layer will be designated true. The comparison of profile values will continue downward. When certain number of consecutive values are found to be less than the threshold, a bottom-of-layer will be located where the first of the consecutive samples was found and the presence of layer will return to false. This process will continue to ground level. The location of the ground level will be the average of the ground levels derived from the 5Hz profiles, as described in Section 3.3.1.8. If no ground signal was detected, the layer search algorithm will continue to the minimum of the 4 DEM minimums associated with the 4-second segment. When this procedure is complete, the set of layer boundaries and ground location of the 4-second profile will be known and stored.

Next, the procedure to find cloud boundaries for each of the 1 second profiles contained in a 4 second segment will be applied to the GLAS backscatter coefficient profiles. The algorithm will be the same as that described for the 4-second profile, with the following alteration. No boundaries outside of those defined by the results from the four-second profile(plus a small delta) will be accepted. If such a boundary or layer is found, it will be considered a false positive result caused by relatively larger random noise. Layers that are wholly outside of 4-second layers will be eliminated. Each 1 Hz result will be assigned a ground height computed from the average of the

corresponding 5 Hz profiles. In a like manner, the layer boundary processing of the 5 Hz data will be same as the 0.25 Hz and 1 Hz. The 5 Hz layers will be required to exist in layers defined by the 1 Hz results.

Finally, the 40 Hz profiles will be processed. Two factors force the processing to be somewhat different than that at the other frequencies. First, the 40 Hz data extend only from –1km to 10 km. Second, the low signal to noise precludes reliable detection of rarefied, optically thin clouds. In general, it is expected that only dense clouds will be reliably detected at 40 Hz. But knowledge of the location of cloud layer boundaries of these types of clouds in the lowest part of the atmosphere is very important for certain types of studies. For these reasons, the processing of 40 Hz data will proceed as follows. A ground height search algorithm will be applied independently to each of the profiles. The random noise factor will be estimated from the background portion of each profile. A threshold profile will be developed for the region 0-4km. If any cloud layers are detected, only the lowest one of those, confined to layers detected at 5 Hz, will be designated as a layer.

4.3.3   Interpreting the Output

The output of GLA09 will consist of the following products, for each 4 second processing segment:
1) Results at 0.25 Hz frequency, 1 set
   a) Vertical locations of the top and bottom of up to ten cloud layers, 0-22 km ;
   b) probability that each detected layer is a false positive result;
   c) probability of one or more false negative results
   d) probability that this layer is a cloud
   e) probability that each detected boundary is within 0.116 km of the algorithm result
   f) Ground height which will be the average of 20 5 Hz ground height results or indication of negative results if no ground was detected in the 4 second interval;
   g) probability that the ground height is within 0.116 km of the algorithm result
   h) time and location information
2) Results at 1.0 Hz frequency, 4 sets
   a) Vertical locations of the top and bottom of up to ten cloud layers, 0-22 km. confined to the layer boundaries detected at 0.25 Hz;
   b) probability that each detected layer is a false positive result;
   c) probability of one or more false negative results
   d) probability that each detected boundary is within 0.116 km of the algorithm result
   f) Ground height which will be the average of 5 Hz ground height results or indication of negative results if no ground was detected in the 1 second interval;
   g) probability that the ground height is within 0.116 km of the algorithm result
   h) time and location information
3) Results at 5 Hz frequency, 20 sets
   a) Vertical locations of the top and bottom of up to ten cloud layers, 0-22 km. confined to the layer boundaries detected at 1 Hz;
   b) probability that each detected layer is a false positive result;
   c) probability of one or more false negative results
   d) probability that each detected boundary is within 0.116 km of the algorithm result
   e) Ground height or negative results if no ground was detected;
   f) probability that the ground height is within 0.116 km of the algorithm result
   g) time and location information

4) Results at 40 Hz frequency, 160 sets
    a) Vertical locations of the top and bottom of one cloud layer, in the range 0-4 km, the lowest of any detected and confined to layer boundaries detected at 0.25 Hz.
    b) probability that the detected layer is a false positive result;
    c) if no cloud is detected, the probability of a false negative result
    d) probability the detected boundary is within 0.116 km of the algorithm result
    e) Ground height or negative results if no ground was detected;
    f) probability that the ground height is within 0.116 km of the algorithm result
    g) time and location information

The tops and bottoms of layers are the heights h (in km above mean sea level) at which the layer signal becomes distinguishable from the molecular signal. In general, within the meaning of layer boundary at any of the time resolutions, the actual cloud boundary, h_a, will be within a range of h-0.116km$<h_a<$h+0.116km.

If a ground signal is detected, than all layer boundaries are considered valid within the uncertainty limits. If no ground signal is detected, then the value of the bottom of the lowest layer has no meaning other than to indicate the height at which random noise first conceals the atmospheric signal. Any layer of sufficient density and optical depth to cause multiple scattering to obliterate the location of the bottom of the layer will be assumed to fully attenuate the laser pulse. The bottom of the layer would not be meaningful in any such case.

4.3.4   Quality Control

The quality of the results of the GLA09 boundary procedure will be judged by how successful it is at finding all detectable cloud layers and locating their boundaries in the atmospheric profile. A significant advantage to the algorithm is that its application to a given time segment is independent of any GLAS observations outside of the segment. Quality of the results will be primarily controlled by the signal to noise ratio at any point in the profile. Modeling studies will be used to assign quality assessments based upon the signal to noise of any detected layer. The results for each layer will be flagged with quality flag based upon the noisiness of the signal.

The best way to judge the general quality of the results of the boundary algorithm is to plot the computed cloud boundaries on top of image segments constructed from lidar profiles. Such images reveal readily systematic and random faults in the results of the procedure. These inspections will be done on samplings of the results on a routine basis. If these reveal significant shortcomings in the method, the parameters used in the computation of thresholds will be adjusted to fix the discrepancies.

4.4   PBL and Elevated Aerosol Layer Height

4.4.1 Required Input Data

The algorithm requires the 5 Hz profiles of the 532 nm attenuated backscatter and selected other components of the GLA07 output. These include the ground bin and various data quality flags. In addition, GLA08 requires the 5 Hz (high resolution) cloud boundaries output from the cloud detection algorithm (GLA09) and the 4 second aerosol layer heights (which are found by the

GLA09 algorithm, but not output to the GLA09 product). Also required from GLA09 is the 5 Hz ground detection flag. Profiles of molecular backscatter cross section are also required since they are used to determine the bottom threshold as discussed in section 3.4.1.2. The MET data, temperature as a function of height is also required to help identify the likelihood of polar stratospheric clouds.

4.4.2 Algorithm Implementation

The algorithm can be implemented on any standard workstation with sufficient memory and CPU resources. To be most efficient, the 150 km record (100, 5 Hz profiles) of lidar data used to find the average PBL height should be kept in memory. The total memory required is less than 1 Mb, and the CPU requirements fairly minimal. We estimate that processing all the data from one orbit (about 27,000 profiles at 5 Hz) would take less than 10 CPU minutes on a low-end workstation such as an HP-715 or SGI Indigo II.

Even though there are similarities between the PBL and EAL algorithms, we believe they should be implemented separately. For instance, the need for 20 second and 4 second averaged profiles is common for both the PBL and EAL portions of the algorithm. However, the criteria for the composition of the 20 second averages is not quite the same. For the elevated aerosol layer, all shots are used regardless of the presence of a ground return or clouds. The PBL height, on the other hand, eliminates all shots without a ground return that have clouds above 5 km. This means that the EAL algorithm will process nearly 100 percent of the data, while the PBL algorithm may discard 30 or 40 percent of the data (due to clouds). In addition, the EAL algorithm requires the PBL algorithm output to determine the lower bound for the aerosol layer search. Thus, the PBL height algorithm must be run prior to the EAL algorithm.

Note that the 4 second aerosol heights determined by GLA09 are passed as input to GLA08. There will be a flag that tells GLA08 whether to execute the routine to find the 4 second aerosol heights or simply to output the heights that were passed to it by GLA09. This value of this flag will also be included in the GLA08 output so that we can tell which routine (GLA08 or GLA09) was used to produce the 4 second aerosol layer heights.

4.4.3 Interpreting the Output

The output from GLA08 will consist of planetary boundary layer height at high resolution (5 Hz or 1.5 km) and low resolution (0.25 Hz or 30 km). It will also contain the top and bottom height of a maximum of five elevated aerosol layers below 20 km at 0.25 Hz resolution, and a maximum of three aerosol layers above 20 km at a horizontal resolution of 0.05 Hz (150 km). When an aerosol layer is found above 10 km, and the temperature at the height of the layer is below –80 °C, and the latitude is poleward of 65 degrees, a Polar Stratospheric Cloud (PSC) flag is set to indicate a very high likelihood of the layer being a PSC. If the layer temperature is above –80 °C, but less than –70 °C, the flag is set to a different value to indicate a lesser likelihood of it being a PSC. The PSC flag will have the value of zero at all other times. All heights generated will be in kilometers above mean sea level. An elevated aerosol layer is defined as a region of increased lidar backscatter (above local ambient values) which has a minimum thickness of 230 meters (3 data bins). The data input to GLA08 will already have been processed by the cloud height detection algorithm (GLA09)

and the EAL algorithm will search only those portions of the data that have been certified cloud free by GLA09. As discussed in section 3.3.1.2, differentiating between a very weak cloud signal (for instance from cirrus) and a strong EAL signal can sometimes be difficult if not impossible. However, an implicit assumption of this (GLA08) algorithm is that any layer detected by the algorithm (after screening the data based on output from GLA09) is an aerosol layer and not an optically thin cloud layer. It should be noted that there will likely be times when this is not correct. However, we anticipate that such occurrences will be very infrequent (less than 1 percent of the EAL heights).

In figure 4.4.1 we have included an example of the output from a prototype version of the PBL height algorithm and the EAL algorithm from GLA08. It shows the high resolution (5 Hz) PBL height obtained by analyzing the simulated nighttime GLAS attenuated backscatter data shown in the image. The PBL top is superimposed on the image with reddish brown points.
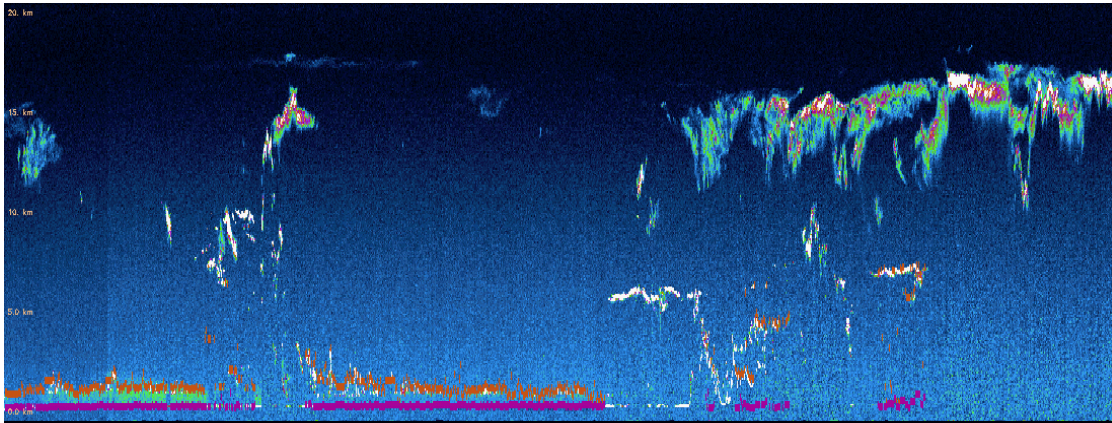

Figure 4.4.1. Output of a prototype PBL height algorithm (GLA08) at a horizontal resolution of 5 Hz for a simulated GLAS attenuated backscattter data set (GLA07 output). The PBL heights are shown as the reddish lines superimposed on top the image.
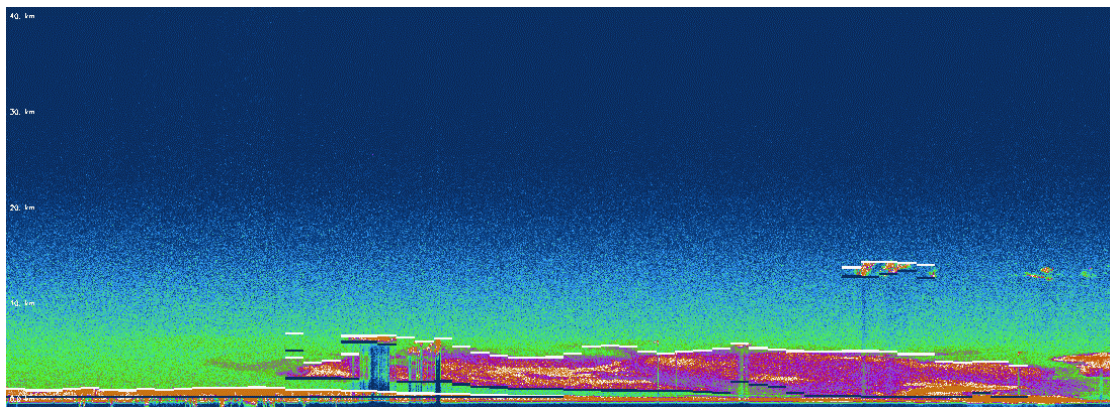
Figure 4.4.2. Output from a prototype EAL algorithm using LITE data as input. The aerosol layer is below about 5 km. The top and bottom of the aerosol layer, as resolved by the algorithm, is shown as the white and black lines superimposed on the image, respectively.

Visual inspection of the backscatter image in figure 4.4.1 reveals the presence of enhanced scattering below two kilometers, especially in the first 20 percent or so of the image. This is indicative of aerosol trapped within the PBL. Beyond this point, the aerosol scattering within the PBL is somewhat less, but still provides enough signal to detect the PBL top. In figure 4.4.2, the aerosol layer top and bottom that has been retrieved by the algorithm is indicated by the overlaid white and black lines, respectively.

A partial list of the output of GLA08 follows:

1   Aerosol layer top and bottom height above 20 km (max 3 layers) at 20 second resolution
2   Aerosol layer top and bottom height below 20 km (max 5 layers) at 4 second resolution
3   Aerosol layer height quality flags (4 and 20 seconds)
4   Flag indicating whether given layer is a Polar Stratospheric Cloud (PSC)
5   Planetary Boundary Layer (PBL) height at 5 Hz and 4 second resolution
6   PBL height quality flags (4 seconds and 5 Hz)
7   Clear/Cloudy flag for PBL height at 5 Hz and 4 second resolution
8   Ground return bin (5 Hz and 4 seconds)
9   Flag indicating whether GLA08 or GLA09 was used to produce the 4 second aerosol layer
         top and bottom heights
10   Precision Orbit Determination (POD) data (1 Hz)
11   GPS time (1 Hz)
12   Orbit Number
13   PAD Pointing Vector (1 Hz)

4.4.4 Quality Control

Validation of the algorithm output can best be accomplished by overlaying the PBL and aerosol layer heights on top of the images, much like what is shown above. We have found from experience that visual inspection can reliably distinguish aerosol boundaries when the data are presented in this form. The lidar retrieved PBL heights can then easily be compared with the visual estimation of PBL height. The same is true for the elevated aerosol layers. Other validation approaches include using nearby radiosonde data to determine PBL depth and checking it against the lidar measurement (provided it is within a certain distance to the radiosonde station). Over land, it may be possible to use the MET data which is ingested by the GLAS ground processing system, and ground based lidar systems.

4.5 Optical Properties of Cloud and Aerosol Layers

4.5.1 Required Input Data

The algorithm that produces the GLA10 and GLA11 level 2 standard products will have as its starting point the 5 hertz GLA07 532 nm backscatter output. One second average, 4 second average, and 20 second average 532 nm intermediate attenuated backscatter profiles and their

corresponding error profiles are created for the optical properties analysis. The error profiles are produces as follows:
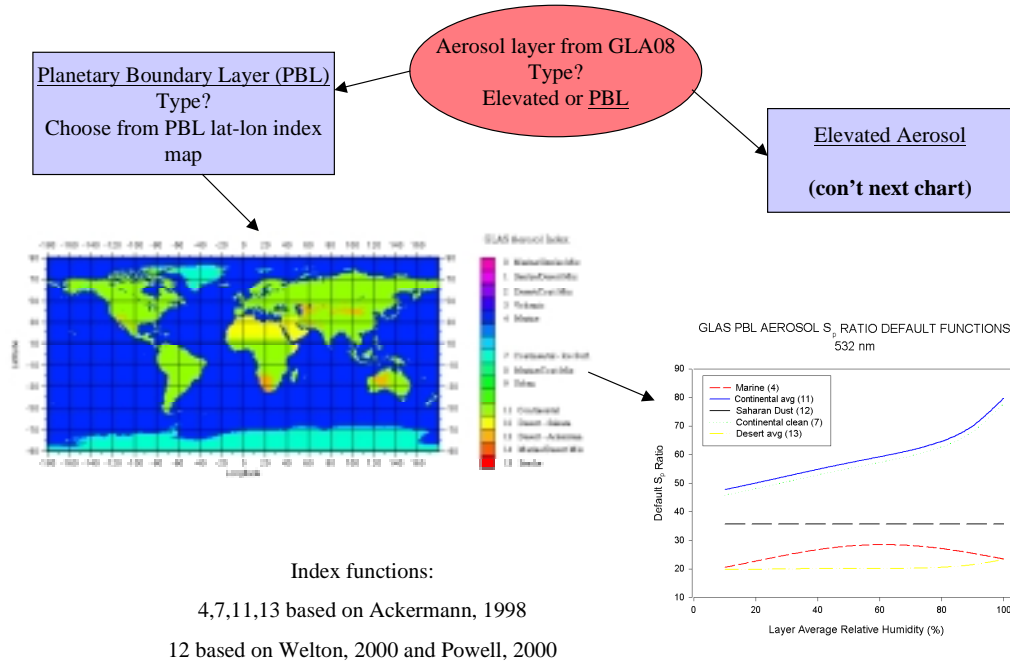
1. Develop standard deviations (sig_dev) while averaging each of the three resolutions:
   - Use 5 hertz data (5 profiles) for 1-second average and deviation
   - Use 1-second data (4 profiles) for 4-second average and deviation
   - Use 4-second data (5 profiles) for 20-second average and deviation
2. Develop vertically smoothed profiles (sig_smo) from each of the 1, 4, and 20 sec average profiles using 5 vertical bin running average
3. Develop difference profiles (sig_avg minus sig_smo) from each of the 1, 4, and 20 sec averages
   - Where difference is zero or positive – add sig_dev to sig_avg
   - Where difference is negative – subtract sig_dev from sig_avg
   - Resultant profiles will be the signal error profiles (sig_err)

These profiles are discarded after GLA10 and GLA11 are calculated. In addition, this algorithm requires MET atmospheric profile data in order to compute the 532 nm molecular backscatter cross section throughout the vertical atmosphere (see sections 3.2.1 and 4.2.1). Temperature and relative humidity from MET profiles will also be used as part of the decision process inside the cloud and aerosol default S_p matrices. Appropriate standard atmosphere profiles will be substituted for the MET profiles when necessary. It is anticipated that the MET data will be refreshed every second and time matched to the three resolutions of the P_n profiles. Other important inputs include the GLA08 aerosol layer location products of PBL height, ground detection height, and top and bottom heights of elevated aerosols (including PSC's) below 20 km, all at low resolution (4 second). GLA08 will also provide top and bottom heights of elevated aerosol layers from 20-40 km (including PSC's) at very low (20 second) resolution. Similarly, cloud location products from GLA09 necessary for input into this algorithm are cloud top and bottom locations and ground detection height at medium resolution (1 second), and cloud top and bottom locations for low resolution (4 second). The cloud and aerosol layer locations will be time matched to the three resolutions of the P_n profiles. The multi-scattering factor, η, (relationships formulated from section 3.6) will all be calculated based in whole or in part on pre-defined look up tables distinguishing between cloud and aerosol regimes. Elevated layers will be assessed for the capability of calculating S'_p from the signal profile. For those particulate layers where S'_p can not be calculated, work done by Ackermann (1998) showed that reasonable estimates of S_p for aerosols can be matrixed using location information (continental, maritime, and desert) with a dependence on relative humidity. Similar estimates can be done for clouds involving cloud phase and temperature. PSC's will be obtained from a subset of the aerosol matrix. S'_p can than be estimated by applying the estimate of η to the S_p value. The following two sections describe the current default decision matrices of the S_p look up tables in detail.

4.5.1.1 Aerosol Extinction to Backscatter Ratio (S_p) Assignments

Aerosol layers will be assigned a best default value of S_p based on the three-chart matrix in figure 4.5.1.

GLAS PBL Aerosol Extinction to Backscatter Ratio (S_p) Default Matrix

Aerosol layer from GLA08
Type?
Elevated or PBL

Planetary Boundary Layer (PBL)
Type?
Choose from PBL lat-lon index map

Elevated Aerosol

(con't next chart)

GLAS PBL AEROSOL S_p RATIO DEFAULT FUNCTIONS
532 nm

Marine (4)
Continental avg (11)
Saharan Dust (12)
Continental clean (7)
Desert avg (13)

Index functions:

4,7,11,13 based on Ackermann, 1998

12 based on Welton, 2000 and Powell, 2000

GLAS Elevated Aerosol Extinction to Backscatter Ratio (S_p) Default Matrix

Polar stratospheric clouds
Type?

Based on lat., T, ht

Elevated Aerosol
Type?

Aerosol layer from GLA08
Type?
Elevated or PBL

Decision based on MET profile or standard atmos.

Stratospheric
Based on Gobbi,1995
model 99

Tropospheric Aerosol
(con't next chart)

GLAS POLAR STRATOSPHERIC CLOUD S_p RATIO DEFAULT FUNCTIONS
532 nm

PSC Type II
PSC Type I

$\beta_p = 1.025(\beta_T - \beta_m)$

Type I

based on Gobbi, 1995
McCormick,1985

model 96

Type II (ice)

only when rh > 95% (rare)

based on Gobbi, 1995

model 86

GLAS STRATOSPHERIC AEROSOL S_p RATIO DEFAULT FUNCTION
532 nm

Stratospheric Aerosol

$\beta_p = 1.025(\beta_T - \beta_m)$

GLAS Elevated Tropospheric Aerosol Extinction to Backscatter Ratio (S$_p$) Default Matrix

Index functions:

11, 15 based on Ackermann, 1998

12 based on Welton, 2000 and Powell, 2000

3 based on Congeduti, 1998 and Liu, 2000

Figure 4.5.1 Flow diagram consisting of 3 charts of default aerosol S$_p$ ratio assignments for use in optical property calculations. The lat-lon index maps are actually composed of 12 layers, one for each month of the year.

The tropospheric and PBL S$_p$ values are primarily formulated from a method developed by Ackermann, which relates relative humidity to S$_p$ in three geographic regions: Maritime, Continental, and Desert through power series coefficients for the following equation:
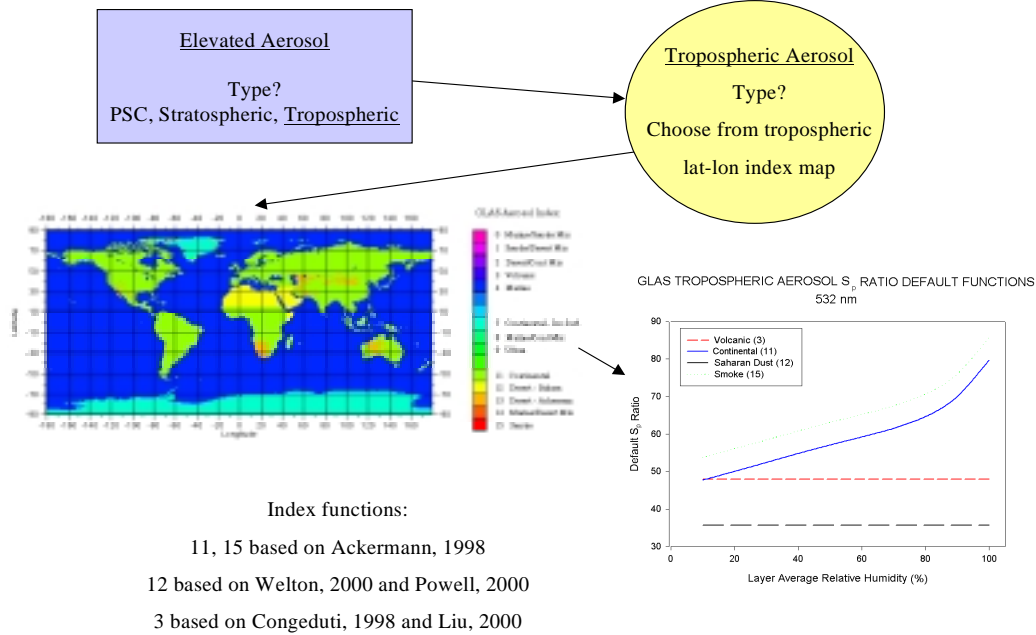
$$(4.5.1) \quad S_p(f) = \sum_{j=1}^{J} a_j f^{j-1},$$

where f is the relative humidity. Details of the S$_p$ used for each aerosol index are as follows:
For PBL:
- Initialize all GLAS PBL aerosol index values (0-15) to 30.0 sr
- Define index 3 (volcanic) to use a constant value of 48.0
- Define index 4 (marine) to use Ackerman maritime
- Define index 7 (continental ice surface) to use Ackerman continental equation with a '-2' offset.
- Define index 11 (continental) to use Ackerman continental equation
- Define index 12 (Saharan dust) to use a constant value of 35.7
- Define index 13 (desert) to use Ackerman desert
- Define index 15 (smoke) to use Ackerman continental equation with a '+6' offset.
For Elevated Tropospheric Aerosol (tropopause definition will follow):
- Initialize all GLAS Elevated Tropospheric aerosol index values (0-15) to 40.0 sr

- Duplicate same index value definitions as is in PBL (indices 3,4,7,11,12,13, and 15)

The S_p ratio of both PSC's and regular stratospheric aerosol layers are based on the following formulation from Gobbi:

$$(4.5.2) \quad S_p = \frac{10^{(a_0 + a_1 \log \beta_p + a_2 \log^2 \beta_p)}}{\beta_p} \, ,$$

where β_p is the aerosol backscatter cross-section in 1/cm-sr. This backscatter value can be estimated by finding the average value of (1.025*total attenuated backscatter – molecular backscatter) over the layer.

To separate Tropospheric and Stratospheric Layers:
- Decide which standard atmosphere to use based on time of year and latitude (use 30N and 30S and Arctic Circle and Antarctic Circle plus use mid October-mid April as winter and mid April-mid October as summer)
- Tropopause height (m)= 17000 for tropical
  9000 for arctic winter
  10000 for arctic summer
  14000 for mid latitude summer
  13000 for mid latitude winter

4.5.1.2 Cloud Extinction to Backscatter Ratio (S_p) Assignments

Cloud layers will be assigned a best default value of S_p based on the matrix in figure 4.5.2. The S_p function ,y, shown in the figure is dependent on mean cloud layer temperature, x (degrees Centigrade) and was created in-house by the GLAS science team based on available information from previous lidar results and ice crystal size and shape studies. For clouds whose temperatures are above –13 C, the S ratio is 17.8 sr.

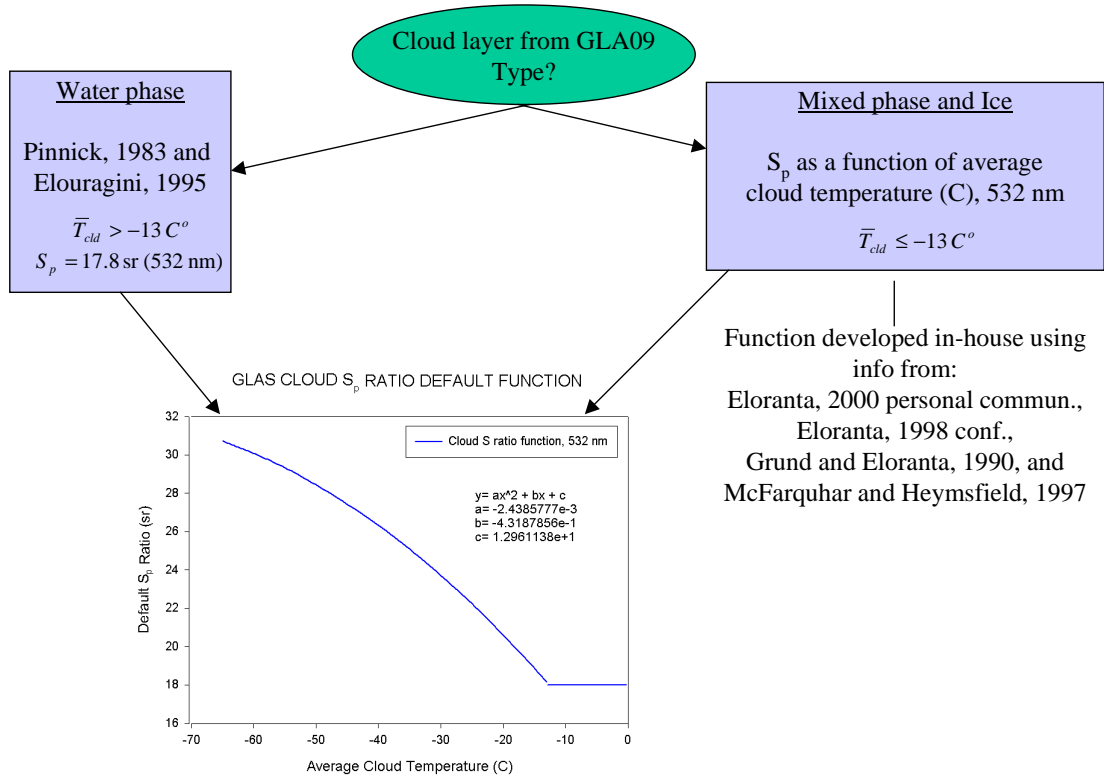GLAS Cloud Extinction to Backscatter Ratio (S$_p$) Default Matrix

Figure 4.5.2 Flow diagram of default cloud S$_p$ ratio assignments for use in optical property calculations.

4.5.2 Algorithm Implementation

The underlying function of this algorithm is to compute molecular and particulate transmission squared for the full vertical profile of the atmosphere starting at 41 km and ending when the value of $T^{\sec\theta}{}_p \leq T_L$ or the lidar profile reaches the earth's surface, whichever occurs first. This will be completed first at four-second resolution, then at 1-second. The following rules will be adhered to:

1. $T'^{2\sec\theta}_p$ for areas between layers will be estimated at 1.0.

2. Average the 5-hertz atb profiles to 1, 4, and 20 second averages and calculate respective standard deviation profiles (Check for invalid bins and do not include them in the averages) [If you don't have at least 50% of your data available in your various averages, then resultant averages are invalid]

    *   Concerning saturation, each 5 hertz bin will have three potential states: 1) unsaturated, 2) saturated but no 1064 conversion done, and 3) saturated and 1064 conversion performed. These three states will be determined from two flags: the 5 hertz saturation flag profile plus the substitution switch. Perform averages and standard deviations no matter which of the three states is active. Processing decisions will be made later with respect to saturation.

However, new saturation flag profiles will have to be created for each of the averaging resolutions as follows:

- During averaging, if less than 'sat_thresh_pct' percent of the bins are in state 2 or 3, then saturation flag for that averaged bin equals 0
- If only the percent of bins that are in state 3 is greater than or equal to 'sat_thresh_pct', then saturation flag of averaged bin equals 1
- If only the percent of bins that are in state 2 is greater than or equal to 'sat_thresh_pct', then saturation flag of averaged bin equals 2
- If the percent of bins in both state 2 and state 3 are greater than or equal to 'sat_thresh_pct', then assign saturation flag to represent the one with the highest percentage. Tie goes to state 3
- Set 'sat_thresh_pct' to 10% for now

3. Initialize optical inversion parameters: set transmission, backscatter, and extinction profiles and their error counterparts to zero's for all resolutions. Set particulate optical depths for all layers to standard defaults
4. Create error profiles for 1, 4, and 20 seconds
5. Process all 20-40 km aerosol layers first using 20-second average data as per the following steps:
   a) Calculate current layer's top and bottom bin locations and set top of layer Tpsq value (ttp or ttp_err) to 1.0 if this is first layer analyzed or, for subsequent layers, to the value at bottom of previous layer
   b) Call Integrated Ratio Technique subroutine to:
      - Decide feasibility of layer to be analyzed using the "integrated ratio technique":
        - Is there enough clean air below the current layer and above the next layer (cloud/aerosol/ground)? (If next layer is a tropospheric cloud or aerosol layer, choose the highest of the 5 4-second layers found to do the decision)
        - If there are no layers below current one, is there a ground return?
        - Is the <u>average</u> Signal to Noise Ratio (SNR) in the calibration zone below the layer higher than the threshold 'calzone_thres_snr'? (SNR will be calculated for this purpose as the atb signal / standard deviation for each bin and 'calzone_thres_snr' has been initially set to 0.4)
        - Is the calculated Tpsq value at the layer bottom below the transmission minimum threshold?
      - If feasible, accept the Tpsq at layer bottom (eq. 3.5.11) and calculate an estimate of tau'p from the Tpsq values at the top and bottom of the layer
      - If feasible, call subroutine SRATIO_CAL to iteratively calculate S'p for the current layer (eq. 3.5.12) Accept if S'p is > 1.0 and less than 130.
   c) Perform saturation decision tree:
      - Does layer have four or more bins with saturated flag equal to 2?
        - If **yes**, do not process this or any further layer in current profile
        - If **no**, does layer have more than 0 bins with saturation flag equal to 2?
          - If **yes**, use Integrated Ratio Technique subroutine output of Tpsq at bottom of current layer and do not process current layer except to estimate real optical depth as tau'p/eta. All subsequent layers in current profile can be processed normally. If Integrated Ratio Technique

subroutine could not be used, do not process current or any subsequent layer in this profile.
- ➢ If **no**, proceed
- Does layer have three or more bins with saturated flag equal to 1?
  - ➢ If **yes**, at the quality flag step at the end of the error processing, bump all quality flags of current layer up 2 categories higher
  - ➢ If **no**, does layer have one to two bins with saturated flag equal to 1?
    - ➢ If **yes**, at the quality flag step at the end of the error processing, bump all quality flags of current layer up 1 category higher
    - ➢ If **no**, proceed normally (no saturation)

d) If current layer is being processed using Integrated Ratio Technique subroutine, call Integrated Ratio Technique subroutine again using ttp_err and the corresponding error profile to calculate a S'p_err

e) Initialize parameters for regular optical inversion of layer profile:
- Set current top Tpsq (ttp or ttp_err) to 1.0 for first layer or to value at bottom of previous layer
- Call Multiple Scattering subroutine to retrieve the multiple-scattering factor (eta), particle size estimate, and range delay estimate from inputs such as layer type, layer top height, layer bottom height, layer average temperature, day of year, latitude, longitude, DEM and estimated <u>effective</u> optical depth (from Integrated Ratio Technique subroutine or default). In order to estimate an optical depth in the 'default' scenario, do the following steps:
  - ➢ Use an estimate of S'p from Sp defaults combined with a guess of the multiple scattering factor (eta) (eq. 3.5.13) by assigning eta=0.5 for all clouds and eta=0.8 for all aerosols
  - ➢ Calculate X term for layer (eq. 3.5.9)
  - ➢ Calculate IB term at layer top (eq. 3.5.9)
  - ➢ Perform Forward Optical Inversion to retrieve an estimate of the true layer optical depth
  - ➢ Estimate effective optical depth: tau'=tau*eta
- Use an estimate of S'p (if you don't have a value from Integrated Ratio subroutine) from Sp defaults combined with the multiple scattering factor (eta) <u>calculated in Multiple Scattering subroutine</u> (eq. 3.5.13). Stratospheric and tropospheric aerosol will be separated by a pre-determined tropopause height based on standard atmosphere defaults.
- Use an estimate of S'p_err from the S'p estimate if you can't calculate one from Integrated Ratio subroutine (S'p_err=S'p+Spct*S'p), where Spct is currently set to 0.05
- Calculate X term for layer (eq. 3.5.9)
- Calculate IB term at layer top (eq. 3.5.9)

f) Decide to use forward or backward optical inversion based on the following:
- Perform Backward Optical Inversion if:
  - ➢ Integrated ratio technique is valid
  - ➢ Zenith angle of the laser is 2 degrees or less

- ➤ Average of SNR of signal in first five bins below layer bottom is greater than 'opt_back_snr', the value of which is initially set to 1.7
- ➤ Optical depth estimate from Integrated Ratio Technique subroutine is greater than 'opt_back_od', currently set at 0.6
- Perform Forward Optical Inversion for all other cases

g) Perform appropriate optical inversion for layer, updating the effective transmission, the total backscatter, the particulate backscatter, and the particulate extinction profiles; plus calculating the final optical depth value, getting rid of the multiple-scattering effect using the variable eta [Use eqs. 3.5.10, 3.5.15, 3.5.17, 3.5.22 for forward inversion; use eqs. 4.5.4, 4.5.5, 4.5.6, 4.5.7 for backward inversion]. If Tpsq is below minimum threshold or signal near ground, stop process and mark rest of layer invalid

h) Repeat Steps e and g for error inversion using the same optical inversion subroutine as you did with the real data:
- Use ttp_err instead of ttp
- Use S'p_err instead of S'p
- Use corresponding error profile instead of atb profile
- Output will be error profiles for transmission, total backscatter, particulate backscatter, and extinction, plus a error value for optical depth
- Calculate quality flags from the error results (See section 4.5.4)
- Use flags will stipulate detailed layer type coming from the Sp ratio default matrices or saturation status

6. Repeat Step 5 in its entirety using a 4-second profile and the below 20.5 km 4-second aerosol and cloud layers, initializing all output profiles (transmission, total backscatter, particulate backscatter, and extinction [and their error counterparts] to the corresponding 20-second output profiles. Initialize ttp and ttp_err to the appropriate 20-second values. Process each cloud and aerosol layer in sequence from top to bottom, but do not save cloud optical property information in output profiles after updating ttp or ttp_err.
- PBL special case: Do not process any PBL which has 1) its cloudy flag turned on or 2) a 4-second cloud bottom at or below the PBL top.

7. Repeat Step 5 in its entirety using a 1-sec profile and 1-second cloud and 4-second aerosol layer information (for setting IB term correctly). Initialize all output profiles (transmission, total backscatter, particulate backscatter, and extinction [and their error counterparts] to the corresponding 20-second output profiles. Initialize ttp and ttp_err to the appropriate 20-second values. Whenever a 1-second cloud layer is the next layer below a corresponding 4-second aerosol layer (already processed), then ttp= ttp*Tpsq(aerosol layer), where Tpsq(aerosol layer) = exp(-2*tau*eta(aerosol layer)). If multiple aerosol layers are directly above the current cloud layer, sum up all the aerosol layer effective tau's in order to calculate ttp. The same goes with ttp_err.
- PBL special case: Do not process any cloud whose top is more than one bin below the PBL top. Also, for clouds whose tops are one bin below the PBL top or higher, but have bottoms below the PBL top, process normally, ignoring PBL as a layer.

8. End result of a 20-second output package should have 20 1-second cloud backscatter and extinction profiles that contain calculated data in only those bins where cloud layers were found. All other bins contain defaults. The output package should contain 5 4-second aerosol backscatter and extinction profiles that contain calculated data in only those bins where

aerosol layers were found. All other bins contain defaults. Layer quantities saved in output (clouds and aerosols separate) include Sp calculated from Integrated Ratio Technique (Sp=S'p/eta), Sp pulled directly from defaults, and a flag stipulating which Sp was actually used in the optical inversion, plus layer true optical depth

The multiple scattering warning flag will be based on the total column optical depth at the end of processing of each 1 second profile as follows:

FLAG VALUE	OPTICAL DEPTH RANGE
0	from 0.00 up to 0.01
1	from 0.01 up to 0.03
2	from 0.03 up to 0.06
3	from 0.06 up to 0.10
4	from 0.10 up to 0.15
5	from 0.15 up to 0.225
6	from .225 up to 0.30
7	from 0.30 up to 0.40
8	from 0.40 up to 0.50
9	from 0.50 up to 0.67
10	from 0.67 up to 0.90
11	from 0.90 up to 1.20
12	from 1.20 up to 1.60
13	from 1.60 up to 2.00
14	greater than or equal to 2.00
15	invalid

 A flow chart showing an overview of the optical parameter calculations is found in figure 4.5.3.

The critical component of the algorithm is the evaluation of the integral to compute γ (see equation 3.5.20). The flow of the algorithm proceeds as follows. For each profile P_n (first the four second and then the one second resolutions), the levels where aerosol and cloud boundaries exist are obtained and differentiated. The molecular transmission to the top of the highest layer is computed to the $2X\sec\theta$ power and used as $I_B(z_t)$ in equation 3.5.10. S'_p for the layer is computed (see section 3.5.1.1) when the backscatter profile for a given layer is found to be appropriate for independent S'_p analysis. Otherwise a default value is used based on whether it is cloud, PSC, or aerosol. The integral for forward inversion is evaluated using a straight-forward rectangular summation. The terms of the summation are $T_{m_i}^{2(X-1)\sec\theta} P_{n_i} \Delta z$. The value of $T_p'^{2\sec\theta}$ is computed for each level z in the layer. Computation for any subsequent layer will use the same method except that the $I_B(z_t)$ value will be re-computed as :

(4.5.3) $I_B(z_t) = T_p'^{2\sec\theta}(z_a)T_m^{2X\sec\theta}(z_t)$,

where $T_p'^{2\sec\theta}(z_a)$ is the particulate slant transmission squared a the bottom of the layer above and $T_m^2(z_t)$ is the molecular transmission squared calculated down to the level of z_t, the top location of the current layer. The backward inversion method initializes particulate backscatter to

zero one bin below layer bottom and calculates corrected particulate backscatter, $\beta_p(z)$, at each bin based in part on the particulate and molecular backscatter at one bin below, starting at the layer bottom and ending at the layer top. Once the backscatter profile is calculated for the layer, extinction and transmission profiles can be calculated. The computer equations governing the backward inversion algorithm for each bin location (ib) in the layer are as follows:

(4.5.4) $A = (S'_p - S_m)(\beta_m(ib) + \beta_m(ib+1))\Delta Z$

(4.5.5) $\beta_p(ib) = \dfrac{P_n(ib) * \exp(A)}{\dfrac{P_n(ib+1)}{\beta_p(ib+1) + \beta_m(ib+1)} + S'_p(P_n(ib+1) + P_n(ib)\exp(A))\Delta Z} - \beta_m(ib)$

(4.5.6) $\sigma_p(ib) = \dfrac{S'_p}{\eta}\beta_p(ib)$

(4.5.7) $T'^2_p(ib) = \dfrac{P_n(ib)}{T_m^2(ib)(\beta_p(ib) + \beta_m(ib))}$

The backward or forward inversion continues throughout each particulate layer as per the eight rules outlined above until $T'^{\sec\theta}_p(z) \le T_L$ or the signal from the earth's surface is detected.

The algorithm is moderately computationally intensive. Results indicate that to process an orbit of data for the GLA10 and GLA11 products would take about 1.05 minutes of cpu time.
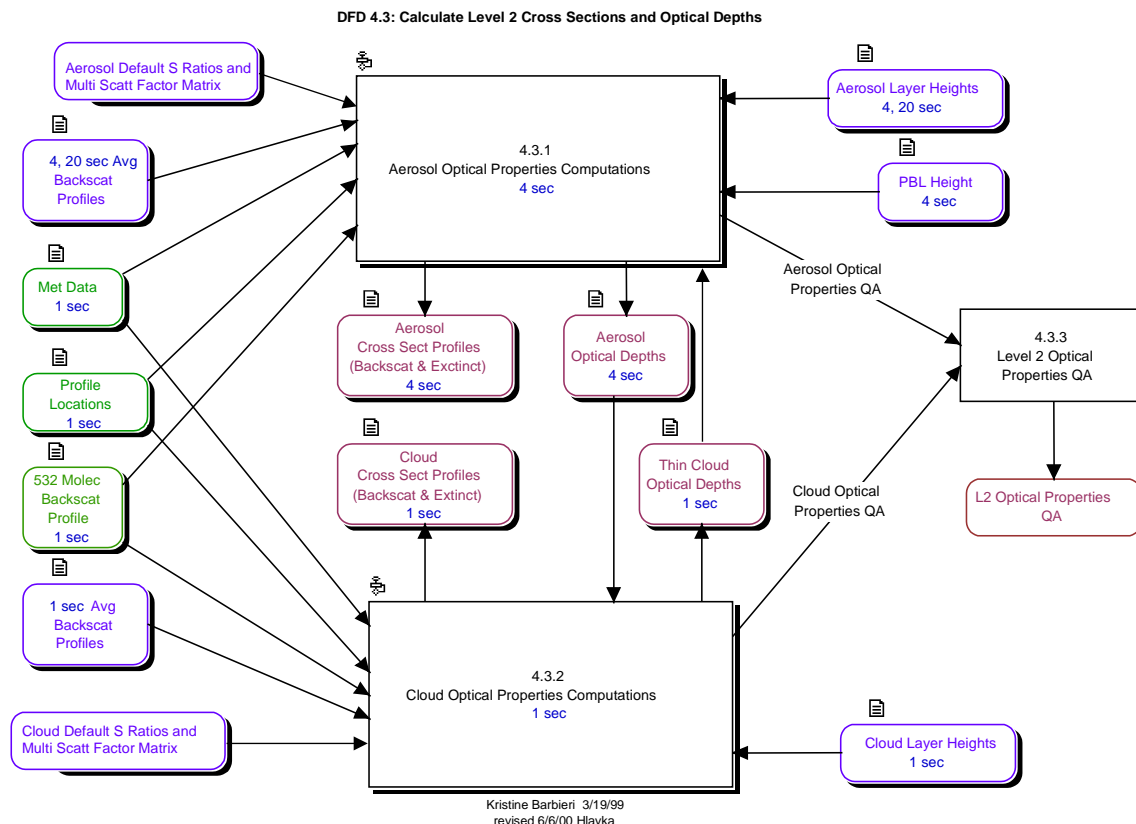
Figure 4.5.3 Flow diagram of level 2 optical parameter calculations.

4.5.3 Interpreting the Output

The output of this algorithm is separated into two standard product packages, GLA10 and GLA11. GLA10 focuses on the output of vertical profiles: cloud and aerosol backscatter cross section and cloud and aerosol extinction cross section. All layer locations are referenced from sea level. GLA11 focuses on particulate optical depths (cloud and aerosol). All extinction and optical depth values have been corrected for multiple scattering. Polar stratospheric clouds in both packages are part of the aerosol category. A complete list of the scientific output for GLA10 follows:

14   532 nm aerosol backscatter cross section, 41 to –1 km above mean sea level , 4 second averages (zero outside layers)
15   Aerosol backscatter layer use and quality flags at 4 second resolution, 1 each per layer, 9 layers, (15 where not processed) [use flag will stipulate saturation state]
16   532 nm cloud backscatter cross section, 20.4 to –1 km above mean sea level, 1 second averages (zero outside layers)
17   Cloud backscatter layer use and quality flags at 1 Hz, 1 each per layer, 10 layers, (Value of 15 where not processed) [use flag will stipulate saturation state]
18   532 nm aerosol extinction cross section, corrected for multiple scattering, 41 to –1 km above mean sea level, 4 second averages (invalid outside layers)

19   Aerosol extinction layer use and quality flags at 4 second resolution, 1 each per layer, 9 layers, (15 where not processed) [use flag will stipulate aerosol type]

20   Calculated aerosol true extinction to backscatter ratios at 4 second resolution, 1 per layer, 9 layers, (invalid where not processed) [PSC ratio, if layer is PSC]

21   Default aerosol true extinction to backscatter ratios at 4 second resolution, 1 per layer, 9 layers, (invalid where not processed) [PSC ratio, if layer is PSC]

22   Flag stipulating which extinction to backscatter ratio was <u>used</u> in algorithm at 4 second resolution, 1 per layer, 9 layers, (invalid where not processed) [PSC ratio, if layer is PSC]

23   532 nm cloud extinction cross section, corrected for multiple scattering, 20.4 to –1 km above mean sea level at 1 Hz, (invalid outside layers)

24   Cloud extinction layer use and quality flags at 1 Hz, 1 each per layer, 10 layers, (15 where not processed) [use flag will stipulate cloud type]

25   Calculated cloud true extinction to backscatter ratios at 1 Hz, 1 per layer, 10 layers, (invalid where not processed)

26   Default cloud true extinction to backscatter ratios at 1 Hz, 1 per layer, 10 layers, (invalid where not processed)

27   Flag stipulating which extinction to backscatter ratio was <u>used</u> in algorithm at 1 Hz, 1 per layer, 10 layers, (invalid where not processed)

28   Medium resolution cloud top heights for layers which were selected for optical processing at 1 Hz, 1 per layer, 10 layers (invalid where not detected or used)

29   Medium resolution cloud bottom heights for layers which were selected for optical processing at 1 Hz, 1 per layer, 10 layers (invalid where not detected or used)

30   Medium resolution processed ground detection height at 1 Hz, 1 per profile (invalid where not processed)

31   Low resolution aerosol layer top heights for layers which were selected for optical processing at 4 second resolution, 1 per layer, 9 layers, including the planetary boundary layer and PSC (invalid where not detected or used)

32   Low resolution aerosol layer bottom heights for layers which were selected for optical processing at 4 second resolution, 1 per layer, 9 layers, including the planetary boundary layer and PSC   (invalid where not detected or used)

33   Low resolution processed ground detection height at 4 second resolution, 1 per profile, (invalid where not processed)

34   Precision Orbit Determination (POD) data (1 Hz)

35   GPS time (1 Hz)

36   Orbit Number

37   PAD Pointing Vector (1 Hz)

Items 1 through 14 are calculated by the optical properties algorithm. Items 15 through 20 are taken from GLA09 and GLA08 particulate boundaries output, but modified to suit the rules listed in section 4.5.2 so that only cloud and/or aerosol layers processed optically will show up in this data set's layer locations. The remaining output is passed along from GLA07 or from another input source.

A complete list of the output for GLA11 follows:

1. 532 nm cloud optical depth, corrected for multiple scattering, at 1 Hz, 1 per layer, 10 layers, (invalid where not processed)

2. Cloud optical depth use and quality flags at 1 Hz, 1 each per layer, 10 layers, (Value of 15 where not processed) [use flag will stipulate cloud type]
3. 532 nm elevated aerosol optical depth, corrected for multiple scattering, at 4 second resolution, 1 per layer, 8 layers, (invalid where not processed)
4. Elevated aerosol optical depth use and quality flags at 4 second resolution, 1 each per layer, 8 layers, (15 where not processed) [use flag will stipulate aerosol type, including PSC]
5. 532 nm planetary boundary layer aerosol optical depth, corrected for multiple scattering, at 4 second resolution, 1 per layer, 1 layer, (invalid where not processed)
6. Planetary boundary layer aerosol optical depth use and quality flags at 4 second resolution, 1 each per layer, 1 layer, (15 where not processed) [use flag will stipulate aerosol type]
7. Medium resolution cloud top heights for layers which were selected for optical processing at 1 Hz, 1 per layer, 10 layers, (invalid where not detected or used)
8. Medium resolution cloud bottom heights for layers which were selected for optical processing at 1 Hz, 1 per layer, 10 layers, invalid where not detected or used)
9. Medium resolution processed ground detection height at 1 Hz, 1 per profile, (invalid where not processed)
10. Low resolution elevated aerosol layer (including PSC) top heights for layers which were selected for optical processing at 4 second resolution, 1 per layer, 8 layers (invalid where not detected or used)
11. Low resolution elevated aerosol layer (including PSC) bottom heights for layers which were selected for optical processing at 4 seconds, 1 per layer, 8 layers (invalid where not detected or used)
12. Low resolution processed ground detection height at 4 second resolution, 1 per profile, (invalid where not processed)
13. Low resolution planetary boundary layer height at 4 seconds, 1 per profile, (invalid where not processed)
14. Cloud multiple scattering coefficients used at 1 Hz, 1 per layer, 10 layers, (invalid where not processed)
15. Aerosol multiple scattering coefficients used at 4 second resolution, 1 per layer, 9 layers, (invalid where not processed) [including PSC and PBL aerosol]
16. Multiple scattering effect warning flag at 1 Hz, 1 per profile (Value of 15 where not processed)
17. Estimated Range (Altimetry) Delay (millimeters) at 1 Hz, 1 per profile taken from last layer analyzed
18. Particle size estimate used to calculate warning flag and range delay at 1 Hz, 1 per profile taken from last layer analyzed
19. Range (Altimetry) Delay Uncertainty (millimeters) at 1 Hz, 1 per profile taken from last layer analyzed
20. Multiple scattering spare
21. Precision Orbit Determination (POD) data (1 Hz)
22. GPS time (1 Hz)
23. Orbit Number
24. PAD Pointing Vector

Items 1 through 6 and 14 through 20 are calculated by the optical properties algorithm. The multiple scattering warning flag and range delay will be based on the height and optical depth of the scattering layers and an assumption on the particle size. This is discussed at length in section 3.6.2. In general, for clear regions (no cloud or aerosol layers found), the value of the multiple

scattering warning flag will be zero. The largest value of this flag (14) will occur for optically thick layers. Likewise, the range delay will be near zero for clear conditions and a maximum for low scattering layers comprised of (assumed) large particles. The details on the calculation of the estimated range delay are in section 3.6.2. Items 7 through 13 are taken from GLA09 and GLA08 particulate boundaries output, but modified to suit the rules listed in section 4.5.2 so that only cloud and/or aerosol layers processed optically will show up in this data set's layer locations. The remaining output is passed along from GLA07.

4.5.4 Quality Control

Quality control will be implemented at all stages of the molecular and particulate transmission profile development. All input parameters and arrays will be evaluated for quality before being used:

1. Attenuated backscatter profiles
   - Bad shots will be detected by integration of the lidar signal in the 20 to 40 km height zone.
   - Lidar bins using 1064 nm backscatter in place of a saturated 532 nm condition will be tracked as far as which particulate layer they occur in.
   - Calibration constants which fall outside an expected range will be flagged.
2. Cloud and aerosol layer detection
   - The layers will be screened so they don't overlap or become embedded except in the PBL.
   - Visual screening with imagery will occur to make sure layers are labeled 'cloud' or 'aerosol' or 'polar stratospheric cloud' correctly.
3. Molecular backscatter
   - Backscatter calculations from MET data will be monitored to make sure they fall within expected boundaries based on atmospheric standards.
   - If MET data are missing or bad, they will be defaulted to atmospheric standards.
4. Extinction to backscatter ratios and multiple scattering factors
   - The accuracy of these input parameters are at times uncertain, especially for cirrus clouds, making this a limitation in the algorithm.
   - Calculations of these parameters in level 2 processing involve a decision matrix look up table, which will restrict these parameters to within theoretical and observed limits. If atmospheric conditions are favorable, S'_p will be calculated for thin clouds, elevated aerosols, and PSC's, then compared to matrixed values. If more accurate calculations come out of level 3 processing, these will be used to re-process level 2 products.

As the transmission profiles are processed, the transmission calculations will be tested for out-of-bounds situations such as increasing transmission with range or large negative transmission. Quality flags will be produced for each particulate layer or profile to help pinpoint how many and which output parameters are suspect. This information will be transferred to each of the individual output parameter's quality flags by the following algorithm:
1. After calculating optical inversion for layer (eq. 3.5.10, etc), re-calculate with a S ratio with error (Sp_err) and a signal profile with error (sig_err) as inputs to determine percent error for each of the following parameters:
   - Percent backscatter error profile: $|\beta p - \beta p\_err| / \beta p$
   - Percent extinction error profile: $|\sigma p - \sigma p\_err| / \sigma p$

- Percent optical depth error for layer: $|\tau p - \tau p\_err| / \tau p$

2. Layer quality flags will be set 0-15 based on layer averages of the above two percent error profiles plus optical depth percent error as follows:

FLAG	%ERROR	FLAG	%ERROR
0	0-5	12	60-65
1	5-10	13	65-70
2	10-15	14	70 and greater
3	15-20	15	could not process
4	20-25		
5	25-30		
6	30-35		
7	35-40		
8	40-45		
9	45-50		
10	50-55		
11	55-60		

3. Layer use flags are designated as follows:

a) for backscatter cross section, the use flag gives saturation status as follows:

FLAG	SATURATION STATUS
0	no saturation detected
1	one or two bins were saturated with 1064 nm conversion performed
2	at least three bins were saturated with 1064 nm conversion performed
3	at least one but less than four bins were saturated with no conversion performed
4	four or more bins were saturated with no conversion performed
15	invalid

b) for extinction cross section and layer optical depth, the use flag designates layer type category as follows:

Aerosol: {based on S ratio default index, PSC flag, and tropopause height}

00	PBL generic (all PBL indices not mentioned below)
01	PBL maritime (index 4)
02	PBL continental ice (index 7)
03	PBL continental haze (index 11)
04	PBL Saharan dust (index 12)
05	PBL desert (index 13)
06	PBL smoke (indices 15,3)
07	TROP generic (all TROP indices not mentioned below)
08	TROP volcanic (index 3)
09	TROP continental haze (index 11)
10	TROP Saharan dust (index 12)
11	TROP smoke (index 15)
12	STRATO aerosol (any non-PSC layer whose top is > tropopause
13	PSC type I (PSC with rh less than or equal to 95%)

| 14 | PSC type II (PSC with rh greater than 95%) |
| 15 | invalid |

Cloud: {based on average cloud temperature, water cloud is warmer than –13 C}

00	less than or equal to –75.0 C
01	-75.0 through –68.5
02	-68.5 through –62.0
03	-62.0 through –55.5
04	-55.5 through –49.0
05	-49.0 through –32.5
06	-32.5 through –26.0
07	-26.0 through –19.5
08	-19.5 through –13.0
09	-13.0 through –6.5
10	-6.5 through 0.0
11	0.0 through 6.5
12	6.5 through 13.0
13	13.0 through 19.5
14	greater than 19.5 C
15	invalid

5 Mitigating Multiple Scattering Induced Ranging Errors

It has been calculated that the effects of multiple scattering from cloud and aerosol will introduce significant errors for precision surface altimetry. These results are presented in detail by Duda et al. (1999, a and b and available from the GLAS ftp site). The pulse spreading from multiple scattering will tend to introduce a positive bias to the range determination. The magnitude of the effect can be considerable under certain atmospheric conditions, ranging to larger than 1 meter for a single pulse depending on conditions. Since cloud cover varies seasonally and year to year, Duda et al. show that if uncorrected, the multiple scattering effect would introduce significant errors for the GLAS surface altimetry yearly analyses. The atmospheric conditions most conducive to multiple scattering are optically transmissive cloud layers that are between 1 and 3 km above the ground. Over the ice pack, such low optically transmissive clouds appear to be the dominant type.

Application of the atmospheric channel of GLAS to perform an analytic correction to the multiple scattering induced ranging error is being developed. In section 3.6.2 we present a detailed discussion of the approach which is based on the creation of a ranging error table for many different atmospheric conditions. The determining factors are the cloud height range and optical thickness plus an assumption of cloud particle size. The factors are essentially the same as those to be used for the generation of the correction factors for the influence of multiple scattering on cloud and aerosol cross sections and optical thickness as also described in section 3.6. As described in Duda et al., an estimate of the magnitude of the pulse spreading error on the surface is computed based on a centroid analysis of a flat, normal surface. This information can then be used by the altimetry processing to eliminate shots that are likely to be severely affected by multiple scattering. GLA11 will have 3 items in its output that are related to the multiple scattering

induced range delay. They are 1) Multiple scattering warning flag, 2) Particle size used in multiple scattering computation and 3) Calculated range-to-surface delay. They are described in detail in section 3.6.2 and listed in section 4.5.3. A separate ATBD document to cover multiple scattering effects on surface ranging may also be developed at a later date. The work presented in Duda et al. would be the basis of such a document.

6 Browse Products

Browse products are used to determine the health of the instrument as well as determining the performance of atmospheric algorithms. A list of possible browse products follows, but should in no way be considered complete. This list may be added to at a later date.

1. Laser energy as a function of time
2. Calibration constants as a function of time
3. Number of saturated 532 nm bins per 5 Hz profile as a function of time
4. Integrated 532 signal from 40 to 20 km as a function of time
5. 532 and 1064 nm background values as a function of time
6. 532 nm background at 70 km vs, 532 background at –5 km
7. Scattering ratio profiles
8. Percentage of time ground return was detected per orbit
9. Percentage of time clouds were detected per orbit
10. Color images of attenuated backscatter cross section with cloud layer, aerosol layer and PBL height superimposed on the image.
11. Cloud and aerosol optical depth as a function of time.

(1) It is important to monitor the laser performance since it is integral to data quality. Producing a plot of laser energy vs. time will be very helpful. (2) We have no idea how consistent the lidar calibration constant calculated from the data will be. We need to know how both the calculated 532 and 1064 calibration constants change with time and moreover, how their values are affected by the varying background conditions. This can be accomplished by plotting the calibration constants as a function of time. Probably, it is best to plot the 532 calibration values separate from the 1064 values with each plot containing the calibration constant calculated at the two calibration heights, with the night calibration distinguishable form the day calibration. (3) There would interest in knowing how many 532 channel bins were flagged as saturated as a function of time. This could be done done by counting the bins in the 5 Hz saturation flag profile that is output from GLA07 and summing over one second. A plot of this value vs time would then be generated. (4) The integrated 532 signal (β') from 40 to 20 km would be of interest because it would tell much about system performance and optical alignment (boresite). This could be summed over one second using the 5 Hz profiles output from GLA07 and plotted as a function of time. (5) The 532 and 1064 background values should be computed at second intervals and plotted as a function of time. This would include all four background values – one before the atmosphere (about 70 km) and one after the ground (about –5 km) for each channel. (6) A scatter plot of the 532 background at 70 km vs the 532 background at –5 km could be constructed form the 1 second average backgrounds computed to produce (5). (7) The scattering ratio profile can be formed by taking the 5 Hz attenuated backscatter profiles (β'(z)) output from GLA07 and dividing by the attenuated molecular backscatter profile and averaging over a given time. Most likely these averages would be

computed from 5 to 10 minute of data. (8) The percentage of time the ground return signal was detected (per orbit) is important for ascertaining cloud cover and optical depth statistics. This can be computed from the output of GLA09 which includes high resolution ground detection and would be plotted as one point per orbit. (9) The percentage of time that clouds were detected is computed from the output of GLA09 using the 4 second average cloud height. Item (10) represents one of the most useful browse products in terms of monitoring overall system performance and for validating the performance of the cloud, aerosol and PBL height algorithms. The image is made from the output of GLA07 for a specified time segment and the output of GLA08 and GLA09 are read and plotted on top of the image. Cloud and Aerosol optical depth would be useful mainly as a way to check the validity of the processing algorithms.

7 Development Plan

The development of the production algorithms for the lidar processing should be a team effort between the software development team under Jay Zwally and the atmospheric lidar group under Jim Spinhirne. The lidar group will work closely with the software development team to assist in the design, implementation, and testing of the atmospheric ATBD specified I-SIPS software components that will produce the level 1 and level 2 standard atmospheric data products (GLA02, GLA07, GLA08, GLA09, GLA10 and GLA11). Dr. Spinhirne's group will develop a set of working algorithms (protocode) and associated documentation for the lidar processing that will utilize their past experiences and the design of the I-SIPS software. The lidar group will consist of 3 to 5 senior research programmers, each of whom has ample experience in the processing and analysis of aircraft and ground-based lidar data. The development team during this period will be implementing the shell to provide the data and control into and from the lidar processing algorithms. During this protocode development period there will be working meetings between the teams to track progress, exchange designs and to insure that compatible systems are being developed. The lidar group protocode will be delivered to the software development team for use as examples, recode, or actual use in the I-SIPS software. The lidar group will work with the development team for testing and verification of the I-SIPS production software, using simulated GLAS data sets produced by the lidar group. The objective of the testing and verification stage will be to produce the same results with the protocode and the final I-SIPS software. The development and turning over of the protocode should be accomplished during FY99. The implementation and test support should be FY00 with some small extension into FY01.

After launch the lidar group will ascertain the performance of the algorithms using the browse products defined in section 6 and the validation methods presented in section 8. Based on these assessments, the lidar group will work toward refinement of the I-SIPS production software by tweaking individual algorithms for peak performance. The protocode may be useful to the lidar group for this process or for special analysis. That work will not be part of the I-SIPS sustaining engineering efforts but is considered part of the lidar science team investigation. There will remain a need, as with all science team members, to work with the sustaining engineering team for the production software to correct errors and implement improved algorithms.

8 Validation Plan

8.1 Validation Criterion

8.1.1 Overall Approach

The validation program will consist of pre-launch and post-launch activities aimed at establishing the accuracy of the GLAS algorithms for retrieval of atmospheric parameters. Prior to launch, simulated GLAS data sets will be produced using the GLAS Atmospheric Lidar Simulator (GALS) program which uses data acquired by the Cloud and Aerosol Lidar System (CALS). We believe these simulations closely resemble the characteristics of actual GLAS data in terms of signal to noise and atmospheric variability. In addition to GALS, we have developed a second GLAS simulation program (Cloud and Aerosol Simulator (CAS)) that is based on a simulated, hypothetical atmosphere which is generated by the program using pre-defined input parameters of the cloud and aerosol layer characteristics. The first method has the advantage of being realistic by providing actual atmospheric variability while the second method has a distinct advantage when using the data to verify atmospheric retrieval algorithms, since all the answers are known (as they are inputs to the model). The GLAS data analysis algorithms will be developed and tested using the simulated GLAS data sets produced by these programs. The algorithm output will be validated in a number of ways. For certain GLAS atmospheric products (cloud top height, PBL height and aerosol layer height), validation is possible by assembling the GLAS backscatter data into color images which show backscatter strength as a function of height and along track distance. The output from the cloud top, PBL top or aerosol layer height algorithms are overlaid onto the color backscatter image (as in Figure 1). If the cloud heights have been correctly retrieved, they will line up with the clouds easily discernable on the backscatter image. The same is true for aerosol layers and PBL height. In addition, when the layer height algorithms are run on the output of the CAS program, the exact cloud and aerosol layer heights are known inputs to the CAS program and the algorithm output will be verified by comparing it to this input file. The validation of optical depth and extinction profiles during the algorithm development phase will be made by running the algorithms on simulated GLAS data produced by the Cloud and Aerosol Simulator (CAS) program. The GLAS calculated values of optical depth and extinction can be directly compared with the known values used by CAS.

We are also working on assembling a global network of Micro Pulse Lidar (MPL) systems (this is discussed further in Section 4.2.2) which would most likely be located at existing AERONET sites. After launch the AERONET data will be used to validate the GLAS retrieval of aerosol optical depth (total column). The co-located MPL data will be used to validate aerosol optical thickness, extinction profiles boundary layer height, and cloud and aerosol heights. In addition to the MPL-AERONET sites, we plan on placing 3 MPL lidars along an eight day repeat orbit track separated by about 100 – 200 km. This will enable better characterization of the atmosphere along the flight track and will provide a more representative sampling of the atmosphere for comparison with the GLAS data. In this effort, we hope to involve the education community by installing the MPL systems at a middle or high school and enlisting the help of the students with data gathering activities. This will most likely take place in Oklahoma, as discussed in section 4.2.2.

8.1.2 Post-Launch

A crucial validation activity that will occur after launch is the design and deployment of an aircraft field mission specifically designed to collect validation measurements along numerous GLAS ground tracks. This would entail flying the NASA ER-2 with at least the Cloud Physics Lidar (CPL)

and the MODIS Airborne Simulator (MAS). A detailed description of this activity is given in section 5. Missions of opportunity will also be exploited where field experiments, not necessarily related to EOS, are using aircraft which can accommodate a lidar system. Piggy-backing in this way will give us more opportunities to acquire coincident data while keeping costs to a minimum. Post launch validation efforts will also rely on ground based lidar networks such as MPLNet and EARLINET throughout the lifetime of the GLAS mission. While the aircraft missions are invaluable, we realize they occur infrequently and that ground based measurements are extremely important. We also plan to involve the global ground based lidar community, giving them an opportunity to collect coincident data during times of GLAS overpasses.

8.1.3 Sampling Requirements and Tradeoffs

The major difficulty in obtaining validation measurements for the GLAS atmospheric products lies in the sampling coincidence requirements. The atmosphere has various length and time scales which determine how close in space and time a validation measurement must be to a GLAS observation in order for it to be useful. These scales depend on atmospheric state and the phenomena being measured, but are generally about 2 – 10 km and 10 – 30 minutes for the troposphere. For ground based validation measurements, this puts limits on both how close an overpass must come to the ground site, and how many GLAS profiles can be validated. GLAS travels at about 7 km/s and therefore will cover 10 km in about 1.4 seconds. Thus, a ground based measurement will be useful for validating no more than one and a half seconds of GLAS data. The ground based validation measurements will have to be carefully screened to eliminate cases where the atmosphere is highly variable (close to fronts), so that the horizontal averaging of the GLAS data (which may be required to obtain a given measurement) does not render it unrepresentative of the ground based point measurement. This could be accomplished using the ground based data itself by computing the variance of the atmospheric backscatter as a function of time. High variance situations would require a more stringent space/time coincidence in the two measurements while low atmospheric variance with time would indicate that the space/time coincidence criteria could be more relaxed.

The situation improves considerably if a fast moving aircraft is used to collect the validation measurements. The NASA ER-2 travels at about 200 m/s and can be flown directly underneath the GLAS track. In 20 minutes, the ER-2 can travel 240 km and can thus be used to validate over 30 seconds of GLAS data. The footprint size for the CPL is only about 1 meter, versus about 70 meters for GLAS. The major difficulty will be in aligning the ER-2 flight track with the GLAS overpass. With the high precision pointing ability of GLAS and the use of GPS positioning for the ER-2, aligning the ER-2 underneath the GLAS track should not be a problem.

8.1.4 Measures of Success

Validation experiments are conducted to evaluate the accuracy of the GLAS retrieved atmospheric parameters. The validation measurements themselves will of course have errors associated with them. A very important part of the validation process is correctly assessing the magnitude of the validation measurement error. We will assume agreement when the error bar of the validation measurement overlaps with the estimated error bar of the GLAS retrieval. For instance, to validate aerosol optical depth using a ground truth measurement obtained by sun photometer, the

magnitude of the error associated with the sun photometer measurement must be known so that the accuracy of the GLAS measurement error can be evaluated.

Table 8.1. Expected Resolution and Accuracy for the new Cloud Physics Lidar System.

Measurement	Spatial Horizontal	Resolution Vertical	Range of Measurement	Expected Accuracy
Cloud Optical Depth	1 km	___	0.01 - 2.0	20%
Cloud Scattering Cross Section	1 km	30 m	10^{-6} - 10^{-1} (1/m-sr)	10%
Aerosol Scattering Cross Section	2 km	30 m	10^{-7} - 10^{-4} (1/m-sr)	10%
Aerosol Optical Depth	2 km	___	0.01 - 2.0	20%
Cloud Top Height	50 m	30 m	300 m-18 km	30 m
Cloud Bottom Height	50 m	60 m	200 m-18 km	60 m
Tropospheric Aerosol Top and Bottom Height	2 km	60 m	200m-18 km	60 m
PBL Height	500 m	60 m	150 m-6 km	60 m

The Cloud Physics Lidar (CPL) will undoubtedly be one of our prime validation tools. It has much better horizontal and vertical resolution than the GLAS measurements and should be able to retrieve extinction and optical depth more accurately as well. Table 8.1 lists tentative information on the spatial resolution and relative accuracy of the various atmospheric measurements made by the CPL. While the spatial resolutions are correct, the accuracy of the products has yet to be verified. An important factor for the CPL measurements is that the system field of view is sufficiently small that multiple scattering is not a significant factor. Therefore GLAS retrieval algorithms can be tested without the complication of an uncertain correction for multiple scattering. Similarly in GLAS underflights it is believed that the CPL cloud optical thickness will be a true independent measurement to compare with the GLAS data product.

8.2 Pre-launch Algorithm Test/Development Activities
8.2.1 Field Experiments and Studies

In most cases, algorithm validation will proceed hand-in-hand with the algorithm development cycle. Coding of the GLAS atmospheric channel algorithms requires the use of actual lidar data sets with which to test the algorithm as it is being developed. Ideally, the test data sets would come from a system that is similar to GLAS and would span large areas of the globe. Unfortunately, no

such data sets exist. However, in 1994 the Lidar In-space Technology Experiment (LITE) was flown aboard the shuttle and acquired global lidar measurements from space for the first time. The lidar instrument flown in LITE is considerably different than GLAS, and in general the data quality is completely unsuitable for development and testing of GLAS data products. However the data set does exist and we think it is possible to use LITE data for testing of a very limited set of the GLAS data products, and indeed, such testing has already begun. In addition, we will test the algorithms using the GLAS simulated data sets generated by the GALS and CAS programs as described in section 8.1.

Since GALS uses actual lidar data acquired from prior field missions, and essentially adds noise to and degrades the data, the original aircraft lidar data can be used as input to an independent set of algorithms to retrieve a given GLAS atmospheric product. This retrieval, whether it be cloud top height, boundary layer height or optical depth, will be more accurate and much easier to retrieve than from the simulated GLAS data because of the much higher signal to noise ratio of the aircraft data. Additionally, during most of the aircraft missions, ancillary and in-situ data are available which can be used to verify and/or supplement the retrievals made from the aircraft lidar data sets. The retrievals made from the aircraft data sets as well as the in-situ observations (where available) will then be used to validate the retrievals made from the GLAS simulated data using the GLAS algorithms. It should be noted that the algorithms used to process the aircraft data to generate the validation data set will be similar to, but distinct from, the actual GLAS algorithms. There is an extensive CALS data base archived at Goddard Space Flight Center which can be used to generate numerous GLAS simulations for algorithm development and testing. Table 8.2 lists the more recent experiments in which CALS has flown on the ER-2 in conjunction with other instruments.

In addition to the CALS flights, the new CPL instrument completed its first field deployment in the Safari 2000 experiment in southern Africa. The field campaign involved close collaborative measurements with instrumented ground sites and in situ aircraft measurements. In the six week deployment extensive observation of thick haze layers were acquired in addition to clear air and cloud conditions. The experiment concluded in September 2000. The data will be used to test GLAS retrievals in the manner described elsewhere.

Table 8.2. Prior ER-2 field experiments using CALS.

Field Campaign	Year	Principle Sensors	Primary Purpose
FIRE	1991	CALS, MAS, CAR	Synoptic scale cirrus
ASTEX	1992	CALS, MAS, CAR, microphysics probes	Marine stratocumulus clouds over the ocean
TOGA-COARE	1993	CALS, MAS, microphysics probes	Tropical cirrus clouds and multi layer clouds over the ocean
CEPEX	1993	CALS, MAS	Tropical cirrus and radiation budget
MAST	1994	CALS, MAS, microphysics probes	Marine stratocumulus clouds over the ocean
ARESE	1995		
ARMCAS	1995	CALS, MAS, CAR, AVIRIS, microphysics probes	Arctic stratus clouds over sea ice; multi- layer clouds; surface bidirectional reflectance
SCAR-B	1995	CALS, MAS, CAR, AVIRIS, microphysics, aerosol properties, AERONET	Smoke, clouds and radiation from biomass burning
SUCCESS	1996	CALS, MAS, HIS, AERI	Mid-latitude cirrus clouds over continents
WINCE	1997	CALS, MAS, HIS,	Cloud detection and properties over snow and ice
FIRE III / ACE	1998	CALS, MAS, HIS,	Arctic stratus clouds over sea ice
WISC-T2000	2000	CALS, MAS, HIS,	Cirrus clouds over snow

8.2.2 Operational Surface Networks
8.2.2.1 AERONET

As mentioned in section 8.1, the validation of GLAS aerosol optical thickness retrievals will be largely done using the AERONET global network of sun photometers. This network is currently comprised of over 75 sites worldwide and has been in operation (though with fewer sites) since the early 90's (Holben et a., 1998). In Figure 8.1, we have made a map of all the AERONET stations that lie within 50 km of the GLAS 8 day repeat orbit that will be used in the GLAS validation phase which lasts about 3 months. Of the 76 total AERONET sites, 38 of them lie within 50 km of the proposed GLAS 8 day repeat orbit. The ICESat spacecraft has the ability to routinely point off nadir such that it can hit targets as far as 50 km from the sub-satellite point. Thus, all ground sites shown in Figure 8.1 can be used for GLAS validation. In Table 8.3, we have listed the geographic coordinates of the 12 AERONET sites that are within 25 km of the expected GLAS 8 day repeat orbit. The last column of Table 8.3 gives the approximate distance from the AERONET location to the expected GLAS overpass. The off nadir pointing required to hit these sites is less than 2.5 degrees and will be easy to accomplish.
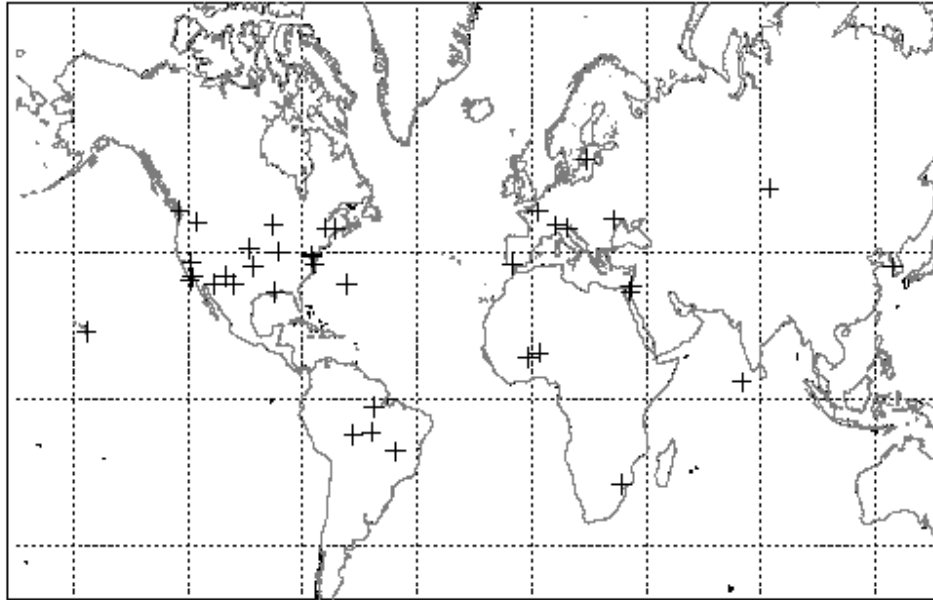
Figure 8.1. The locations of the 38 AERONET sites that lie within 50 km of the expected GLAS 8 day repeat orbit during the validation phase which occurs for a period of about 3 months after launch. As of this year, there are a total of 76 AERONET sites worldwide.

Table 8.3. The 12 AERONET sites that are within 25 km of the projected GLAS 8 day repeat ground track.

AERONET SITE	LATITUDE	LONGITUDE	DISTANCE(KM)
1	-10.70	-62.35	13.0
2	-15.50	-47.65	19.8
3	-9.91	-56.01	7.2
4	36.51	126.31	19.9
5	53.00	83.00	8.9
6	-2.63	-54.95	23.3
7	45.36	-71.91	16.1
8	37.10	-6.70	15.0
9	48.70	2.20	21.6
10	33.25	-119.40	11.9
11	30.51	34.47	24.3
12	30.36	-89.61	22.2

8.2.2.2 MPLNet

In addition to and complimentary with the AERONET sites, plans are underway for the establishment of a global MPL network (MPLNet) for use in EOS validation efforts including GLAS. Currently there are about 8 working MPL sites worldwide (Figure 8.2) and MPLNet will build upon this foundation to eventually double the number of MPL sites. The MPLs will be located at existing AERONET sites as the sunphotometer data is important for the analysis and interpretation of the MPL data. We hope to have MPL-net up and running by the middle of 2001. Data from other

119

ground-based lidar sites around the world as well as sun photometer data from the AERONET global network of radiometers will be used as verification of aerosol optical thickness retrievals. The retrieval of boundary layer height and in some cases cloud layer height can be verified using data from the NWS radiosonde network. Preliminary results from current analysis of MPL data indicate that the MPL, when used in conjunction with sun photometer data, can retrieve aerosol layer optical depth with an accuracy of about 20 percent.
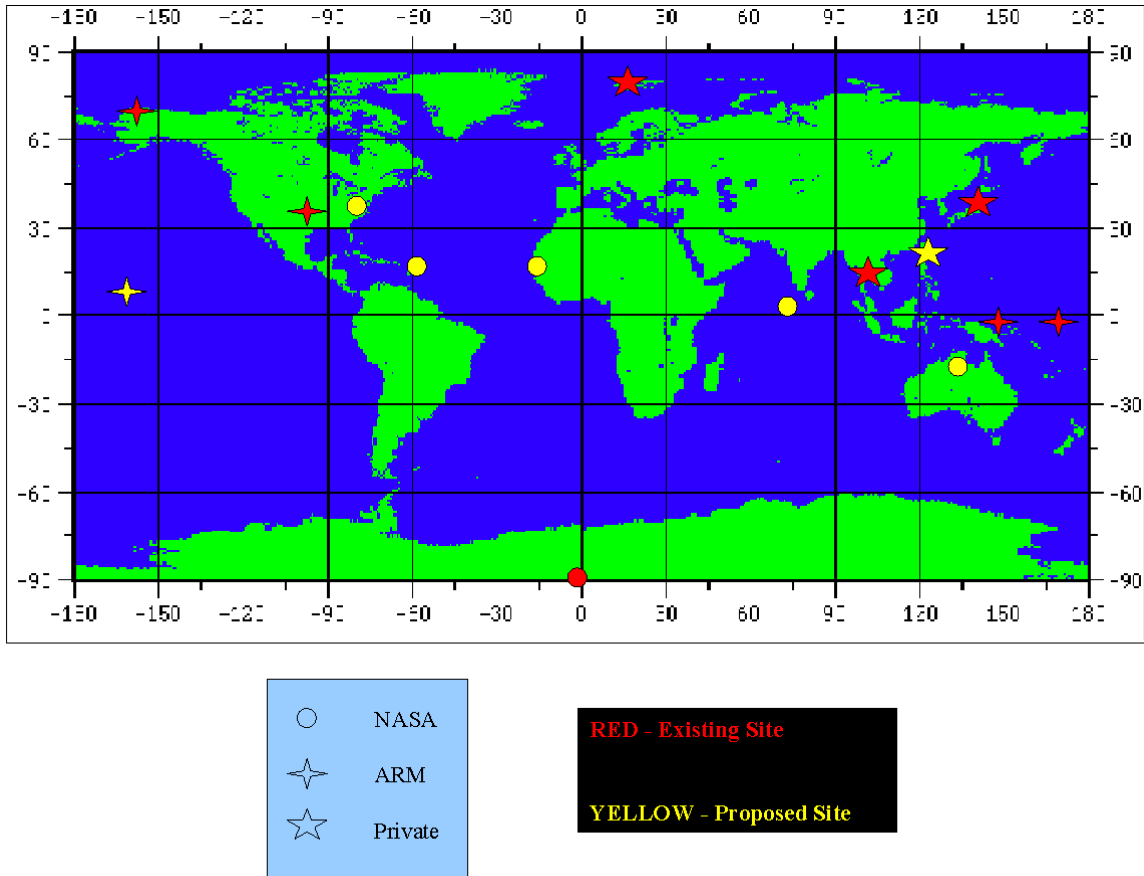

Figure 8.2. A map of the locations of existing and proposed MPL sites.

Table 8.4. The locations of the 9 MPL sites scheduled to be operating by the end of 2001 and the distance between them and the closest approach of the GLAS 8 day repeat orbit.

MPL SITE	LATITUDE, LONGITUDE	GLAS CLOSEST POINT	DISTANCE (KM)
South Pole	-90.00, 0.00	-86.02, -6.20	437
Greenbelt, MD	39.02, -76.87	39.19, -77.25	38
ARM, Manus	-2.07, 147.42	-2.26, 147.66	35
ARM, Naru	-0.50, 166.92	-0.23, 167.65	86
Barrow, Alaska	71.30, -156.68	71.42, -155.94	29
ARM Oklahoma	36.62, -97.50	36.87, -97.66	31
Barbados	13.18, -59.43	13.00, -58.97	53
Saudi Arabia	24.91, 46.41	25.11, 46.08	40
Jabiru, Australia	-15.00, 130.00	-15.16, 130.38	45

8.2.2.3 EARLINET

Another valuable source of ground based validation data can be obtained from the European Aerosol Research Lidar Network (EARLINET). Consisting of 21 ground based stations distributed over most of Europe, the goal of EARLINET is to establish a quantitative and comprehensive data base of both the horizontal and vertical distribution of aerosols on a continental scale. A further goal of EARLINET is to provide ground truth support for present and future satellite missions dedicated to the retrieval of global aerosol distribution. Thus, the use of EARLINET data for the validation of GLAS

Figure 8.3. Network of EARLINET ground stations.

retrievals is in accordance with the goals established for the network. The ground based lidars are comprised mostly of RAMAN systems, capable of determining the extinction profile separately from the backscatter profile. Thus, EARLINET can provide validation for GLAS extinction profiles and optical depth retrievals as well as providing information on extinction to backscatter ratios. It is yet to be determined how many of the EARLINET stations are close enough (within 50 km) to the GLAS 8 day repeat overpasses to be useful, but we expect to use these sites for validation throughout the lifetime of the GLAS mission.

8.2.2.4 Asian Dust Observing Network

A network of ground based lidar systems has been operating since 1997 to monitor the seasonal outbreaks of dust which originate from vast desserts in China and Mongolia. The dust is blown up by strong wind behind cyclone passages and is transported in the free troposphere by the westerly jet. The dust outbreaks are most frequent in the springtime and can cover large areas. It is not uncommon for the dust to extend across the Pacific Ocean and at times reach North America. Most of these sites include sun photometer measurements as well. We intend to use the observations from a number of these stations to compare cloud and aerosol layer height and optical depth retrievals.
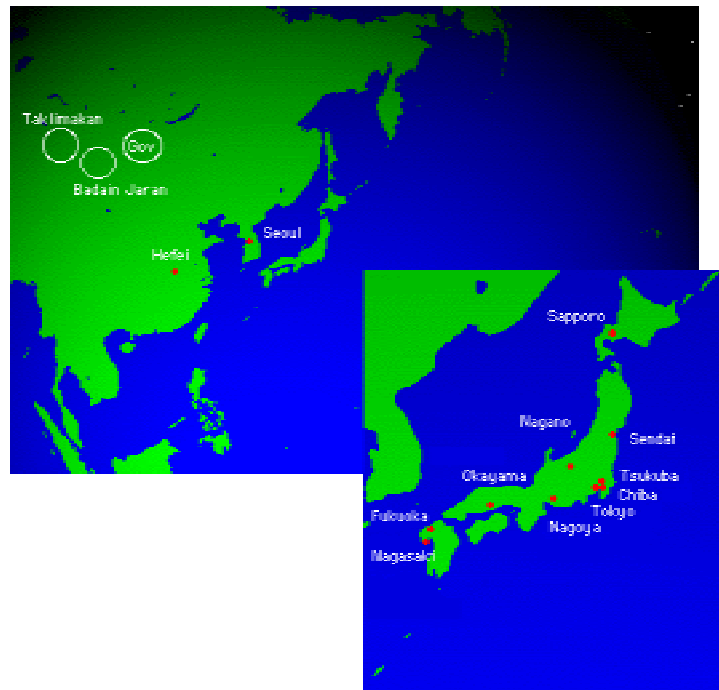

Figure 8.4. Asian Dust observation network

8.3 Existing Satellite Data

During the pre-launch algorithm development phase, satellite data is generally not required for validation activities that can be performed at this time.

8.3 Post-launch Activities

8.3.1 Planned Field Activities and Studies

The products from the GLAS atmospheric channel algorithms will be tested, verified, and validated to the fullest extent possible using available ground based radiation and cloud networks, EOS targeted field validation campaigns, and flights of opportunity which may occur during the lifetime of GLAS (3-5 years). The ground networks cover five main categories:

1) Atmospheric Radiation Measurement (ARM) Sites from DOE:
There are expected to be five sites around the world with micro pulse lidar (MPL) aerosol and cloud profilometers, MFRSR shadowband radiometers, and BBSS balloon sonde atmospheric sounders, all capable of long-term assessments of GLAS derived products. ARM site instrumentation will be involved in intercomparisons of cloud location (especially cloud bottom), attenuated backscatter cross section, aerosol extinction cross section, and optical thickness.

2) Aeronet Radiometer Sites from EOS:
Long term measurements from 78 sites around the world are providing optical ground based aerosol monitoring using automatic sun-sky scanning spectral radiometers. Some of the AERONET sites will be equipped with MPL's to measure vertical distributions of aerosol backscatter and extinction cross sections. The sunphotometer data will provide total column optical depth measurements. This will provide aerosol optical depth validation and possibly thin cloud optical depth validation as well.

3) MPLnet Lidar Sites from EOS:
As part of the general EOS validation scheme, 12 MPL's are now being shipped to various sites around the world to add to the aerosol and cloud database of the EOS ground validation network. They will be used for intercomparisons with GLAS products such as cloud location, aerosol and cloud backscatter cross sections, and optical thickness. The MPL-net locations are shown on the map of Figure 6 in Section 4.2.

4) GLAS MPL sites:
As discussed in 3.1, we plan to deploy 2 additional MPL's along the GLAS orbit track north and south of the existing MPL (ARM) site in Oklahoma. In addition, an MPL site has recently been established at the South Pole and we are examining the possibility of deploying one or two in Greenland as part of the GLAS validation program. These lidar systems will give extra cloud height and boundary layer height validation in climatic zones where ground monitoring is very sparse. If sun photometer data is also available, optical properties will be validated.

5) Ground based lidar community
There are many ground based lidar systems in operation at universities and research institutes around the world. We plan to develop a GLAS correlative measurements group consisting of 10 to 20 lidar sites around the globe. Examples of these include the HSRL[12] at the University of Wisconsin and the lidars at the University of Utah's Facility for Atmospheric Remote Sensing (FARS). Many of the ground based lidar sites will be part of the EARLINET and Asian dust monitoring networks as described in section 4.2. We will keep updated tables posted on the world-

wide-web which indicate when an overpass of GLAS will occur for each site. The lidar data collected during the overpass would then be analyzed for parameters such as cloud top and bottom, backscatter cross section, and cloud and aerosol optical depth. Ideally the analysis will take place at the foreign site, with the results being sent to the GLAS atmospheric science team at Goddard, where they will be archived. The measurements obtained by these groups will themselves have to be verified for accuracy to as great an extent as possible. Generally, this verification is most important for thin cloud and aerosol optical depth, and less important for layer heights. Other instruments (sun photometers for instance) and satellite observations (MODIS, MISR) should be used whenever possible for this purpose. The main burden of this effort would be placed on the institution acquiring the validation data.

After an initial checkout phase lasting about a month, an intense inter-comparison (validation) period is scheduled during the next three months after launch. The ICESat orbit will be configured to enable an increase in overflights over targeted ground networks. Methodologies already developed by NASA/GSFC to generate cloud and aerosol products from MPL systems and AERONET radiometers will be directly adaptable when comparing to the GLAS products. Less intense inter-comparisons will be done after this period when the satellite will be in its normal orbit configuration. These will continue throughout the life of GLAS. We hope to take advantage of planned ER-2 field missions during this time (some of which are listed in Table 6), where one or more flights can be dedicated to flying under the GLAS ground track. The performance of the GLAS algorithms will be statistically evaluated and their accuracy within the different cloud and aerosol types will be classified. The goal of the inter-comparison during the dedicated evaluation period will be to certify the GLAS algorithm accuracy to within a known range of tolerance.

The products produced by the GLAS atmospheric channel algorithms will be extensively tested, verified, and validated by means of aircraft observations after the satellite has been launched into orbit. Since the algorithms were based upon many years of aircraft lidar remote sensing experiments, airborne validation procedures are evidently very appropriate for testing their efficacy and accuracy. Aircraft observations will be made at locations which are inaccessible to ground observations. Aircraft observations can be taken from a large geographical area in a short time compared to ground based observations. The NASA ER-2 aircraft has served as a platform for an atmospheric lidar during many experiments. It remains the best aircraft for this purpose because of its altitude, range, flight stability, and instrumentation capabilities.

8.3.2 New EOS-targeted Field Campaign

To validate the GLAS atmospheric measurements listed in Table 1 will require the use of the Cloud Physics Lidar (CPL) system together with the MODIS Airborne Simulator (MAS) onboard the NASA ER-2 aircraft. Data from the CPL alone will be sufficient to validate cloud and aerosol height, scattering cross section and PBL height. Data from CPL and MAS will be utilized to obtain aerosol and thin cloud optical depth using techniques developed over the years for use with CALS data. It is our understanding that a dropsonde system is under development for the ER-2 aircraft. Measurement of the temperature and pressure structure below the ER-2 will enable us to calibrate the CPL very accurately and to obtain precise measurements of the attenuated backscatter cross section. This will greatly aid our ability to vaidate the GLAS GLA07 data product.

We plan to perform a total of six validation flights, each about 4-6 hours in length. The flights will originate from Dryden Research Center in California. Basing the ER-2 at Dryden Research Center will minimize costs, yet enable the ER-2 to sample a wide area from the mid-west to the eastern Pacific Ocean, encompassing a wide variety of atmospheric conditions. After flying from Dryden to the selected GLAS orbit track, the ER-2 will fly underneath the GLAS orbit for about 1-2 hours. The exact track and location of the GLAS laser footprints can be calculated to a high degree of precision (within 100 m) well ahead of time. The ER-2 will then use GPS positioning to fly directly along the GLAS ground track. The flight will be timed such that GLAS will overfly the ER-2 at the midpoint of the time spent on orbit. The ER-2 then returns to Dryden. The total time of the flights will vary, but should be generally less than 6 hours.

A comprehensive ground-based validation effort will take place in White Sands, New Mexico during the 3 month validation phase. Every eight days the GLAS orbit will pass over White Sands. Much of the effort at White Sands will be geared toward the validation of the pointing accuracy of GLAS and the range measurements derived from the altimeter channel. However, current plans also call for the operation of a ground-based Micro Pulse Lidar (MPL) and sun photometer at White Sands and possibly another location along the orbit track that passes through White Sands. In addition, three MPL's will be located along an 8 day GLAS repeat orbit track in Oklahoma, centered on the ARM CART site as shown in Figure 8.5. We would probably fly the White Sands and Oklahoma orbit tracks twice during the validation period. In addition to these four ER-2 flights, we would make another 3 or 4 flights of GLAS orbits that are within 1500 km or so of Dryden. Of these, one should be chosen which comes close to the Los Angeles metropolitan area (to obtain data that would include anthropogenic aerosol) and another off the coast of California (marine boundary layer and stratus). The other flights would be determined mainly by the weather, as there is a particular interest in the retrieval of thin cloud (cirrus) height and optical depth. At least one of the flights should occur at night, so that we may assess the impact of background light on the GLAS atmospheric retrievals.

The total time required to execute the 7 ER-2 flights will be on the order of 2-3 weeks. We anticipate roughly 35 hours of ER-2 flight time (including ferry time) will be required to accomplish the validation objectives. Assuming a mid December, 2001 launch date, the two weeks required for the mission would occur sometime between late March and early June, 2002. The CPL data will be analyzed in the field at Dryden for cloud and aerosol height, while the optical depth retrievals will be done later at Goddard using the combined analyses of both the CPL and MAS data. These results will then be compared with those obtained from the ISIPS software for the co-aligned data obtained by GLAS.
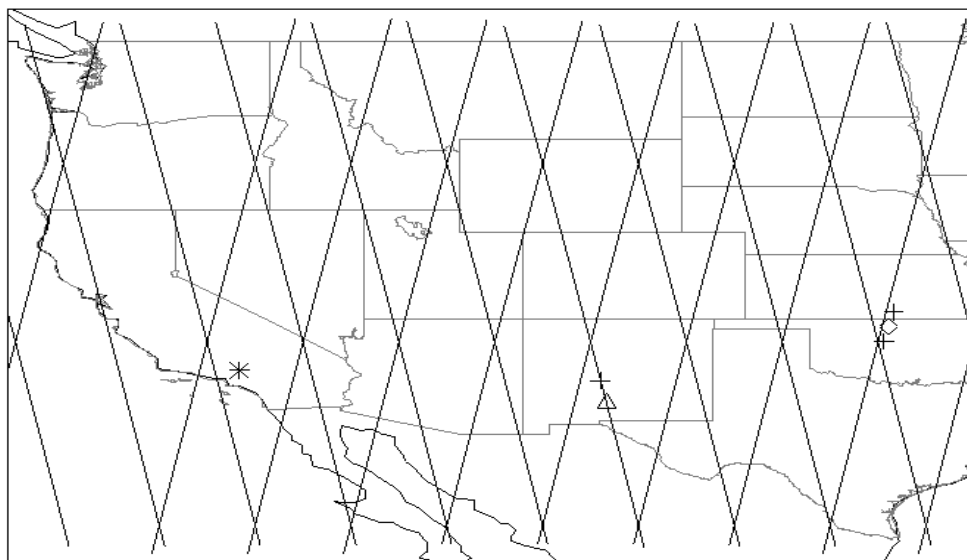
Figure 8.5. A map of the central and western US with the 8-day repeat GLAS orbit tracks and the locations of Dryden Research Center (*), White Sands, New Mexico (Δ), and the ARM CART site in Oklahoma ( ). Also shown are the proposed locations of MPL sites (+) for use during the 3 month validation phase.

An alternative scenario for the ER-2 field mission during the validation phase would be to deploy the aircraft to Fairbanks, Alaska. A mission flown out of Fairbanks would have the advantage of being able to fly 3 or 4 consecutive GLAS overpasses in a single day. This is possible because at the latitude of Fairbanks, the spacing of consecutive GLAS tracks is roughly 500 km, whereas over the central US, the track spacing is close to 1200 km. The ER-2 can fly about 500-600 km/hr and there is about 90 minutes between GLAS overpasses. Thus, over Alaska, the ER-2 could spend about ½ hour on a GLAS ground track, then spend an hour flying to the next GLAS track under which it would fly for another ½ hour, etc. Flying 3 such GLAS underflights would take about 4.5 hours, and with an estimated 3 hour return trip to Fairbanks, would entail a 7.5 hour total mission time. If this is repeated on 3 days, we would have acquired 9 coincident measurements for validation while expending a total of 22.5 flight hours. The mission described above flying out of Dryden would use about 35 flight hours, span 2 to 3 weeks, and yield only 6 coincident validation measurements. While the cost to deploy the ER-2 out of Fairbanks is considerable, it may be largely offset by the reduced number of flight hours.

When the GLAS spacecraft assumes its nominal orbit (after the initial 3 month validation period), the performance of the GLAS algorithms will be reevaluated with ER-2 and other aircraft flights on an episodic basis. This will be done when a situation of opportunity arises for GLAS underflights during the many atmospheric aircraft experiments which typically take place within the planned lifetime of GLAS. During such experiments, it will often be possible to design one or more aircraft sorties to serve as a GLAS underflight. Depending upon the specific instrumentation of a given flight, the products of one or more of the GLAS algorithms will be evaluated. The performance of the instrument will be evaluated for degradation. Such degradation may require that the algorithms be modified. Also, the performance of the algorithms in additional categories of cloud situations will

be analyzed and these results added to the performance catalog. A tentative list of future aircraft experiments which might serve as GLAS validation opportunities is presented in Table 8.5.

The combination of dedicated aircraft lidar underflights immediately after the launch of GLAS and the episodic flights during its lifetime will give investigators a high degree of confidence in the reliability of its products when they are incorporated into atmospheric studies.

Table 8.5. Future post launch (Dec 2001) field campaigns that may provide opportunities to collect GLAS validation data.

Field Campaign	Date	Principle Sensors	Location	Primary Purpose
LBA E-3	1-Apr-02	AVIRIS, MAS, AirMISR	Brazil	
Mini-CRYSTAL	1-Jun-02	ACLS, MAS, CARS, CPL	Florida	Tropical Cirrus Radiative Properties
LBA E-2	7-Apr-03	AVIRIS, MAS, AirMISR	Brazil	
CRYSTAL	21-Jun-04	ACLS, MAS, CARS, CPL	Guam	Tropical Cirrus Radiative Properties
CAMEX V	1-Aug-04	LASE	Florida	Hurricane Dynamics
CloudSat/ Picasso-CENA	15-Aug-04		West Pacific	Validation

8.3.3 Need for other satellite data

The validation of GLAS atmospheric parameters does not require the use of coincident satellite measurements, but when such coincidences occur, we plan to take advantage of them. Of the GLAS products shown in Table 1, satellite data is useful only for validating cloud and aerosol optical depth. The Terra and Aqua EOS platforms as well as AVHRR can be used for this purpose. Additionally, the multispectral infrared radiometer data from any of these satellites can be used to increase the accuracy of the GLAS retrieved optical depth. For the other GLAS data products, satellite retrievals are either unavailable (as in aerosol layer or boundary layer height) or are not accurate enough (cloud height retrievals) to be of use. We expect that PICASSO-CENA and CloudSat data will be used for validation and comparison when they become available, which most likely will not be until mid to late 2004.

8.3.4 Measurement needs at calibration/validation sites

Intercomparison measurements at the validation sites rely heavily on ground and airborne lidar, sun-photometers and radiosonde. During the 3 month validation period a few months after launch we plan to organize a field campaign using the ER-2, portable lidars (MPL), sun-photometers and GPS receivers. Ideally, 3 or 4 MPL's and sun-photometers would be deployed at separate sites along the GLAS ground track separated by 50 to 100 km. The GPS receivers would give us precise knowledge of the validation measurement location. The ER-2 would carry CPL, MAS, a visible imager and possibly another lidar. A second plane might also be used to acquire vertical profiles of extinction using sunphotometers. This would be extremely valuable to validate GLAS computed extinction profiles. Funding for aerosol sampling aircraft for support of the MODIS/MISR validation has been provided by the EOS program in the past and similar funding may be available for GLAS. The most difficult aspect of this plan is in finding suitable places for the ground based MPL systems, since they must lie exactly along the GLAS flight track. Possible sites are being investigated.

8.3.5 Need for instrument development

A major replacement to the ER-2 Cloud and Aerosol Lidar System (CALS) has taken place over the last year. The Cloud Physics Lidar (CPL) was used in its first field campaign during the SAFARI experiment in South Africa in August and September, 2000. The CPL includes the addition of a third channel (355 nm), multiple fields of view, and the use of photon counting detectors. The new design will allow the direct computation of thin cloud and aerosol optical depth, rendering it a more useful instrument for the validation of the GLAS atmospheric products. Currently, the CPL does not have the multiple field of view channels implemented, but continued work over the next fiscal year (2001) will enable the use of these channels by the time GLAS is launched. The CPL performed very well during the SAFARI experiment, and the large data set collected during SAFARI will provide valuable data for the testing of GLAS algorithms. We will also provide manpower for the assembly and alignment of a number of MPL systems which will become part of MPLNet as shown in Figure 6.

8.3.6 Intercomparisons

The validation measurements will first be subjected to an error analysis to quantify the measurement accuracy. Only those measurements which were taken within a certain distance and time (as discussed in section 8.2) will be used. The comparison of cloud top height will be done using the ER-2 CPL data from the underflights when available. In other areas, ground based lidar and radiosonde data will be used. Cloud bottom will be validated from MPLNet, EARLINET and other ground based lidar sites. Aerosol and thin cloud optical depth derived from the GLAS data will be compared with sunphotometer data, Raman lidar and data from the University of Wisconsin's High Spectral Resolution Lidar[12] (HSRL) ground based lidar system. Satellite data from Terra, Aqua and AVHRR will be used when possible for validation of aerosol optical depth.

8.4 Implementation of validation results in data production
8.4.1 Approach

During the first few months after launch, before field validation measurements have been compiled, we will monitor the performance of the cloud top height, aerosol layer height and PBL height algorithms by simply overlaying the results on height-distance images of lidar backscatter.

Adjustments to the algorithms can be made quickly based on these visual inspections. After field validation measurements have been acquired, detailed comparisons between the output of the GLAS processing algorithms and the validation measurements will be performed here at Goddard Space Flight Center by the GLAS atmospheric algorithm development team. Problems and deficiencies in algorithm performance will be identified and corrected. The improved algorithms will be tested on the GLAS data and compared with the results from as many correlative measurement sites as possible to insure their increased accuracy. After an initial, intensive validation period lasting 3 to 4 months, the processing algorithms will be replaced with improved versions, and all of the GLAS data acquired to that point will be re-processed. About six months to one year later, additional improvements to the algorithms will require a second re-processing of the data, based on a continuing assessment of algorithm performance using the ground based validation sites and aircraft data from missions of opportunity. We view validation as an activity that is to be carried out throughout the lifetime of the mission and plan on using data from mainly the ground based sites whenever possible for this purpose.

8.4.2 Role of EOSDIS

The data sent down from GLAS will be analyzed at Goddard Space Flight Center at the GLAS Science Computing Facility (SCF) apart from EOSDIS. Level 1 and 2 data products will then be generated at the SCF and sent to EOSDIS for archival and dissemination to the science community. EOSDIS will also be utilized to locate data sets from other satellites such as Terra, AVHRR, etc., that may be useful in validating the GLAS data products. An example of this would be the use of EOSDIS search tools to locate the occurrences of Terra data that are coincident with GLAS data.

8.4.3 Plans for archival of validation data

The validation data acquired by the correlative measurements program will be archived at Goddard by the GLAS atmospheric measurements principle investigator's (Dr. Spinhirne) group. This will consist of all data acquired during the EOS dedicated field mission and missions of opportunity (involving aircraft), the data from the MPL-net and AERONET, and possibly coincident data from Terra and or Aqua. Additional data obtained from other ground-based lidar sites will also be archived. We have a dedicated computer system (provided by GLAS funds) that has ample disk storage (up to about a terrabyte) and additional DLT tape storage. The data will be archived here and made available through anonymous ftp or a WEB page type interface. Such a data archive may prove very valuable to other EOS investigators, and we are committed to establishing an easily accessible and well documented validation data archive. These data will also be archived at the National Ice and Snow Data Center (NSIDC) in Colorado, which is one of the EOS Distributed Active Archive Centers (DAAC).

8.4.4 Need for Additional Funding

The science validation effort for any spacecraft mission is a costly, but crucial endeavor. Without comprehensive and accurate validation measurements, the science products produced by the processing algorithms have no real value. Thus, it is imperative to design a robust and well thought out validation plan. Of course, the execution of such a plan requires adequate resources. The cost of organizing one EOS dedicated field mission involving the NASA ER-2 aircraft during the 3 month

validation phase has been included in our GLAS budget. The funding for this mission is adequate for only one aircraft. Ideally, we would like additional funds to involve a second aircraft for the in-situ measurement of aerosol properties and extinction profiles. This would greatly facilitate the validation of the GLAS retrieved extinction profiles. A separate proposal to establish and maintain the MPL-net lidar sites has been submitted to EOS management and has been favorably received. Assuming this is fully funded, the only other area which we would ask for additional funding help would be for establishing the additional MPL sites (as shown in Figure 6) that will be used during the 3 month validation phase. At present, these would have to be borrowed from existing MPL sites. A more desirable scenario would be to use funds to assemble 2 or 3 new MPLs here at Goddard, and use them not only during the 3 month validation phase, but throughout the lifetime of GLAS.

8.5 Validation Summary

We have developed a validation plan which strives to insure the best quality retrievals for all of the GLAS atmospheric data products. Prior to launch we will be using mainly simulated GLAS data based on data gathered by the ER-2 CALS system during the last decade for algorithm development and testing. Development of a next generation lidar (CPL) is underway and will provide data sets that can be used for algorithm testing starting in late fall of 2000. Following launch, the validation efforts center on one or more EOS targeted field campaigns utilizing ground based (MPL) and airborne (CPL on the ER-2) lidar and sunphotometer (AERONET) measurements taken along the flight track of GLAS. Validation data gathered from selected ground based lidar sites around the world will also be used, but the usefulness of these data are limited compared to that obtained with aircraft. Care must be exercised to insure that the correlative measurements are co-located in space and time to within certain thresholds that depend on the local atmospheric variability. Table 8.6 lists, for each atmospheric product, the main correlative measurement that will be used to validate that product. Validation is an extremely important component of the GLAS science mission and careful planning must be done to insure its success.

Table 8.6. Validation Summary

GLAS Science Product	Validation Measurement	Validation Issues
Cloud optical depth	CPL, HSRL, MPL and AERONET	Multiple scattering correction, S ratio knowledge
Cloud scattering cross section	CPL, HSRL	Multiple scattering correction, S ratio knowledge
Aerosol optical depth	AERONET and MPL, Raman lidar, HSRL lidar, MODIS, AVHRR	S ratio knowledge
Aerosol scattering cross section	CPL, MPL	S ratio knowledge
Cloud top height	CPL, Radiosonde	Optical depths > .05
Cloud bottom height	MPL. Radiosonde	Multiple scattering; Optical depths < 2.5
PBL height	CPL, Radiosonde.	Multiple embedded layers; Optical depths > .05

9 Future Research

The level I and II data products discussed in this document form the basis for future research activities and the generation of level III data products. In general, level III data products require a level of analysis which precludes them from being produced routinely and continuously as are the level I and II data products. Level III products may involve inputs from other sensors and external models. They often will require a careful screening of the data and more user interaction and checking of the algorithm output.

In terms of the atmospheric measurements to be provided by the GLAS instrument, the basic height parameters provided in Level II can be expected to be robust and not require much further research beyond the improvements that will come out of algorithm development and testing. There are some exceptions. An example of a level III product would be lifting condensation level (LCL), derived from the output of GLA08. The more difficult parameters to obtain accurately from the lidar data are the optical depth and extinction cross sections for aerosol and cloud. It is expected that the accuracy and applicability of these can be significantly increased through Level III products and post processing. The two areas requiring further work for this are the use of data other than the lidar profile signal and improvements in multiple scattering corrections.

For cloud analysis, a desirable input would be simultaneous IR radiance measurements. With IR radiance obtained in sufficiently close time with the lidar profile it is possible to solve for the vertical profiles of IR absorption cross section (Spinhirne et al., 1990). Simultaneous IR radiance values should be available for a large fraction of the GLAS observations. At the time of the mission there will be over 20 spectral imagers with thermal IR channels in orbit. Since GLAS has a precessing orbit, the GLAS measurements will be within the swath width of the MODIS imagers for about two months of the year for example. The combination of the GLAS data with IR data will be a research topic for level III processing. An additional improvement of the cloud retrieval from GLAS data alone may also be possible from research and modeling on using the molecular and surface signals under thin cloud layers to improve optical depth calculations. The most significant improvement for cloud retrieval will likely come from research on the best approach for the multiple scattering correction. To first order, work is proceeding to develop the best possible corrections tables based on geographic location, cloud height and thickness and cloud structure. Another approach to be studied is to possibly make use of the below ground multiple scattering tail that should be observed by the GLAS ranging channel for a direct measure of the multiple scatter factor leading to improvement of correction tables.

For aerosol optical thickness and extinction cross section, multiple scattering corrections are less of an issue. The largest uncertainties would result likely from the value of extinction to backscatter ratio that is applied for the retrievals. An important factor for improving the retrievals for data time observations is to make use of the 532 and 1064 nm solar background signals. From these data alone, over oceans an optical thickness for aerosol could be obtained directly in the manner that AVHRR data are now used. Future research is needed to model the best approach for incorporating the solar background signals with the lidar return profiles. In addition the GLAS aerosol profiles can be combined with many other sensor data and retrievals. One example would be with AVHRR and MODIS aerosol retrievals. Again the precessing orbit of GLAS will provide large amount of coincident data that can be used to improve extinction to backscatter look up

tables for nighttime and other non-coincident GLAS observations. An especially important combination will be GLAS aerosol profiles with TOMS aerosol retrievals. Currently TOMS data are applied to retrieve absorbing aerosol in the atmosphere, but an assumption on the height profile of the aerosol is needed. For the large amount of coincident data with TOMS expected from the full GLAS mission, future research will enable improvements in the TOMS and GLAS aerosol data results.

The level III products will be produced by the atmospheric lidar group headed by Dr. James Spinhirne. They will be done on a case by case basis as opposed to a continuous processing as are the level I and II products. It may be possible, after enough experience has been gained, to automate certain level III data products.

Another area of future research is the development of methods to correct for the multiple scattering induced errors for surface ranging.

10 References

Ackermann, J., 1998: The Extinction-to-Backscatter Ratio of Tropospheric Aerosol: A Numerical Study, *J. Atmos. Oceanic Technol.*, **15**, 1043-1050.

Ansmann, A., U. Wandinger, M. Riebesell, C. Weitkamp and W. Michaelis, 1992: Independent measurements of extinction and backscatter profiles in cirrus clouds by using a combined Raman elastic-backscatter lidar, *Appl. Opt.*, **31**, 7113-7131.

Ansmann, A., J. Bosenberg, G. Brogniez, S. Elouragini, P. Flamant, K. Klapheck, H. Linn, L. Menenger, W. Michaelis, M. Riebesell, C. Senff, P. Thro, U. Wandinger and C. Weitkamp, 1993: Lidar Network Observations of Cirrus Morphological and Scattering Properties during the International Cirrus Experiment 1989: The 18 October 1989 Case Study and Statistical Analysis, *J. Appl. Meteor.*, **32**, 1608-1622.

Boers, R, E. W. Eloranta and R. L. Coulter, 1984: Lidar observations of mixed layer dynamics: tests of parameterized entrainment models of mixed layer growth rate. J*. Clim. Appl. Meteor*, **23**, 247-266.

Boers, R. and E. W. Eloranta, 1986: Lidar measurements of the atmospheric entrainment zone and the potential temperature jump across the top of the mixed layer. *Bound. Layer Meteor.*, **34**, 357-375.

Boers, R., S.H. Melfi and S.P. Palm, 1991: Cold Air outbreak during GALE: Lidar observations and modeling of boundary layer dynamics. *Mon. Wea. Rev.*, **119**, 1132-1150.

Congeduti, F., J. DeLuisi, T. DeFoor, and L. Thomason, 1998: Optical extinction properties of volcanic stratospheric aerosol derived from ground-based lidar and Sun photometer measurements, *J. Geophys. Res.*, **103**, 13893-13902.

Duda, D. P., J. D. Spinhirne and E. W. Eloranta, 1999: Atmospheric Multiple Scattering Effects on Altimetry. Part I: Calculation of Single Pulse Bias. Submitted February, 1999

Duda, D. P., J. D. Spinhirne and E. W. Eloranta, 1999: Atmospheric Multiple Scattering Effects on Altimetry. Part II: Cloud Climatology Analysis of Expected Seasonal and Interannual Surface Altitude Errors. Submitted February, 1999

Eloranta, E. W., R. E. Kuehn and R. E. Holz, "Cirrus Cloud Backscatter Phase Functions Measured with the University of Wisconsin High Spectral Resolution Lidar" 10th Conference on Atmospheric Radiation, preprint, AMS, Madison, Wisconsin, 28 June–2 July, 1999.

Elouragini, S., 1995: Useful algorithms to derive the optical properties of clouds from a backscatter lidar return, *J. Modern. Opt.*, **42**, 1439-1446

Elouragini, S. and P. H. Flamant, 1996: Iterative method to determine an averaged backscatter-to-extinction ratio in cirrus clouds, *Appl. Opt.*, **35**, 1512-1518.

Gobbi, G. P., 1995: Lidar estimation of stratospheric aerosol properties: Surface, volume, and extinction to backscatter ratio, *J. Geophys. Res.*, **100**, 11219-11235.

Grund, C. J. and E. W. Eloranta, 1990: The 27-28 October 1986 FIRE IFO Cirrus Case Study: Cloud Optical Properties Determined by High Spectral Resolution Lidar, *Mon. Wea. Rev.*, **118**, 2344-2355.

Grund, C.J. and E. W. Eloranta, 1991: The University of Wisconsin High Spectral Resolution Lidar, *Optical Engineering*, **30**, 6-12.

Hlavka, D. L., J. D. Spinhirne, and J. R. Campbell, 1998: "Aerosol Analysis Techniques and Results form Micro Pulse Lidar", 19th International Laser Radar Conference, Annapolis, MD, July 6 - 10, 1998.

Holben BN, Eck TF, Slutsker I, Tanre D, Buis JP, Setzer A, Vermote E, Reagan JA, Kaufman YJ, Nakajima T, Lavenu F, Jankowiak I, Smirnov A, 1998: AERONET - A federated instrument network and data archive for aerosol characterization. Remote Sensing of Environment **66**: (1) 1-16.

IPCC, 1995: Climate Change 1994. *Cambridge U. Press*.

Iqbal, M., An Introduction to Solar Radiation, Academic Press, New York, NY, 1983.

Liu, Z., P. Voelger, and N. Sugimoto, 2000: Simulations of the observation of clouds and aerosols with the Experimental Lidar in Space Equipment system. *Appl. Opt.*, **39**, 3120-3137.

Macke, A., 1993: Scattering of light by polyhedral ice crystals, *Appl. Opt.*, **32**, 2780-2788.

Macke, A., P. N. Francis, G. M. McFarquhar and S. Kinne, 1998: The role of particle shapes and size distributions in the single scattering properties of cirrus clouds, *J. of Atmos. Sci.*, **55**, 2874-2883.

Marenco, F., V. Santacesaria, A. F. Bais, D. Balis, A. di Sarra, A. Papayannis, and C. Zerefas, 1997: Optical properties of tropospheric aerosols determined by lidar and spectrophotometric measurements (Photochemical Activity and Solar Ultraviolet Radiation campaign), *Appl. Opt.,* **36**, 6875-6886.

McClatchey, R.A., R.W. Fenn, J.E.A. Selby, F.E. Volz, and J.S. Garing, Optical Properties of the Atmosphere (Third Edition), AFCRL-72-0497, 1972.

McCormick, M. P., H. M. Steele, W Chu, and T. Swissler, 1982: Polar Stratospheric Cloud Sightings by SAM II. *J. Atmos. Sci.*, **39**, 1387-1397.

McCormick, M. P., P. Hamill and U. Farrukh, 1985: Characteristics of Polar Stratospheric Clouds as observed by SAM II, SAGE, and Lidar, *J. Meteor. Soc. Japan,* **63**, 267-276.

McFarquhar, G. M. and A. J. Heymsfield, 1997: Parameterization of Tropical Cirrus Ice Crystal Size Distributions and Implications for Radiative Transfer: Results from CEPEX, *J. Atmos. Sci.*, **54**, 2187-2200.

Melfi, S.H., J.D. Spinhirne, S.H. Chou and S. Palm, 1985: Lidar observations of vertically organized convection in the planetary boundary layer over the ocean. J*. Clim. Appl. Meteor.*, **24**, 806-821.

Mishchenko, M. I., Wielaard, and B. E. Carlson, 1997: T-matrix computations of zenith-enhanced lidar backscatter from horizontally oriented ice plates, *Geophys. Res. Lett.*, **24**, 771-774.

Nicolas, F., Bissonnette, L. R., and P. H. Flamant, 1997: Lidar effective multiple-scattering coefficients in cirrus clouds, *Appl. Opt.*, **36**, 3458-3468.

Palm, S.P. and J.D. Spinhirne, 1987: Optimization of boundary layer height retrieval. Laser and Optical Remote Sensing of the Atmosphere, Volume **18**, 63-66, and presented at conference.

Palm, S.P. and J. Spinhirne, 1998: The detection of Clouds, Aerosol and Marine Atmospheric Boundary Layer Characteristics from Simulated GLAS Data. The 19th International Laser Radar Conference, Annapolis, Md, July 6-10, 1998.

Palm, S. P., D. Hagan, G. Schwemmer and S.H. Melfi, 1998: Inference of Marine Atmospheric Boundary Layer Moisture and Temperature Structure using Airborne Lidar and Infrared Radiometer Data, J*. Appl. Meteor.*, **37**, 308-324.

Pinnick, R. G., J. M. Rosen and D. J. Hofmann, 1976: Stratospheric Aerosol Measurements III: Optical Model Calculations, *J. Atmos. Sci.*, **33**, 304-314.

Pinnick, R. G., S. G. Jennings, P. Chylek, C. Ham and W. T. Grandy, 1983: Backscatter and Extinction in Water Clouds. *J. Geophys. Res*, **88**, 6787-6796.

Platt, C. M. R., 1979: Remote Sounding of High Clouds: I. Calculation of Visible and Infrared Optical Properties from Lidar and Radiometer Measurements, *J. Appl. Meteor.,* **18**, 1130-1143.

Platt, C. M. R., Reynolds, D. W., Abshire, N. L., 1980: Satellite and lidar observations of the albedo, emittance, and optical depth of cirrus compared to model calculations. *Mon. Wea. Rev.*, **108,** 195-204

Platt, C. M. R., 1981: Remote sounding of high clouds. Part III: Monte Carlo calculations of multiple-scattered lidar returns, *J. Atmos. Sci.*, **38**, 156-167.

Powell, D. M., J. A. Reagan, M. A. Rubio, W. H. Erxleben, and J. D. Spinhirne, 2000: ACE-2 Multiple Angle Micro-pulse Lidar Observations from Las Galletas, Tenerife, Canary Islands. *Tellus B*, **52**, 651-660.

Russell, P. B., T. J. Swissler, M. P. McCormick, W. P. Chu, J. M. Livingston and T. J. Pepin, 1981: Satellite and Correlative Measurements of the Stratospheric Aerosol. I: An Optical Model for Data Conversions, *J. Atmos. Sci.*, **38**, 1279-1294.

Spinhirne, J. D., J. A. Reagan, and B. M. Herman, 1980: Vertical Distribution of Aerosol Extinction Cross Section and Inference of Aerosol Imaginary Index in the Troposphere by Lidar Technique, *J. Appl. Meteor.*, **19,** 426-438.

Spinhirne, J. D., 1982: Lidar clear atmosphere multiple scattering dependence on receiver range, *Appl. Opt.*, **21**, 2467-2468.

Spinhirne, J. D., R. Boers and W. D. Hart, 1989: Cloud Top Liquid Water from lidar Observations of Marine Stratocumulus. *J. Appl. Meteor.*, **28**, 81-90.

Spinhirne, J. D. and W. D. Hart, 1990: Cirrus structure and radiative parameters from airborne lidar and spectral radiometer observations: the 28 October 1986 FIRE study. *Mon. Wea. Rev,* **118**, 2329-2343

Spinhirne, J. D., W. D. Hart, D. L. Hlavka, 1996: Cirrus infrared parameters and shortwave reflectance relations from observations, *J. of Atmos. Sci.*, **53**, 1438-1458.

Spinhirne, J. D. and S. P. Palm, 1996: Space Based Atmospheric Measurements by GLAS. Advances in Atmospheric Remote Sensing with Lidar. Selected Papers of the 18th International Laser Radar Conference, Berlin Germany. 213-216.

Spinhirne, J. D., Campbell, J. R., Hlavka, D. L., Ferrare, R. A., Turner, D. D., and Flynn, C. J., "Aerosol Retrieval Comparison During the SGP Summer '98 IOP from Multiple Lidar Probing", Poster Abstract, Atmospheric Radiation Measurement (ARM) Science Team Meeting, San Antonio, Texas, March 22-26, 1999.

Starkov, A. V., and C. Flesia, 1998: Correction of spaceborne lidar signal for multiple scattering from high clouds, Proc. of the 19th International Laser Radar Conference, July 6-10, Annapolis, MD.

Vigroux, E., Contribution a l'etude experimentale de l'absorption de l'ozone, Ann. Phys., 8, 709-761, 1953.

Welton, E. J., K. J. Voss, H. R. Gordon, H. Maring, A. Smirnov, B. Holben, B. Schmid, J. M. Livingston, P. B. Russell, P. A. Durkee, P. Formenti, and M. O. Andreae, 2000: Ground-based Lidar Measurements of Aerosols During ACE-2: Instrument Description, Results, and Comparisons with other Ground-based and Airborne Measurements. *Tellus B*, **52**, 635-650.

Wielicki, B. A., B. Barkstrom, E. Harrison, R. Lee, G. Smith, and J. Cooper, 1996: Clouds and the Earth's radiant energy system (CERES): An Earth observing system experiment. *Bull. Amer. Meteor. Soc.*, **77**

Wiscombe, W., 1977: Mie scattering calculations: Advances in technique and fast, vector-speed computer codes. NCAR Tech. Note TN140+STR. (Edited and revised 1996, available at ftp://climate.gsfc.nasa.gov/pub/wiscombe/Single_Scatt/Mie_Code/NCARMieReport.pdf

11 Acronyms

ACE	Arctic Clouds Experiment
AEROCE	Aerosol/Ocean Chemistry Experiment
AERONET	Aerosol Robotic Network
AIRS	Atmospheric Infrared Sounder
ARM	Atmospheric Radiation Measurement Program
ARMCAS	Arctic Radiation Measurements in Column Atmosphere-surface System (beaufort Sea, Alaska, June 1995)
ASTEX	Atlantic Stratocumulus Transition Experiment (Azores, June 1992)
AVHRR	Advanced Very High Resolution Radiometer
AVRIS	Airborne Visible / Infrared Imaging Spectrometer
CALS	Cloud and Aerosol Lidar System
CAR	Cloud Absorption Radiometer
CEPEX	Central Equatorial Pacific Experiment
CRYSTAL	
DAAC	Distributed Active Archive Center
DEM	Digital Elevation Model

EAL	Elevated Aerosol Layer
EOS	Earth Observing System
EOSDIS	EOS Data and Information System
FIRE	First ISCCP Regional Experiment
GLAS	Geoscience Laser Altimeter System
GLOBE	Global Backscatter Experiment
HSRL	High Spectral Resolution Lidar
ISCCP	International Satellite Cloud Climatology Project
LITE	Lidar In-space Technology Experiment
MAS	MODIS Airborne Simulator
MAST	Monterey Area Ship Tracks Experiment (Monterey California, June 1994)
MODIS	Moderate Resolution Imaging Spectroradiometer
NSIDC	National Ice and Snow Data Center
PBL	Planetary Boundary Layer
SUCCESS	Subsonic Aircraft Contrail and Cloud effects Special Study (April – May, 1996)
WINCE	Winter Cloud Experiment